University of Alberta

Structural Studies on Antibacterial Peptides

By

Alan C. Gibbs

A thesis submitted to the Faculty of Graduate Studies and Reseach in partial fulfillment of the requirements for the degree of Doctor of Philosophy

in

Pharmaceutical Sciences

Faculty of
Pharmacy and Pharmaceutical Sciences

Edmonton, Alberta
Fall, 2001

National Library of Canada
Acquisitions and Bibliographic Services
395 Wellington Street
Ottawa ON K1A 0N4
Canada

Bibliothèque nationale du Canada
Acquisitions et services bibliographiques
395, rue Wellington
Ottawa ON K1A 0N4
Canada

Your file Votre référence

Our file Notre référence

The author has granted a non-exclusive licence allowing the National Library of Canada to reproduce, loan, distribute or sell copies of this thesis in microform, paper or electronic formats.

L'auteur a accordé une licence non exclusive permettant à la Bibliothèque nationale du Canada de reproduire, prêter, distribuer ou vendre des copies de cette thèse sous la forme de microfiche/film, de reproduction sur papier ou sur format électronique.

The author retains ownership of the copyright in this thesis. Neither the thesis nor substantial extracts from it may be printed or otherwise reproduced without the author's permission.

L'auteur conserve la propriété du droit d'auteur qui protège cette thèse. Ni la thèse ni des extraits substantiels de celle-ci ne doivent être imprimés ou autrement reproduits sans son autorisation.

0-612-68936-0

Canada

University of Alberta

Library Release Form

Name of Author: Alan C. Gibbs

Title of Thesis: Structural Studies on Antibacterial Peptides

Degree: Doctor of Philosophy

Year this Degree Granted: 2001

Permission is hereby granted to the University of Alberta Library to reproduce single copies of this thesis and to lend or sell such copies for private, scholarly or scientific research purposes only.

The author reserves all other publication and other rights in association with the copyright in the thesis, and except as herein before provided, neither the thesis nor any substantial portion thereof may be printed or otherwise reproduced in any material form whatever without the author's prior written permission.

Alan Gibbs

Faculty of Pharmacy and
Pharmaceutical Sciences
University of Alberta
Edmonton, Alberta
T6G 2N8

Date: June 19, 2001

University of Alberta

Faculty of Graduate Studies and Research

The undersigned certify that they have read, and recommend to the Faculty of Graduate Studies and Research for acceptance, a thesis entitled "Structural Studies on Antibacterial Peptides" submitted by Alan C. Gibbs in partial fulfillment of the requirements for the degree of Doctor of Philosophy in Pharmaceutical Sciences.

Dr. David S. Wishart

Dr. John C. Vederas

Dr. James M. Diakur

Dr. Edward E. Knaus

Dr. Mavanur R. Suresh

Dr. Julie Forman-Kay
University of Toronto

Date: June 13, 2001

Abstract

This thesis describes a series of structural and spectroscopic studies conducted on a number of antibacterial peptides. In Chapter 2, a sequence length dependence on β–sheet formation in small cyclic peptides (gramicidin S analogs) is described. ^{1}H–NMR and CD data reveal, that small cyclic peptides will form β–sheets if, and only if, they contain the following features: 2(2n+1) residues [where (n= 1, 2, 3...)], two equally spaced type II' β–turns (or type I' β–turns) and proper placement of turn and sheet forming residues. In Chapter 3, the synthesis and characterization of D–Leucocin A is described. This represents the first synthesis of an all–D–amino acid class IIa bacteriocin. We show that the unnatural D–enantiomer of Leucocin A is devoid of activity. This result strongly suggests a chiral recognition step is necessary to Leucocin A's mechanism of antibacterial action. Chapter 4 details, by way of ^{1}H–NMR spectroscopy and molecular dynamics, the structural determinants of type II' β–turn formation. The gramicidin S model is used to determine the effects of: a) backbone chirality, b) backbone N–alkylation and c) side–chain/side–chain interaction, on β–hairpin and type II' β–turn formation. It is shown, that proper backbone chirality may account for up to 60%, N–alkylation for up to 20% and proper side–chain/side–chain interactions for up to 10% of type II' β–turn stabilization. In Chapter 5, the folding and unfolding kinetics of small cyclic β–hairpins (gramicidin S analogs) is described. These studies were performed by temperature–jump IR, and the results correlated to all–atom molecular dynamics simulations in an attempt to gain detailed structural and dynamic insight into the

unfolding events of β–sheets.

Acknowledgements

This thesis work was inspired by three excellent scientists and teachers: Dave Wishart, Jim Diakur and John Vederas. My thanks goes to, my supervisor Dr. David Wishart for providing me with the intellectual insight, guidance and the resources to perform this interesting and rewarding research. To Dr. Jim Diakur for your friendship and stimulating conversations ranging from chemistry to sports and all things in between. And to Dr. John Vederas for your contagious enthusiasm for chemistry and inherent generosity.

I would like to express my gratitude and thanks to all my colleagues and fellow grad students that I have had the pleasure of associating with through out the last four years. In particular, I would like to thank Scott Watson, Gary Van Domselaar, Dr. Kevin Morin and Don Husereau who have all been good friends, providing many intellectual discussions and a constant source of emotional support.

I must acknowledge various, invaluable contributions from Dr.'s, Alex Nip (Linux), YunJun Wang (NMR), Liang Zeng Yan and Michael Stiles (Leucocin A). I am very grateful to Dr.'s Brian Sykes and Robert Hodges for their involvement and initiation of the gramicidin S project (Chapters 2 and 4). I wish to thank Dr. Brian Dyer and Shelia Maness for their contributions of T-jump IR data (Chapter 5). I would like to thank Dr.'s Edward Knaus and Len Wiebe for accepting me into the Faculty of Pharmacy and Pharmaceutical Sciences back in the Summer of 1996. For technical assistance, I would like to thank Marc Genest (peptide synthesis) and

Ashenafi Abera (lab boss). My thanks also goes out to Dr.'s Wasimul Haque and Albert Friesen for encouragement and support over the last couple of years.

My greatest appreciation is for my wife and son, Kim and Christopher. Without their constant support, encouragement and patience over the last four years, this thesis and research would not have been accomplished.

Finally, I would like to acknowledge PENCE, the Dorothy Whiteman graduate scholarship foundation and the Mike Wolowyk graduate scholarship foundation for financial support.

Table of Contents

Page

Chapter 1: Introduction 1

1.1 Antibacterial Peptides 3

1.2 Peptide Synthesis 13

1.3 NMR Spectroscopy 15

1.4 Molecular Mechanics and Dynamics 21

1.5 Objectives 25

References 27

Chapter 2: Unusual β–sheet Periodicity in Small Cyclic Peptides (GS Analogs) 49

2.1 Introduction 49

2.2 Materials and Methods 51

2.3 Results and Discussion 54

2.4 Conclusion 62

References 64

Chapter 3: Bacteriocin Analogs: Antibacterial Activity and Interactions of Leucocin A with its Enantiomer, Carnobacteriocin B2 and Truncated Derivatives 80

3.1 Introduction 80

3.2 Materials and Methods 82

3.3 Results and Discussion....86
3.4 Conclusion....93
References....95

Chapter 4: Probing the Structural Determinants and Conformational Space of Type II' β–turns....105

4.1 Introduction....105
4.2 Materials and Methods....109
4.3 Results and Discussion....113
4.4 Conclusion....128
References....132

Chapter 5: Folding and Unfolding of Small Cyclic β–sheet Peptides (GS Analogs)....161

5.1 Introduction....161
5.2 Materials and Methods....164
5.3 Results and Discussion....168
5.4 Conclusion....175
References....177

Chapter 6: General Discussion and Conclusion....187

References....196

List of Tables

Page

Table 1.1.....33

Table 1.2.....35

Table 2.1.....68

Table 2.2.....69

Table 2.3.....70

Table 2.4.....71

Table 2.5.....72

Table 2.6.....73

Table 2.7.....74

Table 2.8.....75

Table 3.1.....98

Table 4.1.....137

Table 4.2.....138

Table 4.3.....139

Table 4.4.....140

Table 4.5.....141

Table 4.6.....142

Table 4.7.....143

Table 4.8.....144

Table 4.9.....145

Table 4.10.....146

Table 4.11.....147

Table 4.12.....148

Table 4.13.....149

Table 5.1.....179

Table 5.2.....179

List of Figures

Page

Figure 1.1.....36

Figure 1.2.....37

Figure 1.3.....38

Figure 1.4.....39

Figure 1.5.....40

Figure 1.6.....41

Figure 1.7.....42

Figure 1.8.....43

Figure 1.9.....43

Figure 1.10.....44

Figure 1.11.....45

Figure 1.12.....46

Figure 1.13.....47

Figure 1.14.....48

Figure 2.1.....76

Figure 2.2.....78

Figure 2.3.....79

Figure 3.1.....99

Figure 3.2.....100

Figure 3.3.....101

Figure 3.4.....102

Figure 3.5.....103

Figure 3.6.....104

Figure 4.1.....151

Figure 4.2.....152

Figure 4.3.....154

Figure 4.4.....155

Figure 4.5.....157

Figure 4.6.....158

Figure 4.7.....159

Figure 4.8.....160

Figure 5.1.....180

Figure 5.2.....181

Figure 5.3.....182

Figure 5.4.....183

Figure 5.5.....184

Figure 5.6.....186

List of Abbreviations

Coded Amino Acids:

A (Ala)	=	L–Alanine
C (Cys)	=	L–Cysteine
D (Asp)	=	L–Aspartic Acid
E (Glu)	=	L–Glutamic Acid
F (Phe)	=	L–Phenylalanine
G (Gly)	=	Glycine
H (His)	=	L–Histidine
I (Ile)	=	L–Isoleucine
K (Lys)	=	L–Lysine
L (Leu)	=	L–Leucine
M (Met)	=	L–Methionine
N (Asn)	=	L–Asparigine
P (Pro)	=	L–Proline
Q (Gln)	=	L–Glutamine
R (Arg)	=	L–Arginine
S (Ser)	=	L–Serine
T (Thr)	=	L–Threonine
V (Val)	=	L–Valine
W (Trp)	=	L–Tryptophan
Y (Tyr)	=	L–Tyrosine

Non-coded Amino Acids (mentioned in this thesis):

Sar	=	Sarcosine (N-Methlyglycine)
Phg	=	L-Phenylglycine
Pip	=	L-Pipecolic acid (Homo-proline)
Deh	=	L-3,4-Deydroproline
O (Orn)	=	L-Ornithine
AIB	=	α-Aminoisobutyric acid

Δp	=	protonmotive force
Å	=	angstrom
μs	=	microsecond
2-Cl-Z	=	2-chlorobenzyloxycarbonyl
Boc	=	t-butyloxycarbonyl
BOP	=	Benzotriazole-1-yl-oxy-tris-(dimethylamino)-phosphonium hexafluorophosphate
CbnB2	=	carnobacteriocin B2
CD	=	circular dichroism
CPU	=	central processing unit
CSI	=	chemical shift index
Da	=	dalton
DCC	=	N,N'-dicyclohexyl-carbodiiimide
DMAP	=	4-dimethylaminopyridine
DMF	=	N,N-dimethylformamide
DMSO	=	dimethyl sulphoxide

DCM	=	dichloromethane
DSS	=	3–(trimethylsilyl)–1–propanesulfonic acid
DTT	=	dithiothreitol
DPC	=	dodecylphosphocholine
FID	=	free induction decay
Fmoc	=	9–fluorenylmethoxycarbonyl
GS	=	gramicidin S
GS1	=	gramicidin S synthetase 1
GS2	=	gramicidin S synthetase 2
HATU	=	O–7–azabenzotrizol–1–yl–N,N,N',N'–tetramethyluronium hexafluorophosphate
HBTU	=	O–benzotriazole–N,N,N',N'–tetramethyluronium hexafluorophosphate
HOBT	=	N–Hydroxybenzotriazole
HPLC	=	high performance (pressure) liquid chromatography
HCl	=	hydrochloric acid
IR	=	infrared spectroscopy
K	=	Kelvin
LAB	=	lactic acid bacteria
LeuA	=	leucocin A
MD	=	molecular dynamics
MIC	=	minimum inhibitory concentration
MM	=	molecular mechanics
NMM	=	N–methyl morpholine

NMR	=	nuclear magnetic resonance
NOE	=	nuclear overhauser effect
NOESY	=	nuclear overhauser effect spectroscopy
PEF	=	potential energy function
Pmc	=	2,2,5,7,8–pentamethyl–chroman–6–sulphonyl
PTS	=	phosphotransferase system
RMSD	=	root mean square deviation
ROESY	=	rotating frame nuclear overhauser effect spectroscopy
SAR	=	structure activity relationships
SPC	=	single point charge
SPPS	=	solid phase peptide synthesis
T–jump	=	temperature jump
TASP	=	template assembled synthetic protein
TFA	=	trifluoroacetic acid
TFE	=	trifluoroethanol
TOCSY	=	total correlation spectroscopy
Trt	=	triphenylmethyl
UV	=	ultraviolet spectroscopy
amu	=	atomic mass units
ns	=	nanoseconds
ppb	=	parts per billion
ppm	=	parts per million
preCbnB2	=	precarnobacteriocin B2
ps	=	picoseconds

tBOC	=	t–butyloxycarbonyl
tBu	=	t–butyl

Chapter 1

Introduction

The *antibiotic era* began in 1941 with the first clinical use of penicillin by Howard Florey (Chain et al., 1940). Florey's therapeutic application of penicillin was heralded as a modern medical miracle and provided reassurance that devastating pandemics like the bubonic plague would never happen again. The advent of the *antibiotic era* produced an explosion of new antibacterial compounds; streptomycin (Schatz et al., 1943), chloramphenicol (Bartz, 1948; Ehrlich, et al., 1948), chlortetracyclin (Duggan, 1948), erythromycin (McGuire et al., 1952), and by 1965 over 25,000 antibacterial compounds had been identified. However, shortly after penicillin's introduction, resistant bacteria began to emerge. In 1950, penicillin displayed 100% bacteriocidal efficacy on *Staphylococcus aureus* and 35 years later it was effective against less than 5%. By 1992, the only effective antibiotic for 40% of *Staphylococcus aureus* strains was vancomycin. Then, in 1997 the first case of *Staphylococcus aureus* resistance to vancomycin was reported.

It is currently believed that antibiotic resistance may eventually lead to the end of the so called *antibiotic era* and usher in a more threatening *post-antibiotic era* for the twenty-first century. The emerging threat of bacterial resistance to conventional antibiotics has renewed interest in the discovery of novel antibacterial compounds, a field which has been somewhat complacent over the last 20 years. One class of antibacterial compounds which has seen recent interest are antibacterial

peptides (Hancock, 1997; Hancock and Chapple, 1999; Hwang and Vogel, 1998). Although antibacterial peptides have been known and used topically (gramicidin S and polymyxins) for quite some time, most of them exhibit undesirable properties making them relatively poor therapeutic agents. Many of these undesirable properties are inherently related to the stability and three–dimensional structure of the peptide.

In this thesis I will explore the relationship between structure, stability and activity for two different classes of antibacterial peptides 1) gramicidin S (Schwyzer, 1958) and 2) leucocin A (Hastings et al., 1991). Gramicidin S is a small, cyclic peptide that adopts a well–defined antiparallel β–sheet structure while leucocin A is a longer, linear peptide that prefers an α–helical structure. Both peptides have demonstrated therapeutic potential. Please see Figures 1.1 and 1.2 for structural information concerning these two peptides.

In characterizing the structure/function relationships of these peptides it was necessary to employ solid phase peptide synthesis to prepare a large number of chemically and structurally unique analogs. These analogs were then characterized using a variety of spectroscopic and computational techniques such as NMR spectroscopy, CD spectroscopy, IR spectroscopy and molecular dynamics. Through this kind of detailed structural and dynamic analysis it has been possible to gain important insights into general aspects of protein folding as well as the chemical and structural parameters that control the activity of these antibacterial peptides. These

results are presented and discussed in more detail in Chapters 2 – 5.

The remainder of this introductory chapter is concerned with providing the reader with some basic background concerning antibacterial peptides. Brief, introductory discussions on a number of key techniques that were critical to the success of this research project (solid phase peptide synthesis, NMR spectroscopy and molecular dynamics) are also provided.

1.1 Antibacterial Peptides

Antibacterial peptides are ubiquitous in nature and are thought to play an important role in the innate first–line–of–defense against infectious bacteria (Boman, 1995). Antibacterial peptides are produced by nearly every living organism, including: mammals, amphibians, insects, spiders, fish, plants, invertebrates and bacteria (Tossi et al., 2000). Table 1.1 contains a representative list of antibacterial peptides found in nature. From this table one can see there is considerable diversity in: amino acid composition, biosynthesis, mechanism of action, and three–dimensional structure.

Amino acid composition. There is considerable variability in antibacterial peptide composition. Indeed, close inspection of Table 1.1 demonstrates that these peptides include a wide variety of coded, non–coded and post–translationally modified amino acids. Certain peptides have abnormally high numbers of tryptophan [gramicidin A, indolicidin (Rosek et al., 2000)], proline [pyrrhocoricin (Kragol et

al., 2001)], α–amino isobutyric acid (AIB) [alamethicin (Sansom, 1991)], or histidine [histatin (Grogan et al., 2001)] residues. Many peptides also have high concentrations of arginine and lysine, making them quite cationic. Frequently, the cationic peptides have alternating arrangement of hydrophobic and charged residues which imparts an amphipathic (usually helical) structure. There are also examples of antibacterial peptides containing amino acids that are unnatural D enantiomers (gramicidin S), whereas other amino acids are functionalized by lipids [daptomycin (Carrier et al., 1998)] or carbohydrates (pyrrhocoricin).

Biosynthesis. The biosynthesis of antibacterial peptides is accomplished either via direct translation by the ribosome (Demain and Fang, 2000) or through template–directed synthesis by multi–domain peptide synthases (Marahiel, et al. 1997). Many ribosomally synthesized antibacterial peptides require post–translational modifications in order to become active or mature. Some of the more important post–translational modifications known to occur on antibacterial peptides (Andreu and Rivas, 1998) include: halogenation, disulphide formation, phosphorylation, O–glycosylation, hydroxylation, methylation, C–terminal amidation, carbon epimerization and proteolytic cleavage.

Leucocin A is synthesized as a 61 residue protein via standard ribosomal synthesis (Hastings et al., 1991). Following synthesis, Leucocin A undergoes post–translational cleavage to yield a mature 37 residue peptide. In contrast, gramicidin S is synthesized non–ribosomally by a two–subunit multimodular enzyme, gramicidin S synthetase 1 (GS1) and 2 (GS2), by way of the thio–template mechanism (von

Döhren et al., 1997; Luo and Walsh, 2001). The synthesis of one GS molecule is accomplished in 16 individual reactions in a concerted effort by both subunits (see Figure 1.3). GS1 activates and epimerizes phenylalanine, then transfers the resulting D–Phe to a condensing domain on GS2. GS2 subsequently activates proline, valine, ornithine and leucine and catalyzes elongation reactions to produce the pentapeptide, D–Phe–Pro–Val–Orn–Leu. After two pentapeptide intermediates are synthesized GS2 then cyclizes them in a head–to–tail fashion by an undetermined mechanism (von Döhren et al., 1997). Elongation/condensation and epimerization are initiated through the formation of a thioester intermediate (thio–template mechanism). The thioester intermediate is formed from thioesterification of an aminoacyl–AMP by a 4'–phosphopantetheine cofactor, a reaction catalyzed by a so–called aminoacyl carrier protein (domain). Incidentally, the aminoacyl carrier proteins of peptide synthases are thought to be structurally similar to the acyl carrier proteins of polyketide synthases (Dieckmann and von Döhren, 1997).

Mechanisms of Action. Antibacterial peptides exert their bacteriocidal activity through various mechanisms of action. A schematic diagram illustrating possible modes of action for antibacterial peptides is shown in Figure 1.4. A small number of peptides act by inhibiting/disrupting cell–wall synthesis. Glycopeptides (eg. vancomycin) inhibit the binding of the host transpeptidase to D–alanyl–D–alanine. This inhibits crosslink formation, thereby greatly weakening the cell wall (Walsh, 1999). Bacitracin, on the other hand, inhibits cell wall synthesis by inhibiting the dephosphorylation of the pyrophosphate form of the C_{55} isoprenyl carrier lipid, an integral molecule in cell wall synthesis (Epperson and Ming, 2000). It is well

established, however, that the majority of antibacterial peptides actually act on the lipid membrane. Because our understanding of lipid–peptide interactions is still quite primitive, the details of how peptides disrupt the lipid bilayer are still not known. It is understood that positively (cationic) charged peptides have a high affinity towards bacterial cell membranes. Cationic peptides typically displace membrane stabilizing cations attached to the lipopolysaccharide (LPS) layer of gram–negative bacteria (Eppand and Vogel, 1999). On the other hand, cationic peptides are thought to interact with negatively charged teichoic acid on gram–positive bacteria. After their initial membrane contact, some peptides are known to aggregate and disrupt the membrane via one of two possible models (Huang, 2000; Oren and Shai, 1998): 1) the barrel–stave model or 2) the carpet model. The carpet model proposes that binding of a critical concentration of peptide to the surface membrane leaflet causes a large scale breakdown of the plasma membrane. Alternatively, the barrel–stave model suggests peptides aggregate (resembling staves of a barrel) and form pores that extend through the membrane. All membrane disruption models suggest that the bacteriocidal activity arises from upsetting the protonmotive force (Δp) or electrochemical gradient, osmotic gradients and/or cytoplasmic pools of small organic molecules.

Membrane active peptides may also act in other less membrane obtrusive (or invasive) ways. It has been hypothesized that some peptides may, after binding to the outer membrane, flip inward. In doing so, these peptides carry lipids with them (Matsuzaki et al., 1997; 1998). Dr. Bob Hancock (University of British Columbia)

has recently reported that no clear correlation could be found between peptide concentrations leading to complete membrane permeabilization and their minimal inhibitory concentration (MIC), no matter what type of peptide structural class (Wu et al., 1999). This result suggests that bacteriocidal activity of certain membrane active peptides may lie in their ability to pass across the membrane and subsequently affect cytoplasmic targets. Regardless of how antibacterial peptides may enter the cell, there are many targets in the cytoplasm they could exert their influence upon. One example is a class of peptides called the streptogramins, which act on the 50S ribosomal subunit. A–type streptogramins bind the peptidyl transferase domain thus inhibiting translation whereas B–type streptogramins inhibit the formation of the 50S ribosomal subunit itself.

Synergy between two or more peptides to impart bacteriocidal activity appears to be an important aspect for a number of antibacterial peptides (Zhang et al., 1999). Interestingly, the streptogramins are bacteriostatic (i.e. orders of magnitude less active) by themselves and bacteriocidal when acting together. Synergistic action is quite common amongst many classes of antibacterial peptides. Bacteriocins, for example, have a sub–class (IIb) dedicated for synergistic peptides produced by lactic acid bacteria (LAB).

Structure. As shown in Table 1.1, there are many different types of structural motifs found in antibacterial peptides. The structures listed in Table 1.1 correspond primarily to the structures for the biologically active forms. Some of the peptides are unstructured until they interact with a membrane, a protein receptor or with each

other (Hancock and Chapple, 1999). Interestingly, different structures can affect similar targets while, similar structures can influence different targets. Inspection of Table 1.1 reveals that secondary and tertiary structures found in antibacterial peptides are composed of elements ranging from common α–helices and β–sheet's to relatively rare cystine–knot's and chealated–metal complexes. Figure 1.5 illustrates a few of the structural classes found in antibacterial peptides. Two structural types of antibacterial peptides examined in this thesis are α–helical peptides (class IIa bacteriocins) and β–sheet peptides (gramicidin S analogs).

While cyclic non–helical (gramicidin S and polymyxins) peptides were the first antibacterial peptides to be identified and characterized, the most extensively studied antibacterial peptides are the helical peptides. The majority of these helical, antibacterial peptides are cationic and amphipathic (Table 1.1). Interestingly, although many membrane active peptides contain cationic amphipathic helices, the lack of inter–species sequence homology has been suggested as being evidence of convergent evolution within this structural class (Hancock and Chapple, 1999).

Exhaustive SAR studies have indicated that up to seven different physical characteristics may influence the potency and spectrum of activity of α–helical antibacterial peptides. These include size, sequence, percent helix content, net charge, hydrophobicity, amphipathicity and size of the hydrophilic and hydrophobic faces (Tossi, et al., 2000). It is believed that the size of the hydrophilic/hydrophobic face relates to the method of peptide–membrane interaction (Dathe and Wieprecht,

1999). In particular, it has been shown that peptides with a small hydrophilic angle and large overall hydrophobic content will aggregate and form pores. In contrast, peptides with equal amounts of hydrophilic/hydrophobic content will orient parallel to the membrane surface (Brasseur et al., 1997).

Although most helical antibacterial peptides contain cationic amino acids, there are also other types of helical antibacterial peptides. The AIB rich peptide called trichogin, is composed of a 3_{10}–helix (Epand et al., 2001). As shown in Figure 1.5, the 3_{10}–helix is longer than other helices composed of the same number of amino acids. Therefore peptides with 3_{10}–helices need fewer residues to traverse lipid membranes. Gramicidin A, a pentadecapeptide composed of alternating L and D amino acids, forms a right handed β–helix – a sort of helical parallel β–strand (Ketchem et al., 1996). When two gramicidin A molecules are oriented with their N termini touching each other in a lipid membrane, a pore is formed. The proline/tryptophan rich peptide indolicidin is known to form type II poly–L–proline helices with some evidence of β–turn elements as well (Rozek et al., 2000). Another rare class of helical antibacterial peptide is the proline and arginine rich molecule bactenecin, which has been shown to adopt a γ–helix (Niidome et al., 1998). Incidentally, the γ–helix has similar backbone torsion angles to the type II poly–L–proline helix.

Less common among membrane active peptides is the β–sheet or β–hairpin structure. Most antibacterial peptides that adopt antiparallel β–sheet structures are

cyclic. There are actually two primary forms of cyclization; backbone cyclization (homodetic) as in the case of gramicidin S and related tyrocidines; and side–chain cyclization (heterodetic) as in lactoferricin, protegrins and defensins. Peptide cyclization may assist in β–haripin formation because the loss in entropy that small peptides encounter during β–hairpin formation is not well compensated for by hydrogen bonding or non–covalent interactions (Epand and Vogel, 1999).

Often, local structure is quite important in defining antibacterial peptide function. Local structure may be defined as the effect certain residues have on structure and/or function. Local structure is important for both buforin II (Park et al., 2000; Kobayashi et al., 2000) and melittin (Sansom and Weinstein, 2000) activity. The evidence gathered to date suggests these peptides require a 'proline hinge' for proper activity. Usually proline acts as a helix breaker. However, in the case of buforin II and melittin, proline only slightly kinks the helix. In buforin II, the substitution of proline to leucine renders the peptide unable to pass through the plasma membrane, hence the kink or hinge mediates the peptides passage through the membrane. Tryptophan residues have also been shown to play an important role in antibacterial peptide function. In gramicidin A, the β–helices are anchored in the membrane via many tryptophan residues, as shown by its solid state NMR structure, 1MAG (Ketchem et al., 1996). Tryptophan has also been implicated in modulating the activities of cecropin A (Andreu et al., 1983) and the porcine myeloid peptide PMAP–23 (Kang et al., 1999). Interestingly, PMAP–23 requires a C–terminal tryptophan for activity as do many non–related bacteriocins. Another example of

local structural effects is shown in chapter 4 of this thesis where we investigated the influence of β–turns on gramicidin S analogs. A favorable electrostatic interaction between aromatic rings and proline (or proline like) side–chains were shown to stabilize type II' β–turns. This type of local interaction was also found in type IVa β–turns (Nardi et al., 1997; 2000; Demchuk et al., 1997).

Gramicidin S (GS). In their desperate search for agents to cure war time infections, two Russian scientists discovered a cyclic decapeptide that they named gramicidin S (Gause and Brashnikova, 1944). First isolated in the Soviet Union (hence the S in gramicidin S) from *Bacillus brevis*, gramicidin S has been used as a topical antibiotic since its discovery in 1944. It was not until 1957 that preliminary X–ray data gave insights into its unique three–dimensional structure (Schmidt et al., 1957). Over the next 20 years numerous theoretical, NMR, IR and UV/CD studies revealed more and more about GS's three–dimensional conformation (Vanderkooi et al., 1966; Balasubramanian, 1967; Ohnishi and Urry, 1969). However, it was not until 1978 that Hull and coworkers were finally able to solve the crystal structure of GS (Hull et al., 1978). This structure revealed a slightly twisted, amphipathic, anti–parallel β–sheet structure enclosed by two evenly spaced type II' β–turns (Figure 1.1).

Following the three–dimensional characterization of GS, numerous SAR studies ensued (Kato et al., 1970; Tamaki et al., 1995; Kondejewski et al., 1996; 1999). In this thesis I will describe three additional studies where the structure and

dynamics of GS have been explored at new levels of detail. In chapter 2, we characterize the peptide–length dependence on β–hairpin formation within cyclic peptides. In chapter 4, we investigate the role of β–turns (more specifically type II' β–turns) on β–hairpin formation and stability in cyclic peptides. These results may have important implications for the *de novo* design of peptides and peptidyl mimetics. Chapter 5 examines β–hairpin stability as defined by the kinetics of peptide unfolding–refolding via T–jump IR and molecular dynamics studies.

Bacteriocins. Bacteriocins have been described as compounds that are proteinaceous in nature, produced by bacteria and bacteriocidal to closely related bacteria (Jack et al., 1995; van Belkum and Stiles, 2000). The first account of a bacteriocin was reported by Louis Pasteur in 1877 (Pasteur and Joubert, 1877). Pasteur and his colleague, Joubert, noticed an antagonistic interaction between bacteria. The first specific identification of a bacteriocin was made in 1925, with the discovery of colicin V (Gratia, 1925) and soon after, the discovery of nisin (Rogers, 1928) in 1928. Since that time, large numbers of bacteriocins have been discovered from a variety of bacteria, both gram–negative and gram–positive strains. Klaenhammer has recently proposed four classes of lactic acid bacteriocins (Klaenhammer, 1993), see Table 1.2.

In chapter 3, we describe the investigation of a class IIa bacteriocin (Ennahar et al., 2000; Nes and Holo, 2000) produced from gram–positive LAB – called Leucocin A (LeuA). Although most class IIa bacteriocins contain cationic,

amphipathic α–helices, other structural elements may be present as well. Such is the case for LeuA. In addition to having an α–helix, LeuA contains a small, N–terminal, antiparallel β–sheet. To help elucidate the possible roles of these structural elements and LeuA's mechanism of action, its enantiomer was synthesized and tested for activity. Interestingly, our results suggest that LeuA acts through a receptor or synergistic protein–protein interaction – and not through a classical membrane disruptive mechanism, as opposed to literature reports (Wade, et al., 1990; Maloy and Kari, 1995).

1.2 Peptide Synthesis

Basic Principles of Solid Phase Peptide Synthesis (SPPS). Peptide synthesis via the solid phase approach is the most efficient and commonly used technique for the chemical synthesis of peptides and proteins. Since the invention of SPPS by Bruce Merrifield in the 1960's, advances in chemistry have led to the synthesis of peptides and peptoids of impressive sizes and complexity (Merrifield, 1963; 1965; 1997). There are two main chemistries employed in SPPS. Each is named after their respective α–amino protecting groups, t–butyloxycarbonyl (tBoc) (Erickson and Merrifield, 1976) and 9–fluorenylmethoxycarbonyl (Fmoc) (Chang and Meienhofer, 1978). The difference between the two strategies lies in the acid/base–lability of their respective α–amino and side–chain (orthogonal) protecting groups.

SPPS involves the step–wise linking of individual amino acids, in a C– to

N–terminal direction, to create a peptide. The C–terminal amino acid is initially attached to a solid support matrix. The matrix is an insoluble polymer that has accessible reactive *handles*, such as nucleophilic –OH groups. During the step–wise synthesis, all soluble/excess reagents and free protecting groups can be removed from the solid support by solvent washing. After the desired sequence of amino acids has been assembled, the peptide is then cleaved from the solid support with concurrent orthogonal deprotection. The resulting peptide is usually purified to homogeneity via reversed phase high performance liquid chromatography (HPLC). The scheme for SPPS is shown in Figure 1.6.

For simplicity, the synthetic scheme can be broken down into three steps that are repeated until the desired peptide is synthesized.

1. Deprotection: The α–amine (of the growing peptide chain) is deprotected via acid or base catalysis. Common conditions are: 30% piperdine in N,N'–dimethylformamide (DMF) or 50% triflouroacetic acid (TFA) in dichloromethane (DCM) [for Fmoc and tBoc chemistries respectively].

2. Activation: Convergent to amine deprotection (Step 1), is the *activation* of a protected amino acid. Commonly used reagents are tetra–methyluronium salts (see Figure 1.7), O–benzotriazole–N,N,N',N'–tetramethyluronium hexafluorophosphate (HBTU) and O–7–azabenzotriazol–1–yl–N,N,N',N'–tetramethyluronium hexafluorophosphate (HATU). In the presence of a catalytic amount of N–methylmorpholine (NMM) these compounds

activate by forming (in situ) the HOBt or HOAt esters, thereby rendering the carbonyl carbon more electrophilic.

3. Coupling: The activated amino acid is allowed to react with the deprotected, solid–support attached, amino acid. A nucleophilic substitution, via the free amine, at the carbonyl carbon takes place, thus extending the peptide chain in a C– to N–terminal direction.

Initial amino acid attachment to the solid support is similar to the Coupling step (Step 3), however, dicyclohexylcarbodiimide (DCC) is commonly used as the coupling agent. Cleavage of the peptide from the solid support is accomplished via acid hydrolysis. Typically, hydrogen flouride (HF) or TFA are used for t–Boc and Fmoc resins respectively. Often cleavage conditions contain reducing agents (thioanisole, dithiothreitol, etc.) and cation scavengers (anisole, water, etc.) to minimize side reactions. It is important to mention, as with many chemistries, SPPS reaction conditions often need to be modified and optimized to maximize yield.

1.3 NMR Spectroscopy

Basic Principles of NMR. Since its discovery in 1945, NMR spectroscopy has become one of the most powerful techniques for biomolecular structure determination and analysis (Wuthrich, 1986). Developments resulting in two Nobel Prizes (F. Bloch and E.M. Purcell in 1952 and R.R. Ernst in 1991) along with recent advances in multidimensional pulse sequences, have made possible the structure

elucidation of large molecules such as peptides and proteins (Gardner and Kay, 1998).

NMR spectroscopy uses a nuclear magnetic property, called spin (I). When nuclei with I=1/2 are placed in an external magnetic field they adopt two (2I+1) possible orientations, parallel or antiparallel, see Figure 1.8. The different orientations correspond to different energy levels (ΔE) which are directly proportional to the strength of the external magnetic field (B_o).

$$\mathbf{[1.1]} \quad \Delta E = \gamma h B_o / 2\pi$$

Where h is Planck's constant (6.6262×10^{-34} J s) and γ is the gyromagnetic ratio (1/s T).

A nucleus in an external magnetic field can move between higher or lower energy levels, with concomitant absorption or emission of energy, at its Larmor frequency. The Larmor frequency (ω_o) is defined as the nuclei's characteristic rate of precession in an external magnetic field. Larmor frequency is dependent on the strength of the magnetic field (B_o) and intrinsic properties of the nucleus defined in its gyromagnetic ratio γ. The Larmor frequency is given by:

$$\mathbf{[1.2]} \quad \omega_o = -\gamma B_o$$

The nuclei create a net magnetization (M) while in an external magnetic field due to unbalanced populations of spin–defined energy levels. The population ratio of the energy levels can be expressed by the Boltzmann equation:

$$\mathbf{[1.3]} \quad N\beta / N\alpha = \exp(-\Delta E / kT)$$

Where $N\beta$ and $N\alpha$ are the population of the upper and lower energy states

respectively.

Molecular information can be measured if the net magnetization (M) of a sample is perturbed (Derome, 1987). By applying a magnetic pulse (B_1) in the form of a radiofrequency pulse perpendicular to the external magnetic field (B_o), a magnetic precession of the nuclei occurs. Because the precession eventually returns to equilibrium, it can be detected and recorded by metal coils in the XY plane. The precession is recorded in the form of a oscillating current and is subsequently converted to an electronic signal called a free–induction decay (FID). Finally, a Fourier transformation is applied to the FID (time domain) in order to convert it to the familiar NMR spectrum (frequency domain). See Figure 1.9 for a more detailed picture of the process.

Chemical shifts. Electron density shields the nucleus from the applied magnetic field, thus the magnetic field at the nucleus is not equal to the applied magnetic field. This is described by the following equation:

$$\mathbf{[1.4]} \quad \mathbf{B = B_o (1-\sigma)}$$

Where σ is the shielding constant, B_o is the applied magnetic field and B is the net magnetization.

An increase in electron density around a nucleus corresponds to an increase in shielding σ, hence a stronger magnetic field is needed to bring the nucleus into resonance. The electron density surrounding a nucleus is influenced by the

proximity of: π electron systems (including carbonyl groups and aromatic rings), solvent, metal ions, etc. Simply stated, chemical shifts (δ) are defined as the difference between the frequency (Hz) at which a nucleus absorbs, relative to the absorption frequency of a nucleus of a given chemical shift standard such as 2,2'–dimethyl–2–silapentane–5–sulfonate (DSS). Chemical shifts are reported in parts per million (ppm) and are calculated using the following equation:

$$[1.5] \quad \delta(\text{ppm}) = \frac{\text{Shift from standard (Hz)} \times 10^6}{\text{Spectrometer frequency (Hz)}}$$

Coupling constants. Nuclei are also influenced by the spins of nuclei, less than or equal to, three bonds away. This is known as through–bond spin–spin coupling (J) and manifests itself in the NMR spectrum as resonance–peak splitting. The magnitude of this resonance splitting contains torsion angle information between the two coupling nuclei. Martin Karplus of Harvard University, has derived the following equation (Karplus, 1959):

$$[1.6] \quad {}^3J_{ab} = A\cos^2(\theta) + B\cos(\theta) + C$$

Where ^3J is the coupling constant through three bonds and A, B, and C are empirically derived constants for each type of coupling constant.

Figure 1.10, provides a graphical representation of a typical Karplus equation for protein $^3J_{HNHA}$ coupling constants. The sinusoidal nature of the curve illustrates how multiple dihedral values correlate to one coupling constant value.

Nuclear Overhauser Effect (NOE). An important phenomenon that indirectly yields nuclei–to–nuclei distance information by way of NMR, is the nuclear Overhauser effect. The nuclear Overhauser effect was discovered by Albert Overhauser and was first confirmed experimentally in 1953 (Carver and Slichter, 1953). The effect can be observed if the saturation of one nucleus (promotion to the high spin state) results in energy transfer to a neighboring nucleus (less than 5 Å apart), with the net effect being an enhancement of the NMR signal of the neighboring nucleus.

Structure related NMR data. To use NMR to generate realistic three–dimensional solution structures of peptides, it is necessary to collect a variety of different types of spectral data. The more information obtained, the more accurate the resulting structures will be. In this thesis homo–nuclear chemical shifts, NOE data, coupling constants, amide temperature coefficients and chemical shift anisotropies were used to help solve the structures of many of the peptides discussed herein.

To acquire this information, all proton resonances must be assigned to specific amino acid protons. This is accomplished through the use of two types of NMR experiments: through–bond correlation experiments and through–space correlation experiments. The homonuclear experiments, COSY (Marion and Wuthrich, 1983) and TOCSY (Bax and Davis, 1985) (see Figure 1.11 for an example TOCSY spectrum) are commonly used for through–bond proton correlation, whereas NOESY (Jeener et al., 1979) and ROESY (Bothner–By et al., 1984) are most common for through–space correlations. The total resonance

assignment can be broken down in to two steps: (1) individual spin system assignment via through–bond connectivities, and (2) sequential residue assignment via through–space connectivities. Following this resonance assignment step, one can collect coupling constant and amide temperature coefficient data through 1–D, TOCSY and/or COSY experiments.

Chemical shifts, coupling constants, NOE's and temperature coefficients all yield important information on local and global (secondary and tertiary) structure of peptides and proteins. Chemical shifts are particularly sensitive measures of peptide structure. The Chemical Shift Index (CSI) is a simple method for identifying polypeptide structure through chemical shift analysis (Wishart et al., 1992). In particular, α protons shifted down–field, relative to random coil values, are known to exist in β–sheet backbone conformations where as protons shifted up–field, relative to random coil values, exist in α–helical regions. NOE data, in addition to its important role in sequential assignment, also yields secondary and tertiary structural information as well. Since the magnitude of the NOE is proportional to $1/r^6$ (where r is the distance between coupling nuclei), specific NOE patterns are commonly observed for different secondary structural elements. For example, strong NOE's between $d_{NN}(i,i+1)$ and $d_{\alpha\beta}(i,i+3)$ are characteristic for residues in α–helical regions and $d_{\alpha N}(i,i+1)$ NOE's suggest residues in β–sheet conformations, see Figure 1.12. Coupling constants also give information on torsion angles. In particular $^3J_{HNH\alpha}$ measurements yield peptide backbone phi (ϕ) dihedral data (see Figure 1.13). The value of $^3J_{HNH\alpha}$ directly relates to secondary structure, for

example:

$^3J_{HNH\alpha} \cong 3.9$ Hz correspond to α–helices with phi (ϕ) angles of ~ –60°

$^3J_{HNH\alpha} \cong 9.0$ Hz correspond to β–sheets with phi (ϕ) angles of ~ –140°

Chemical shifts, coupling constants, NOE's and other NMR accessible data may be used to generate polypeptide structures via molecular mechanics in the form of restraints.

1.4 Molecular Mechanics and Dynamics

Basic Principles of Molecular Mechanics. Molecular mechanics is a computational technique used to simulate molecular structure and dynamics (Burkert and Allinger, 1982; Boyd and Lipkowitz, 1982). Classical Newtonian mechanics is used to approximate the molecular system of interest. In essence the molecule may be simply described as a network of balls with point charges, connected by springs. More specifically, an empirical energy funtion is used to approximate the potential energy of a molecular system as a function of geometric variables (Bowen and Allinger, 1991). Unlike quantum mechanics, electrons are not considered explicitly and the molecular system is described as a collection of atoms that interact with one another by simple analytical functions that are based on equations of classical mechanics. A group of analytical functions (terms) make up the potential energy function (PEF) or force field (Dinur and Hagler, 1991). The PEF describes the energy of the system for any conformation and configuration of atomic coordinates. A typical empirical PEF takes the form:

$$[1.7] \quad V(R) = V_{bonded}(R) + V_{nonbonded}(R)$$

Where V(R) is the potential energy function, that calculates the potential energy for any molecular conformation, as defined by the cartesian coordinate vector R. The bonded terms are covalent interactions and reflect energy contributions from: bond stretching, bond angle bending, improper angle twisting (chirality) and dihedral angle twisting. Nonbonded terms are non–covalent interactions and reflect interactions between two nuclei not mediated by bonds: coulombic or Lennard–Jones (vdW) interactions. More specifically,

$$
\begin{aligned}
V_{bonded}(R) \;=\; & {}_{bonds}\, K_l \{l - l_{eq}\}^2 + \\
& {}_{angles}\, K_\theta \{\theta - \theta_{eq}\}^2 + \\
& {}_{impropers}\, K_\omega \{\omega - \omega_o\}^2 + \\
& {}_{dihedrals}\, K_\varphi/2 \{1 + \cos[n\varphi - \gamma_o]\} + \\
V_{nonbonded}(R) = {}_{nonbonded} & \{ \varepsilon_{ij}[(A_{ij}/r_{ij})^{12} - 2(B_{ij}/r_{ij})^6]_{vdW} + \\
& q_i q_j/\varepsilon_r \varepsilon_o r_{ij}{}_{coulombic} \}
\end{aligned}
$$

The first bonded sum is over bonds between atom pairs where K_l is a force constant, l is the bond length and l_{eq} is the equilibrium bond length. The second bonded sum is over bond angles defined by three atoms, where K_θ is a force constant, θ is the angle and θ_{eq} is the equilibrium angle. The third and fourth bonded sums are defined by four atoms, K_ω and K_φ are force constants, ω is the improper angle, ω_o is the phase, n is the multiplicity, φ is the dihedral angle and γ_o is the phase. For the nonbonded terms, the sums are over atoms i and j. The Lennard–Jones potential describes van der Waals interactions with a so–called 6–12 potential. The 6–12 potential is used to describe the attractive (6) and repulsive (12) forces, where A_{ij} and B_{ij} are the Lennard–Jones diameters, ε_{ij} is the dispersion well depth and r is the nonbonded distance. Electrostatic interactions are described by coulombic

interations, where q_i and q_j are atomic charges, ε_r is the relative dielectric coefficient of the medium between the charges, ε_o is the permittivity of free space and r_{ij} is the nonbonded distance between two atoms.

A graphical view of the terms in equation 1.7 is shown in Figure 1.14. The figure illustrates how harmonic functions describe the bond and angle bonded terms, and how cosine functions describe improper dihedrals and torsions (dihedrals) (Steinbach, 1999). For a complete system like a polypeptide the function may have many hundreds of bonded and non–bonded terms each with associated parameters and numerical constants. The parameters, the constants and the function itself all require extensive optimization. Simulation and parameter modification iterations are performed to improve agreement between *ab initio* calculations and experimental (usually spectroscopic) data.

Restrained molecular dynamics. Restrained molecular dynamics is the most common technique for macromolecular structure generation and refinement. In restrained MD, initial velocities are assigned to all atoms in the system and then Newton's laws (in the form of a PEF) are invoked to propagate the system through time. The resulting molecular motions have very strict limitations imposed by restraint terms derived from experimental data (chemical shifts, NOE's, coupling constants, amide temperature coefficients, etc.). Most peptide structures described in this thesis were generated using the CHARMM PEF (Brooks et al., 1983) with simulated annealing (Nilges, 1988) or *quenched* MD, as implemented in X–PLOR

(Brunger, 1992). Annealing is a process that involves initial heating of a system followed by slow cooling. A simulated annealing run starts with an increase in the system temperature (10,000 K) that enables the system to surmount energetic barriers in the search for conformations with minimum energies. Following the initial heating stage, cooling (annealing) of the system enables the extraction of various low energy structures for subsequent minimization (local minima). The heating/annealing is repeated until no new energy minima are found and the resulting structures do not violate the experimentally determined restraints. Usually, an ensemble of at least 20 structures are calculated to fully sample the allowed conformational space.

Unrestrained molecular dynamics. Structure determination is an important step to help define biological function. However, peptide function is not determined by structure alone. Indeed most biological activities depend on molecular motions to activate or initiate a chemical process. Unrestrained MD is an common method to investigate the motion and time dependent properties of molecular systems. Properties such as: diffusion constants, viscosities, thermodynamic stabilities etc., can be investigated providing a sufficiently long simulation (trajectory) is calculated. Unrestrained MD usually begins where experimental structure determination leaves off, if not during the structure refinement process itself. The primary differences between unrestrained MD and restrained MD is the absence of experimental (spectroscopic) restraints and a greater emphasis on coloumbic interactions in the form of solvent models (implicit or explicit) in unrestrained MD calculations.

The unrestrained MD trajectories calculated in this thesis use the GROMACS PEF, as implemented in GROMACS (Berendsen, et al. 1995). This PEF is a derivative of the more common GROMOS force field (Berendsen and van Gunsteren, 1987). In GROMACS, the molecular dynamics algorithm used is known as the *Leap Frog* algorithm. This method derives its name from the way in which atomic positions and velocities are calculated in an alternating sequence, continuously leaping past each other until the simulation is complete. Solvent was simulated using SPC explicit water (Berendsen, et al. 1981) along with the SETTLE algorithm (Miyamoto and Kollman, 1992) to constrain water bond lengths and angles.

1.5 Objectives

This thesis follows a paper-based format. Chapter 1 provides some basic background information on antibacterial peptides as well as various peptide synthetic and spectroscopic techniques not fully covered in later chapters. Chapter 2 (published in Nature Structural Biology – Gibbs et al., 1998) describes the synthesis and NMR-based characterization of a series of progressively longer analogs of gramicidin S. Chapter 3 (published in the Journal of Medicinal Chemistry – Yan et al., 2000) describes the synthesis and spectral/functional characterization of an enantiomeric (all D-amino acid) form of leucocin A. Chapter 4 (manuscript submitted to the Journal of the American Chemical Society – Gibbs et al., 2001) describes the synthesis and structural characterization of a series of 14-residue

gramicidin S analogs with varying amino acid substitutions in the β–turn region. Chapter 5 (manuscript in preparation) explores the kinetics of folding of gramicidin S analogs as measured by IR and molecular dynamics simulations. Chapter 6 summarizes the results of this work and describes some possible future directions for further research.

References

Andreu, D., Merrifield, R.B., Steiner, H. and Boman, H.G. (1983) *Proc. Natl. Acad. Sci. USA* 80:6475–6479.

Andreu, D. and Rivas, L. (1998) *Biopolymers* 47:415–433.

Balasubramanian, D. (1967) *J. Am. Chem. Soc.* 89:5445–5449.

Bartz, (1948) *J. Biol. Chem.* 172:445.

Bax, A. and Davis, D.G. (1985) *J. Magn. Reson.* 65:355–360.

Berendsen, H.J.C., van der Spoel, D. and van Drunen, R. (1995) *Comp. Phys. Comm.* 91:43–56.

Berendsen, H.J.C. and van Gunsteren, W.F. (1987) *GROMOS87 manual*, Groningen, University of Groningen.

Berendsen, H.J.C., Postman, J.P.M., van Gunsteren, W.F. and Hermans, J. (1981) *Intermolecular forces*, Dordrecht, Reidel Publishing Co.

Boman, H.G. (1995) *Annu. Rev. Immunol.* 13:61–92.

Bothner–By, A.A., Stephans, R.L., Lee, J. Warren, C.D. and Jeanloz, R.W. (1984) *J. Am. Chem. Soc.* 106:811–813.

Bowen, J.P. and Allinger, N.L. (1991) In *Reviews in Computational Chemistry*, Vol. 2, Lipkowitz, K.B and Boyd, D.B. eds. VCH Publishers, New York, pp. 81–97.

Boyd, D.B. and Lipkowitz, K.B. (1982) *J. Chem. Ed.* 59:269–277.

Brasseur, R., Pillot, T., Lins, L., Vandekerckhove, J. and Rosseneu, M. (1997) *Trends Biochem. Sci.* 22:167–171.

Brooks, B.R., Bruccoleri, R.E., Olafson, B.D., States, D.J., Swaminathan, S. and Karplus, M. (1983) *J. Comp. Chem.* 4:187–217.

Brunger, A. (1992) *X–PLOR Version 3.1. A system of X–ray crystallography and NMR*, New Haven, Yale University Press.

Burkert, U. and Allinger, N.L. (1982) *ACS Monograph 177*, American Chemical Society, Washington, D.C., 339pp.

Carrier, D., Khalil, M.B. and Kealey, A. (1998) *Biochemistry* 37:7589–7597.

Carver, T.R. and Slichter, C.P. (1953) *Phys. Rev.* 93:212.

Chain, E., Florey, H.W., Gardner, A.D., Heatley, N.G., Jennings, M.A., Orr-Ewing, J. and Sanders, A.G. (1940) *Lancet* 1:226–228.

Chang, C.D. and Meienhofer, J. (1978) *Int. J. Pept. Protein Res.* 11:246–249.

Dathe, M. and Wieprecht, T. (1999) *Biochim. Biophys. Acta* 1462:71–87.

Demain, A.L and Fang, A. (2000) *Adv. Biochem. Eng. Biotechnol.* 69:1–39.

Demchuk, E., Bashford, D. and Case, D.A. (1997) *Fold. Des.* 2:35–46.

Derome, A.E. (1987) In *Modern NMR Techniques for Chemistry Research*, Pergamon Press, New York.

Diekmann, R. and von Döhren, H. (1997) In *6th Conference on the Genetics and Molecular Biology of Industrial Microorganisms, extended abstracts*; Am. Soc. Microbiol., Washington DC.

Dinur, U. and Hagler, A.T. (1991) In *Reviews in Computational Chemistry*, Vol. 2, Lipkowitz, K.B. and Boyd, D.B. Eds. VCH Publishers, New York, pp. 99–164.

Duggan, (1948) *Ann. N.Y. Acad. Sci.* 51:177.

Ehrlich, J., Gottlieb, D., Burkholder, P.R., Anderson, L.E. and Pridham, T.G. (1948) *J. Bact.* 56:467–477.

Ennahar, S., Sashihara, T., Sonomoto, K. and Ishizaki, A. (2000) *FEMS Microbiol. Rev.* 24:85–106.

Epand, R.F., Epand, R.M., Formaggio, F., Crisma, M., Wu, H., Lehrer, R.I. and Toniolo, C. (2001) *Eur. J. Biochem.* 268:703–712.

Epand, R.M. and Vogel, H.J. (1999) *Biochim. Biophys. Acta* 1462:11–28.

Epperson, J.D. and Ming, L. (2000) *Biochemistry* 39:4037–4045.

Erickson, B.W. and Merrifield, R.W. (1976) In *The Proteins*, vol. II (Neurath, H. & Hill, R.L. eds.), pp. 255–527, Academic Press, New York

Gardner, K.H. and Kay, L.E.(1998) *Annu. Rev. Biophys. Biomol. Struct.* 27:357–406.

Gause, G.F. and Brazhnikova, M.G. (1944) *Nature* 1944 154:703.

Gibbs, A.C., Hodges, R.S. and Wishart, D.S. (2001) Submitted.

Gibbs, A.C., Kondejewski, L.H., Gronwald, W., Nip, A.M., Sykes, B.D., Hodges, R.S. and Wishart, D.S. (1998) *Nat. Struct. Biol.* 5:284–288.

Gratia, A. (1925) *C. R. Seances Soc. Biol. Fil.* 93:1040–1041.

Grogan, J., McKnight, C.J., Toxler, R.F., Oppenheim, F.G. (2001) *FEBS Lett.* 491:76–80.

Hancock, R.E.W. (1997) *Lancet* 349:418–422.

Hancock, R.E.W. and Chapple, D.S. (1999) *Antimicrob. Agents Chemother.* 43:1317–1323.

Hastings, J.W., Sailer, M., Johnson, K., Roy, K.L., Vederas, J.C. and Stiles, M.E. (1991) *J. Bacteriol.* 173:7491–7500.

Huang, H.W. *Biochemistry* 2000, 39, 8347–8352.

Hull, S.E., Karlsson, R., Main, P., Woolfson, M.M. and Dodson, E.J. (1978) *Nature* 275:206–207.

Hwang, P.M. and Vogel, H.J. (1998) *Biochem. Cell Biol.* 76:235–246.

Jack, R.W., Tagg, J.R. and Ray, B. (1995) *Microbiol. Rev.* 59:171–200.

Jeener, J., Meier, B.H., Bachmann, P. and Ernst, R.R. (1979) *J. Chem. Phys.* 71:4546–4553.

Kang, J.H., Shin, S.Y., Jang, S.Y., Kim, K.L. and Hahm, K.S. (1999) *Biochem. Biophys. Res. Commun.* 264:281–286.

Karplus, M. (1959) *J. Phys. Chem.* 30:11–15.

Kato, T., Waki, M., Matsuura, S. and Izumiya, N. (1970) *J. Biochem.* 68:751–753.

Ketchem, R.R., Lee, K.C., Huo, S. and Cross, T.A. (1996) *J. Biomol. NMR* 8:1–14.

Klaenhammer, T.R. (1993) *FEMS Microbiol. Rev.* 12:39–86.

Kobayashi, S., Takeshima, K., Park, C.B., Kim, S.C. and Matsuzaki, K. (2000) *Biochemisty* 39:8648–8654.

Kondejewski, L.H., Farmer, S.W., Wishart, D.S., Kay, C.M., Hancock, R.E.W. and Hodges, R.S. (1996) *J. Biol. Chem.* 271:25261–25268.

Kondejewski, L.H., Jelokhani–Niaraki, M., Farmer, S.W., Lix, B., Kay, C.M., Sykes, B.D., Hancock, R.E.W. and Hodges, R.S. (1999) *J. Biol. Chem.* 274:13181–

13192.

Kragol, G., Lovas, S., Varadi, G., Condie, B.A., Hoffman, R. and Otvos, L. (2001) *Biochemistry* 40:3016–3026.

Luo, L. and Walsh, C.T. (2001) *Biochemistry* 40:5329–5337.

Maloy, W.L. and Kari, U.P. (1995) *Biopolymers* 37:105–122.

Marahiel, M.A., Stachelhaus, T. and Mootz, H.D. (1997) *Chem. Rev.* 97:2651–2673.

Marion, D. and Wuthrich K. (1983) *Biochem. Biophys. Res. Commun.* 113:967–74.

McGuire, J.M., Bunch, R.L., Anderson, R.C., Boaz, H.E., Flynn, E.H., Powell, H.M. and Smith, H.W. (1952) *Antibiot. Chemother.* 2:281–283.

Matsuzaki, K., Mitani, Y., Akada, K.Y., Murase, O., Yoneyama, S., Zasloff, M. and Miyajima, K. (1998) *Biochemistry* 37:15144–15153.

Matsuzaki, K., Yoneyama, S. and Miyajima, K. (1997) *Biophys. J.* 73:831–838.

Merrifield, B. (1963) *J. Am. Chem. Soc.* 85:2149–2154.

Merrifield, B. (1997) *Methods Enzymol.* 289:3–13.

Merrifield, R.B. (1965) *Science* 150:178–185.

Miyamoto, S. and Kollman, P.A. (1992) *J. Comp. Chem.* 13:952–962.

Nardi, F., Kemmink, J., Sattler, M. and Wade, R.C. (2000) *J. Biomol. NMR* 17:63–77.

Nardi, F., Worth, G.A. and Wade, R.C. (1997) *Fold. Des.* 2:S62–S68.

Nes, I.F. and Holo, H. (2000) *Biopolymers* 55:50–61.

Niidome, T., Mihara, H., Oka, M. Hayshi, T., Saiki, T., Yoshida, K. and Aoyagi, H. (1998) *J. Pept. Res.* 51:337–345.

Nilges, M., Clore, G.M. and Gronenborn, A.M. (1988) *FEBS Lett.* 229:317–324.

Ohnishi, M. and Urry, D.W. (1969) *Biochem. Biophys. Res. Commun.* 36:194–202.

Oren, Z. and Shai, Y. (1998) *Biopolymers* 47:451–463.

Park, C.B., Yi, K., Matsuzaki, K., Kim, M.S. and Kim, S.C. (2000) *Proc. Natl.*

Acad. Sci. USA 97:8245–8250.

Pasteur, L. and Joubert, J.F. (1877) *C. R. Soc. Biol. Paris* 85:101–115.

Rogers, L.A. (1928) *J. Bacteriol.* 16:321–325.

Rozek, A., Friedrich, C.L. and Hancock, R.E.W. (2000) *Biochemistry* 39:15765–15774.

Sansom, M.S.P. (1991) *Prog. Biophys. Mol. Biol.* 55:139–235.

Sansom, M.S.P. and Weinstein, H. (2000) *Trends in Pharm. Sci.* 21:445–451.

Schatz, A., Bugie, E. and Waksman, S.A. (1944) *Proc. Soc. Exp. Biol. Med.* 55:66–69.

Schmidt, G.M.J., Crowfoot–Hodgkin, D. and Oughton, B.M. (1957) *Biochem. J.* 65:744–756.

Schwyzer, R. (1958) *Chimia* 12:53–68.

Steinbach, P.J. (1999)
http://cmm.info.nih.gov/intro_simulation/course_for_html.html

Tamaki, M., Arai, I., Akabori, S. and Muramatsu, I. (1995) *Int. J. Peptide Res.* 45:299–302.

Tossi, A., Sandri, L. and Giangaspero, A. (2000) *Biopolymers* 55:4–30.

van Belkum, M.J. and Stiles, M.E. (2000) *Nat. Prod. Rep.* 17:323–335.

Vanderkooi, G., Leach, S.J., Nemethy, G., Scott, R.A. and Scheraga, H.A. (1966) *Biochemistry* 5:2991–2997.

von Döhren, H., Keller, U., Vater, J. and Zocher, R. (1997) *Chem. Rev.* 97:2675–2705.

Wade, D., Bowman, A., Wahlen, B., Drain, C.M., Andreu, D., Bowman, H.G. and Merrifield, R.B. (1990) *Proc. Natl. Acad. Sci. USA* 87:4761–4765.

Walsh, C. (1999) *Science* 284:442–443.

Wider, G. (2000) *Biotechniques* 29:1278–1290.

Wishart, D.S., Sykes, B.D. and Richards, F.M. (1992) *Biochemistry* 31:1647–1651.

Wu, M., Maier, E., Benz, R. and Hancock, R.E.W. (1999) *Biochemistry* 38:7235–

7242.

Wuthrich, K. (1986) *NMR of Proteins and Nucleic Acids*, New York, John Wiley & Sons.

Yan, L.Z., Gibbs, A.C., Stiles, M.E., Wishart, D.S. and Vederas, J.C. (2000) *J. Med. Chem.* 43:4579–4581.

Zhang, L., Benz, R. and Hancock, R.E.W. (1999) *Biochemistry* 38:8102–8111.

Table 1.1 Structural Diversity of Antibacterial Peptides

Charge	Primary Structure	Compound	Source	2°, 3° or 4° Structure	Mechanism of Action
Positive	Non–coded amino acids	Gramicidin S	Bacteria	Cyclic β–sheet	Membrane active
	Non–coded amino acids	Polymyxins	Bacteria	Cyclic	Membrane active, binds LPS
	Coded amino acids	Defensins	Mammal	Disulfide promoted β–sheet	Membrane active
	Coded amino acids	Indolicidin	Mammal	Type II polyproline helix	Membrane active
	Coded amino acids	Cecropins	Insect	α–helix	Membrane active
	Coded amino acids	Magainins	Amphibian	α–helix	Membrane active
	Post–translationally modified amino acids	Nisin	Bacteria	Mixed (methyl)lanthionine backbone bridges	Membrane active
	Coded amino acids	Leucocin A	Bacteria	Mixed α–helix	Membrane active
	Coded amino acids	Carnobacteriocin B2	Bacteria	Mixed α–helix	Membrane active
	Coded amino acids	Bactenecin	Mammal	γ–helix	Membrane active
	Coded amino acids	Lactoferricin B	Mammal	β–sheet	Membrane active
	Coded amino acids	Tachyplesin I	Crustacean	Disulfide promoted β–sheet	Membrane active
	Coded amino acids	Buforin II	Amphibian	α–helix	Membrane active
	Coded amino acids	Circulin B	Plant	Cystine–knot	Membrane active?
	Coded amino acids	Temporins	Amphibian	α–helix	Membrane active
	Coded amino acids	Lycotoxin	Spider	α–helix	
	Coded amino acids	Styelins	Tunicate	α–helix	
	Coded amino acids	Melittins	Insect	α–helix	Membrane active
	Post–trans. Mod. – Glycosylated	Pyrrhocoricin	Insect	Mixed α–helix	Inhibits ATPase activity of DnaK

Charge	Primary Structure	Compound	Source	2°, 3° or 4° Structure	Mechanism of Action
Positive; pH dependent		Histatin			Metalloprotease inhibitor
Slightly Positive	Metal chealator– peptolide	Bacitracin	Bacteria	Metal complex–distorted 5 or 6 coordination sphere	Blocks lipid carrier–undecaprenylpyrophosphate
	Glycopeptide	Vancomycin	Bacteria	Dimer	Inhibits peptidoglycan synthesis
	Glycopeptide	Teichoplanin	Bacteria	Dimer?	Inhibits peptidoglycan synthesis
	Glycopeptide	Eremomycin	Bacteria	Dimer?	Inhibits peptidoglycan synthesis
Neutral or Negative	Coded amino acids	Pardaxins	Fish	α–helix	
	Lipopeptide–peptaibol	Trichogin	Fungus	3_{10} helix	Membrane active
	Lipopeptide–Non–coded amino acids	Daptomycin	Bacteria	Decapeptide lactone	Membrane active
	Peptolide	Dalfopristin	Bacteria	Lactone	Targets 50S ribosomal sub–unit
	Non–coded amino acids	Quinupristin	Bacteria	Cyclic hexadepsipeptide	Targets 50S ribosomal sub–unit, synergistic with Dalfopristin
	Peptaibol	Alamethicin	Fungus	α–helix	Membrane active

Table 1.2 Klaenhammer[1] Bacteriocin Classification

Class	Sub–Class	Description
I		–Lantionine containing lantibiotics.
II		–Small <10 KDa, non–lantionine containing membrane active peptides.
	a	–Listeria monocytogenes–active peptides containing a YGNGV concensus sequence.
	b	–Two component (synergistic) peptide systems.
	c	–Thiol–activated peptides, requiring reduced cysteine residues for activity.
III		–Large >30 KDa, proteins.
IV		–Bacteriocins that contain lipid or carbohydrate adducts.

1. From Klaenhammer, T.R. (1993) *FEMS Microbiol. Rev.* 12:39–86.

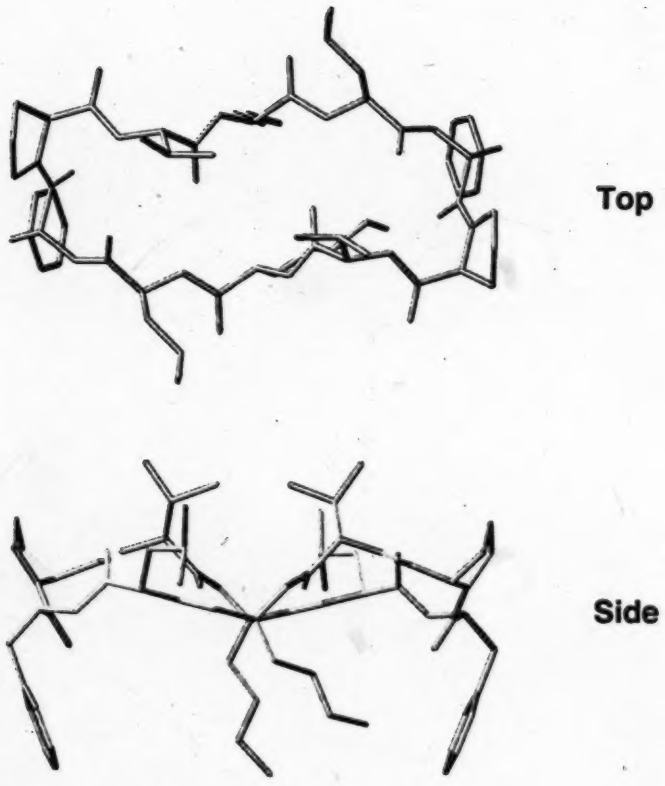

Figure 1.1. Top and side views of gramicidin S

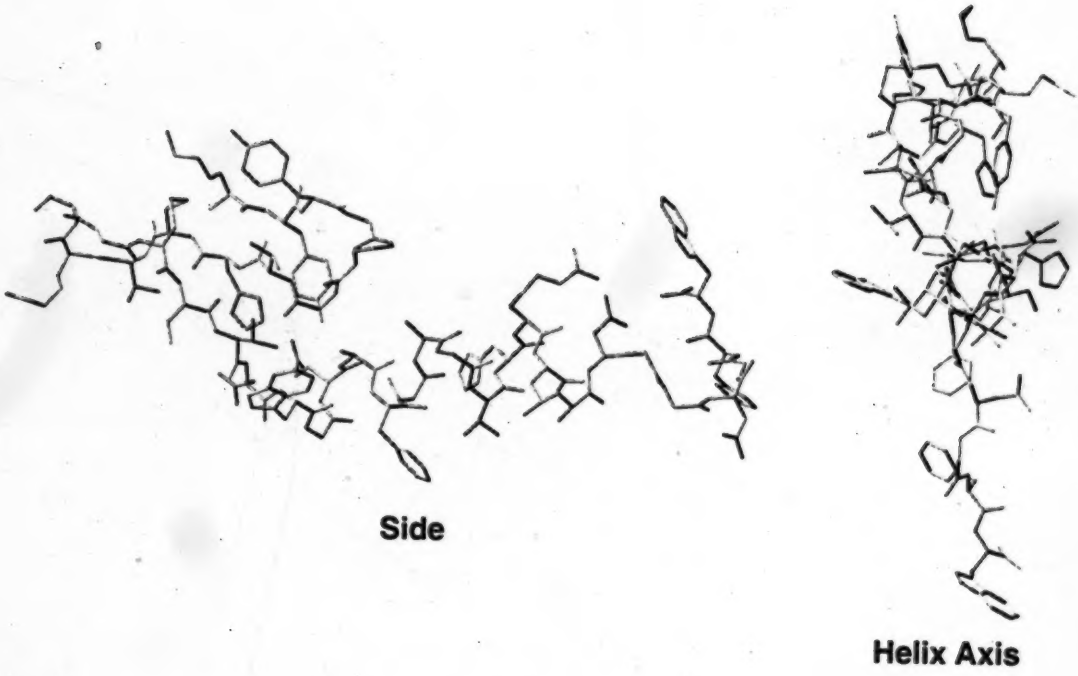

Figure 1.2. Side–view and a view down the helical axis, of leucocin A

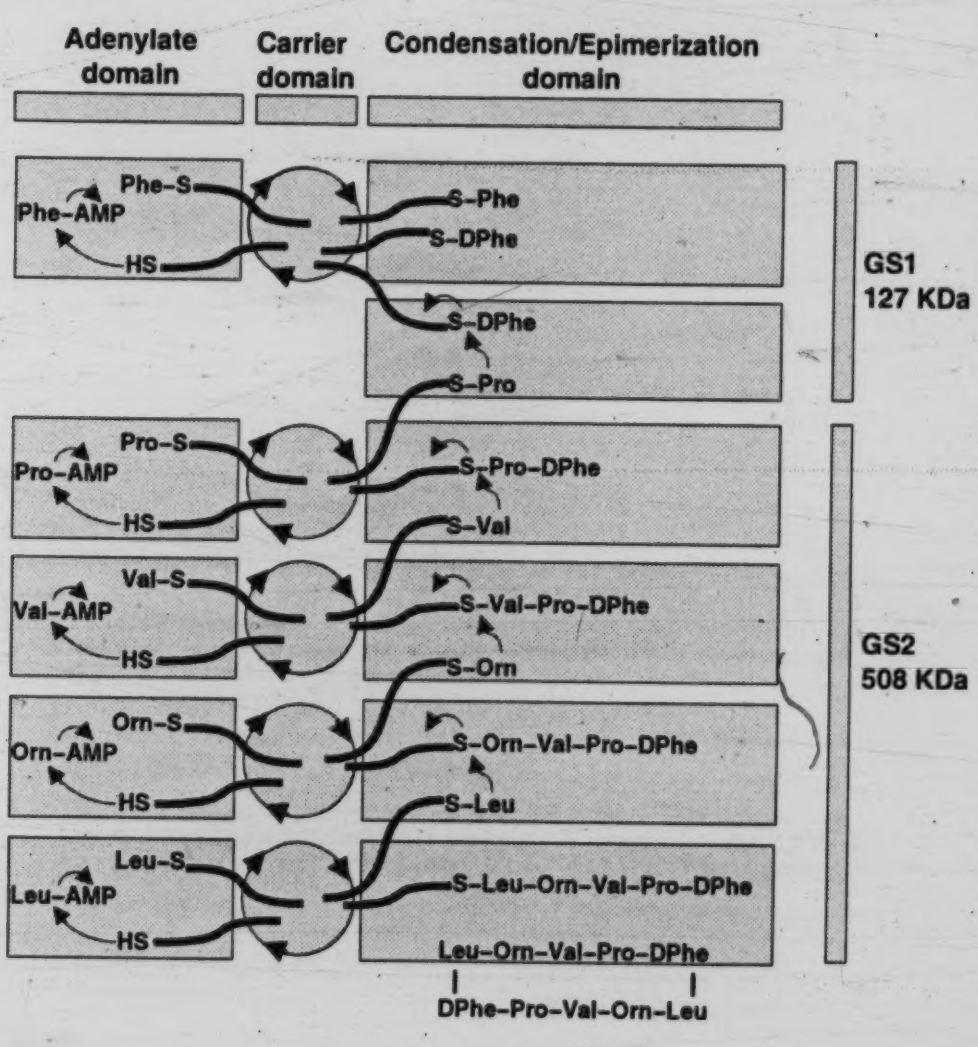

Figure 1.3. Gramicidin S biosynthesis. Biosynthesis is initiated on the adenylate domain of GS1 by way of phe–AMP formation. After epimerization of Phe, the 'activated' amino acids on GS2 can, in turn, condense to form a pentapeptide – where condensation steps are catalyzed by the thiotemplate intermediate (shown cycling through the adenylation and condesation/epimerization modules). The cycle is repeated, then both pentapeptides are linked head–to–tail.

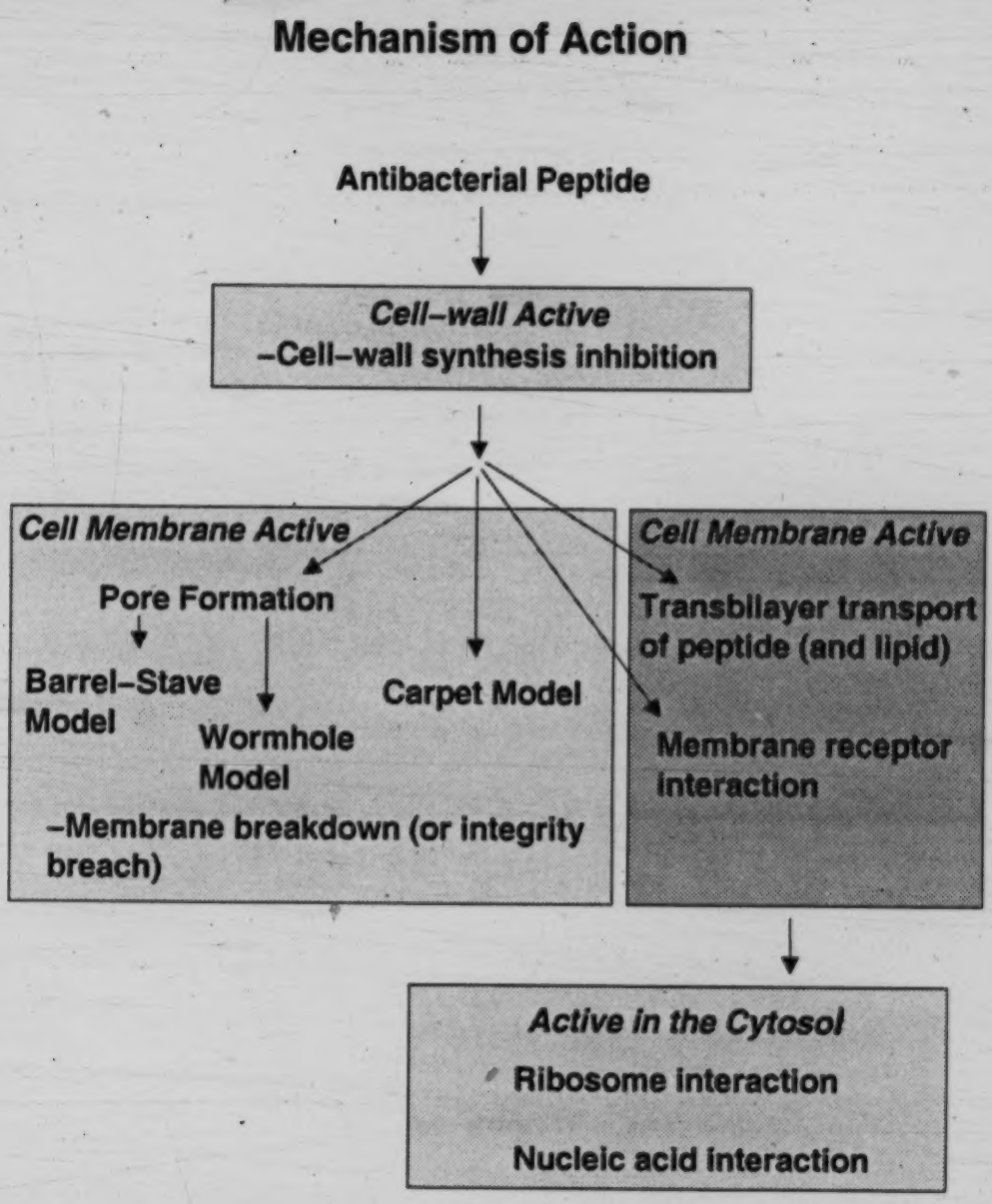

Figure 1.4. Antibacterial mechanism of action. As is shown, the peptides can follow two primary mechanistic routes; membrane disruption or peptide–membrane translocation.

Figure 1.5. A few representative structures of antibacterial peptides. The three helices on the right are made up of 10 residues.

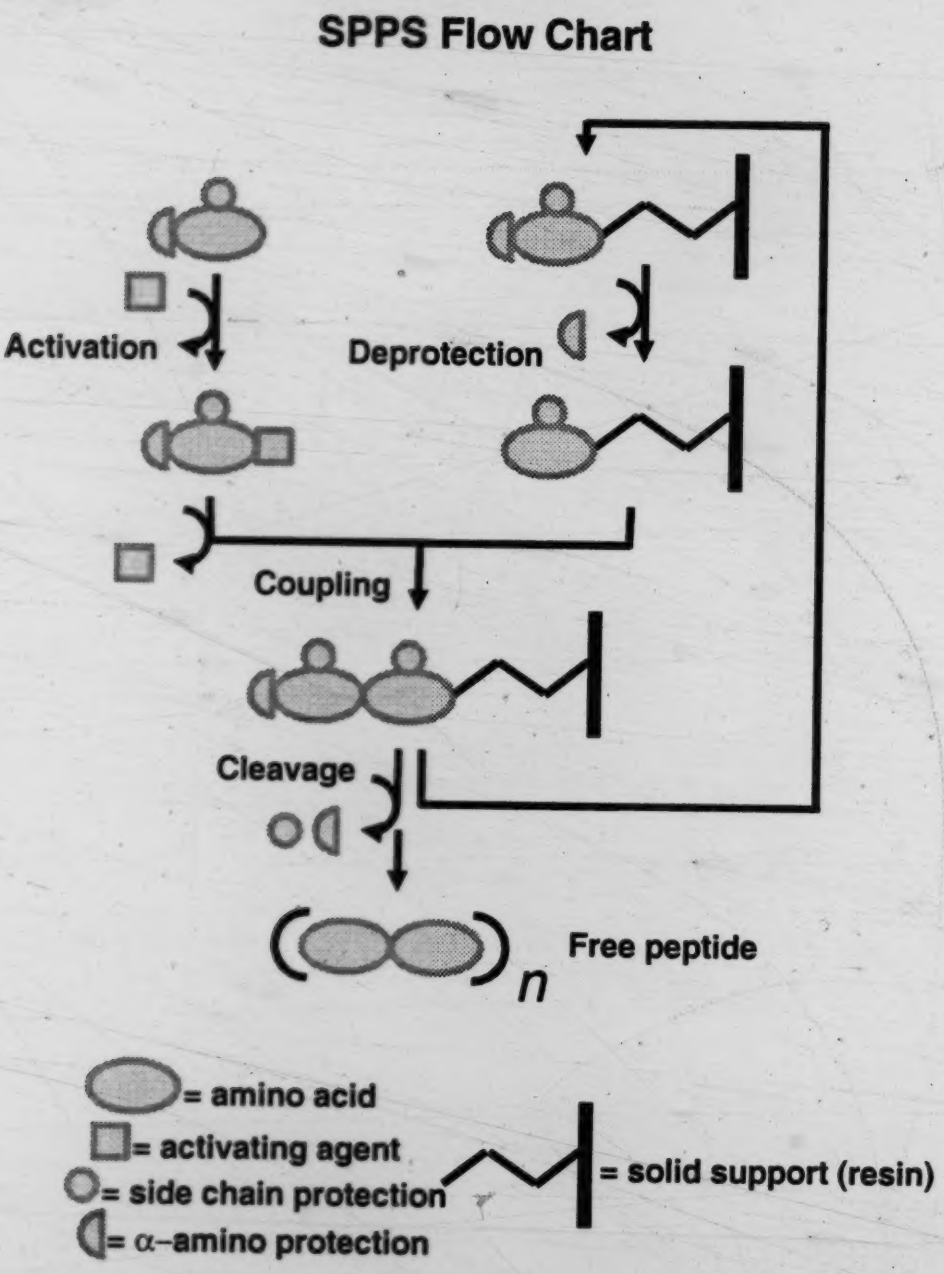

Figure 1.6. Solid phase peptide synthesis. Peptides are synthesized in step–wise fashion beginning with side–chain deprotection concomitant to amino acid activation. The amino acid and growing peptide chain are allowed to couple for a few hours until the cycle is repeated or the peptide is cleaved off the resin.

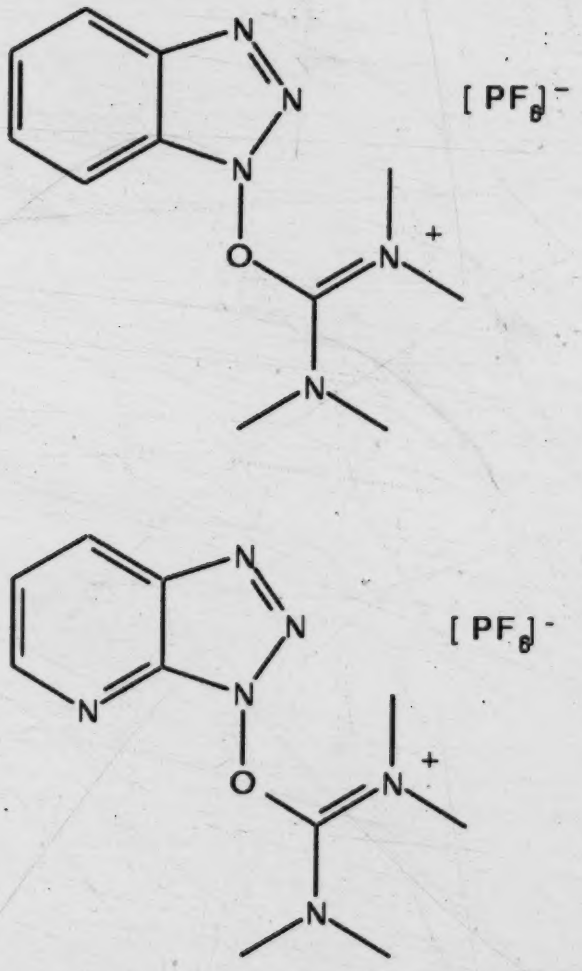

Figure 1.7. Structures of the activating agents HBTU (top) and HATU (bottom).

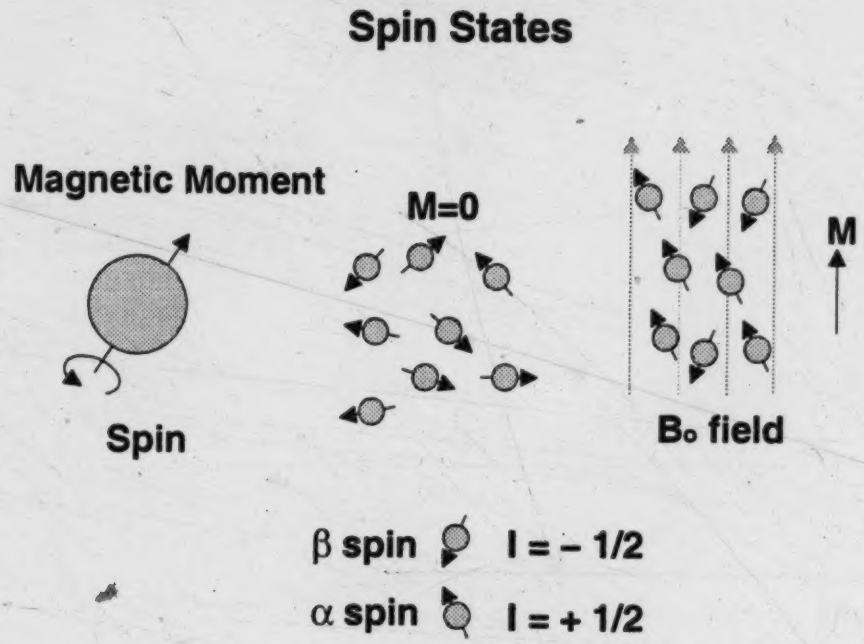

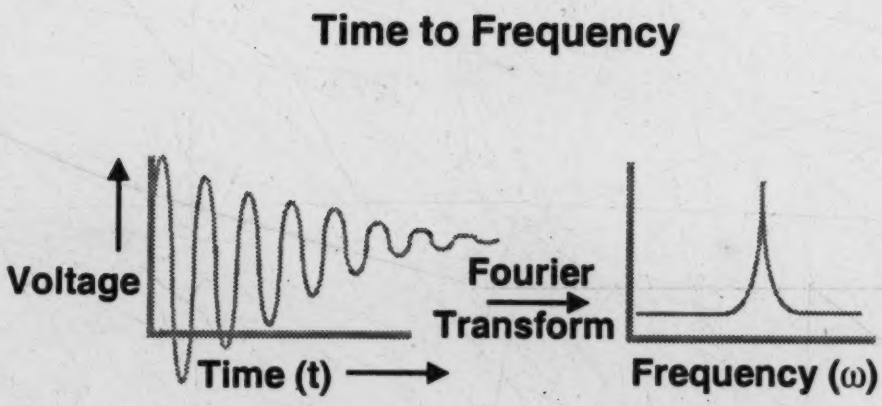

Figure 1.8 (top). Spin states of nuclei in and out of an applied magnetic field.
Figure 1.9 (bottom). Schematic representation of the conversion of an FID to the common frequency domain spectrum.

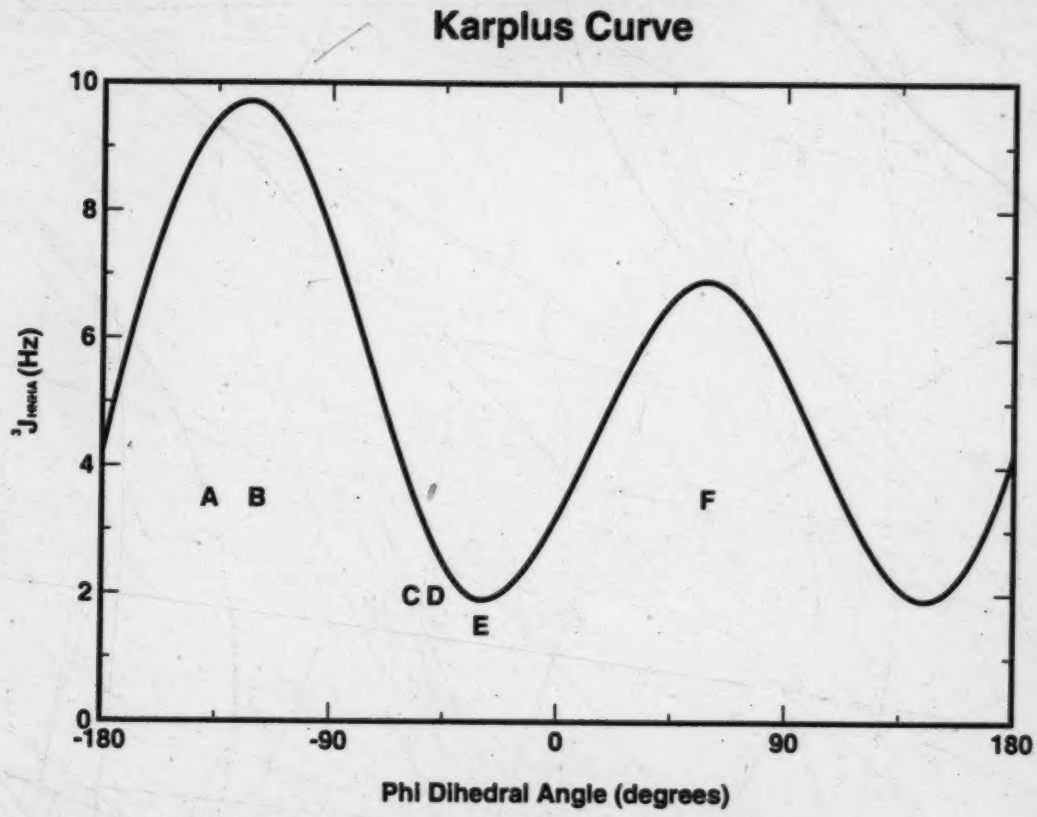

Figure 1.10. Karplus Curve for $^3J_{HNHA}$ as a funtion of the phi dihedral angle. Pointed out are the common secondary structure regions; A = antiparallel β–sheet, B = parallel β–sheet, C = right–handed α–helix, D = 3_{10} helix, E = π helix and F = left–handed helix.

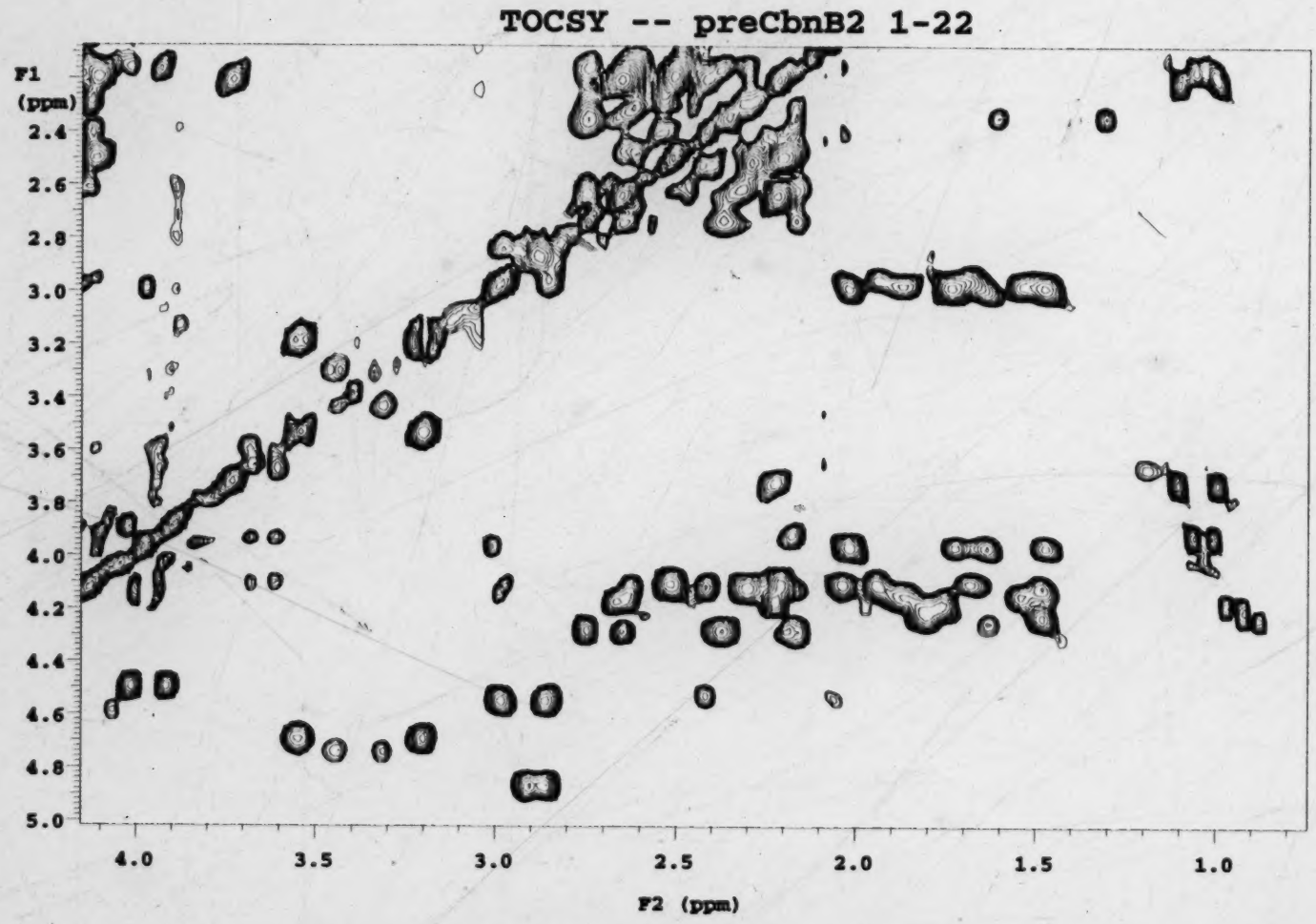

Figure 1.11. Example TOCSY spectrum.

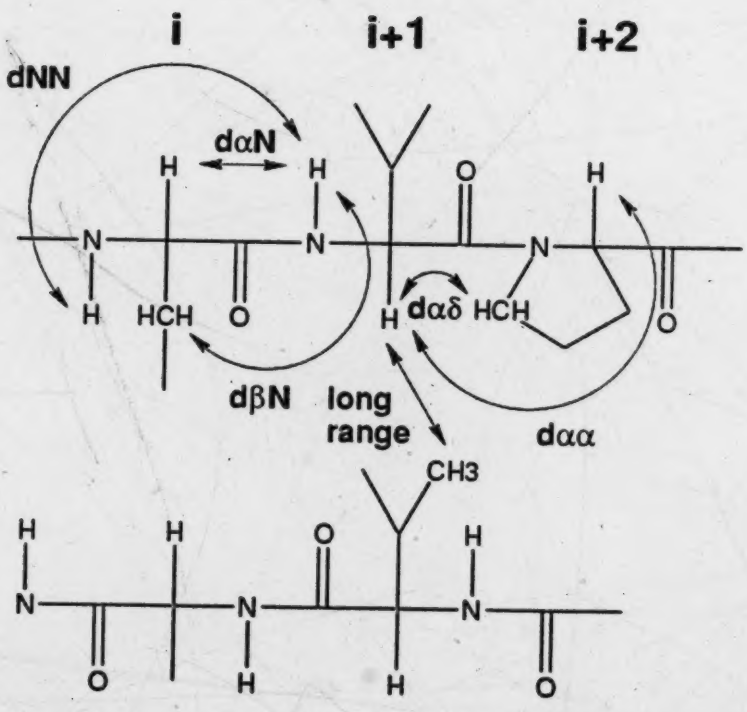

Figure 1.12. Representative NOE's. The top strand (containing residues; i, i+1 and i+2), illustrates the dNN, dαN, dβN, dαδ, dαα NOE's all used to help determine secondary structure. A long range NOE is also shown between a valine side chain and an α proton.

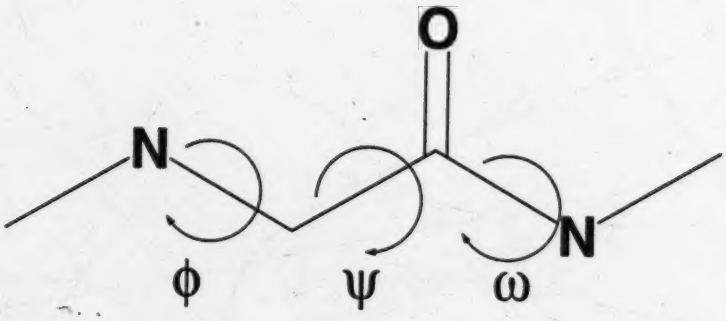

Figure 1.13. Protein backbone dihedral angles.

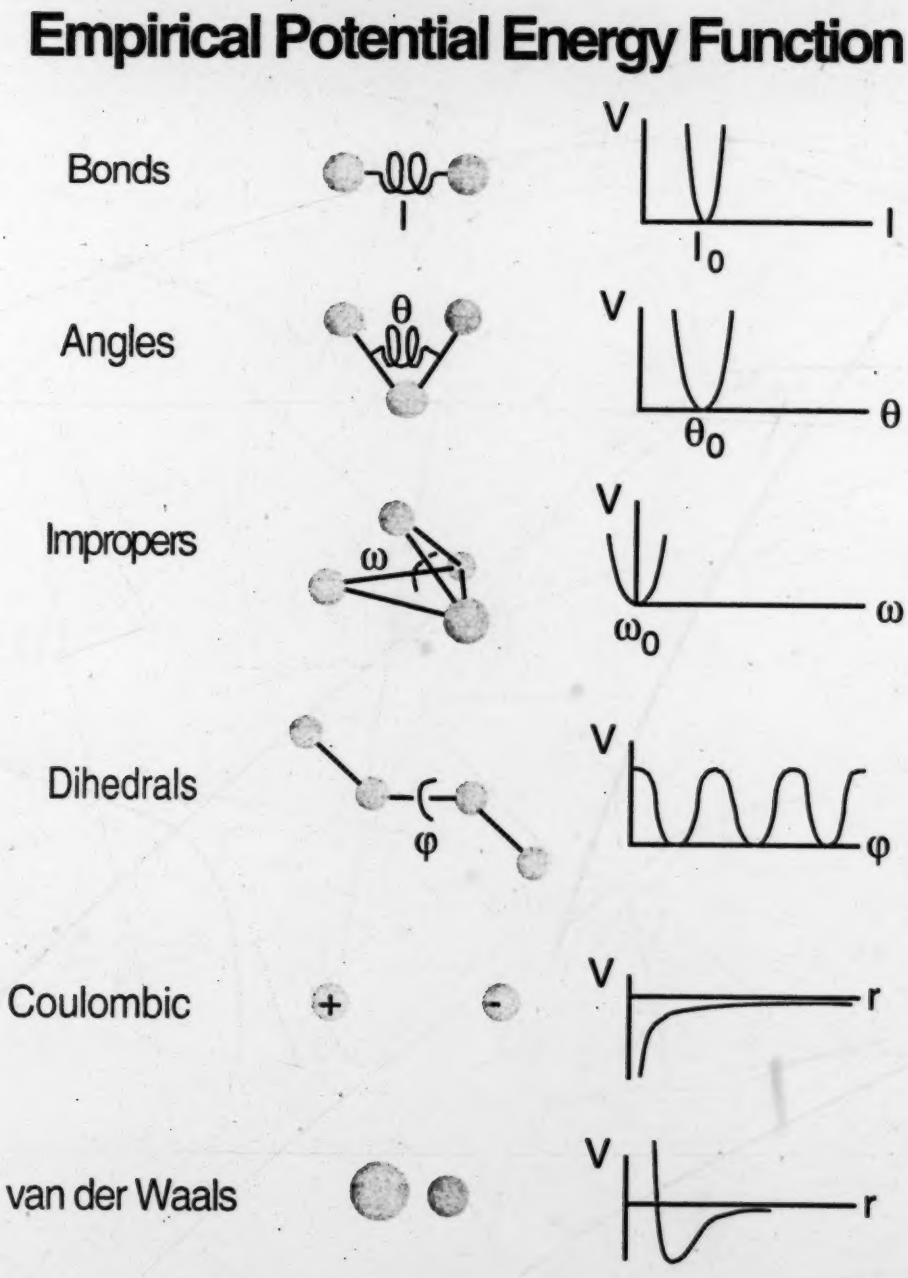

Figure 1.14. A graphical representation of a empirical potential energy function.

Chapter 2*

Unusual β–sheet Periodicity in Small Cyclic Peptides (GS Analogs)

2.1 Introduction

Peptide models of protein secondary structures can yield important insights into the forces that govern protein folding. Indeed, over the past 30 years peptide models of α–helices have taught us much about the energetics and dynamics of this important secondary structure (Padmanabhan et al., 1990; O'Neil and DeGrado, 1990; Zhou et al., 1992; Hill et al., 1990; Horovitz et al., 1992). Unlike α–helices, however, peptide models of β–sheets and β–strands have not been as easily attained (Smith and Reagan, 1997; Gellman, 1998). Recent studies based on peptide mimetics (Hartman et al., 1974; Kemp, 1990), naturally occurring small proteins (Kim and Berg, 1993; Minor and Kim, 1994; Smith et al., 1994), artificial proteins (Richardson and Richardson, 1987; Richardson et al., 1992) and protein fragments (Viguera et al., 1996; Prieto et al., 1997; Najbar et al., 1997) have shown that it is possible to create relatively small, soluble versions of β–strands. Most of these peptide models, however, suffer from a number of limitations, ranging from a propensity to aggregate, excessive size (>50 residues), low β–sheet content (<20%)

---

*This chapter was published as a paper by Gibbs, A.C., Kondejewski, L.H., Gronwald, W., Nip, A.M., Sykes, B.D., Hodges, R.S. and Wishart, D.S. (1998) in *Nat. Struct. Biol.* 5:284–288.

or low stability (molten globule).

In an attempt to overcome some of the limitations found in earlier β–sheet models, we have selected a small, water–soluble peptide known as gramicidin S (GS) to serve as a model β–sheet peptide (Guase and Brshnikova, 1944). GS is a cyclic decapeptide [cyclo(FPVOLFPVOL) – where underlined residues are D–amino acids] that has been shown by X–ray crystallography (Schmidt et al., 1957; Dodson et al., 1978) and NMR spectroscopy (Gibbons et al., 1972; Krauss and Chan, 1982) to form a very stable, amphipathic, antiparallel β–sheet bordered by two type II' β–turns (see Figure 1.1).

Over the past five years, we have devised a number of semi–automated solid phase synthetic schemes to quickly and efficiently prepare analogs of GS (Wishart et al., 1995; Kondejewski et al., 1996 a.; Wishart et al., 1996; Kondejewski et al., 1996 b.). In combination with NMR and CD spectroscopy, these synthetic procedures have allowed us to investigate the influence of amino acid substitutions on β–sheet and β–turn propensity and stability (Kondejewski, et al., 1996 c.). The present study uses this GS model in an attempt to better understand the influence of β–strand length on β–sheet stability. We have designed and synthesized a series of cyclic GS analogs that were both smaller and larger than the native GS peptide (10 residues). Six GS analogs containing 6, 8, 10, 12, 14 and 16 residues (see Table 2.1 for sequences) were prepared having hypothetically paired β–strand lengths of 1, 2,

3, 4, 5 and 6 residues respectively. Preliminary CD data unexpectedly revealed that the structure of these peptides alternated between ordered and disordered forms depending on the length of the hypothesized β–strands (Kondejewski et al., 1996 a.). These results prompted further investigation of the phenomenon using NMR spectroscopy to generate detailed three–dimensional structures of these peptides. As seen below, the data provide unequivocal evidence for a length–dependent periodicity in β–sheet content for this particular group of cyclic peptides.

2.2 Materials and Methods

Peptide Synthesis and Purification. Peptides were synthesized on an Applied Biosystems 430A automated peptide synthesizer using standard t–butyloxycarbonyl (Boc) chemistry (Wishart et al., 1996) on Boc–Pro–PAM resin. For peptides containing more than two lysines orthogonally protected Boc–ε–formyl–lysine, instead of the common Boc–ε–2ClZ–lysine, was used to prevent complications arising from the cyclization process (Kitagawa et al., 1994). The linear peptides were subsequently cleaved from the resin with anhydrous HF in the presence of 10% anisole and 2% 1, 2–ethanedithiol. The crude linear peptides were purified prior to cyclization using reversed–phase HPLC on a Synchropak RP–4 preparative C–8 column. Cyclizations were performed at peptide concentrations of 2 mg/mL in N,N–dimethyformamide (DMF) using 3 equivalents each of benzotriazoyl–N–oxytridimethylaminophosphonium hexafluorophosphate (BOP), 1–hydroxybenzotriazole (HOBT) and diisopropylethylamine (DIEA). The cyclization reaction was generally complete after 12 h. For those peptides containing ε–formyl

lysine, the formyl protecting group was removed (after cyclization) by heating the peptide to 37 °C in 10% methanolic HCl for 24 hours. The resulting cyclic peptides were purified by reverse phase HPLC using a linear AB gradient where solvent A is 0.1% aqueous TFA and solvent B is 0.1% TFA in acetonitrile. Peptide homogeneity was verified via electrospray mass spectrometry.

Circular Dicroism (CD) Spectroscopy. The CD spectra were recorded at 25 °C on a Jasco J–500C spectropolarimeter using 0.02 cm path length quartz cells. Each CD spectrum is an average of four scans, collected at 0.1 nm intervals between 190 and 250 nm. The peptides were prepared at a concentration of 1 mg/mL in 10 mM sodium acetate buffer, pH of 5.5. Ellipticity is reported as mean residue ellipticity [θ], with approximate errors of +/–500 millidegrees at 220 nm.

Nuclear Magnetic Resonance (NMR) Spectroscopy. ^{1}H–NMR experiments were performed on Varian Unity–300 and VXR–500 spectrometers. Each peptide was dissolved in 500 µL of 80% H_2O/20% D_2O or 100% D_2O (depending on the experiment) giving a sample concentration of approximately 1–2 mM. Uncorrected pH readings were between 3.4 – 7.1 and the sample temperature was maintained at 25 °C. All chemical shifts were referenced to internal DSS at 0.00 ppm. Individual spin system assignments were made using total correlation spectroscopy, (TOCSY) (Bax and Davis, 1985). Sequential assignments were made using data collected from ROESY (Bothner–By et al., 1984) and NOESY (Macura et al., 1981) experiments. Mixing times of 80 ms, 150 ms and 350 ms were used for the

TOCSY, ROESY and NOESY experiments respectively. $^3J_{HNHA}$ coupling constants were measured from 1-D ^{1}H-NMR spectra using an in-house curve fitting program. Amide temperature coefficients were measured from a series of 1-D ^{1}H-NMR experiments recorded over a range of temperatures (25 – 45 °C).

Molecular Modeling. Distance restraints were generated from analysis of ^{1}H NOESY and ROESY experiments. Differential NOE crosspeak intensities were assessed to identify upper-distance bounds of 2-3.5 Å (strong), 2-4 Å (medium) and 2-5.5 Å (weak) depending on corresponding crosspeak intensity. Van der Waals radii of 2 Å were set as the lower distance bound. Hydrogen-bond donors were identified by amide temperature coefficients and NH-O distance restraints were determined by chemical shift differences from random coil values of amide protons using a r/1 relationship (Wishart et al., 1991). Hydrogen bond measurements provided an additional 2, 4 and 6 intra-strand NH-O and N-O restraints for the 6, 10 and 14-mers respectively. Additional distance restraints were included to "cyclize" the peptides at the N and C termini using N-C, HN-O, HN-C and N-O distances of 1.22 ± 0.00 Å, 3.17 ± 0.10 Å, 1.99 ± 0.05 Å and 2.09 ± 0.05 Å respectively. Analysis of 1-D ^{1}H-NMR spectra yielded $^3J_{HNHA}$ coupling constants which were converted to an additional 4, 6, 8, 10 and 12 phi dihedral angle restraints for the 6, 8, 10, 12 and 14-mers respectively. Psi angle restraints were obtained via the Chemical Shift Index (Wishart et al., 1992), with CSI values of +1, 0 and -1 corresponding to psi values of 120° ± 30°, -40° ± 180° and -60° ± 40° respectively. Omega dihedral angles were restrained to 180°. An in-house distance geometry program employing a genetic algorithm (Cartwright, 1993) for conformational

sampling was used to generate the 20 "fittest" structures for each of the five peptides. These structures were further refined using the CVFF force field (Biosym), employing a conjugate gradient minimizer for 100 iterations. The mean RMSD's of the final families of analogs were calculated from ensemble–averaged coordinates derived from X–PLOR (Brunger, 1992). The final structures were evaluated by VADAR (Wishart et al., 1997) for coordinate feasibility, bond length and dihedral violations as well as packing defects. Structural statistics for all five peptides are summarized in Table 2.2.

2.3 Results and Discussion

Structure Determination. The NMR spectra for five of the six peptides used in this study were assigned using conventional ^{1}H homonuclear techniques (Wuthrich, 1986). Insufficient material for the sixth peptide (the 16–mer) was available to permit detailed NMR analysis. The small size and good solution behavior of the remaining five peptides made it possible to assign all observable main–chain and side–chain ^{1}H resonances (total = 276), see Tables 2.3 (6–mer shifts), 2.4 (8–mer shifts), 2.5 (10–mer shifts), 2.6 (12–mer shifts) and 2.7 (14–mer shifts). As has been noted by others (Sefler et al., 1996; Fahrner et al., 1996) cyclic peptides in aqueous conditions tend to exhibit relatively few inter–residue NOE's. In addition, resonance degeneracy arising from the molecular symmetry combined with the limited variation in amino acid composition of this particular group of peptides further reduced the number of useful NOE's. This made three–dimensional structural determination through conventional NOE–based techniques somewhat difficult. However, using a protocol similar to that described by Sefler (Sefler et al.,

1996), we were able to overcome these difficulties by supplementing the sparse NOE data with detailed $^3J_{HNHA}$ coupling constant measurements, ^1H chemical shift values, amide exchange rates and amide temperature coefficients (see Table 2.8), for additional dihedral and H–bond constraints. Furthermore, by concentrating on the backbone conformation only and making use of an efficient genetic algorithm (Cartwright, 1993) (see Materials and Methods for further details) for conformational sampling, we were able to reduce the computational complexity of multiple structure determinations to a manageable level.

β–sheet Content Varies Periodically with Peptide Length. Superimposed (20 structures) backbone traces, as determined by conventional ^1H NMR methods, are shown for GS analogs containing 6, 8 , 10, 12 and 14 residues (Fig. 2.1). Also shown are the far–UV CD spectra for the same five peptides plus a sixth CD spectrum for the 16–residue analog. It is clear from these figures that all six peptides alternate between structured (β–sheet) and unstructured forms depending on their sequence length. Peptides containing 6, 10 and 14 residues exhibit well–defined β–sheets and show the spectroscopic hallmarks of rigid, well–defined structures including low amide temperature coefficients (indicative of H–bonds), large ^1H chemical shift deviations from random coil values, and a mixture of both large (> 8 Hz) and small (< 5 Hz) $^3J_{HNHA}$ coupling constants. Furthermore, the backbone RMSD values (based on a superimposed set of 20 structures each) are very small (typically < 0.1 Å), indicating a high degree of structural order.

On the other hand, the peptides containing 8, 12 and 16 residues exhibit no well–defined structure and show strong spectroscopic evidence of high main–chain mobility and a great deal of structural disorder. In particular, all three peptides were characterized by random coil CD spectra, while NMR data for the 8–mer and 12–mer yielded random coil ^{1}H chemical shifts, random coil $^3J_{HNHA}$ coupling constants (~7 Hz), high amide temperature coefficients (> 6 ppb/°C) and no evidence of slow–exchanging protons. Furthermore, the backbone RMSD values for these two "disordered" peptides (based on a backbone superposition of 20 structures each) are typically greater than 0.70 Å.

In Figure 2.2 we illustrate how the periodicity in β–sheet content varies with sequence length in a more quantitative fashion. Note that because these peptides are cyclic, the far–UV CD spectra of the more structured analogs (Wishart et al., 1996; Kondejewski, et al., 1996 b.) tend to resemble those of helical peptides. This prevented quantitative determination of β–sheet content using conventional CD spectral deconvolution techniques (Perczel et al., 1991; Perczel et al., 1992). However, by using a weighted combination of measured ^{1}H chemical shifts and $^3J_{HNHA}$ coupling constants we were able to quantitatively estimate the percent β–sheet content (Table 2.1) in a manner similar to methods described by others for estimating percent helical content in peptides via NMR (Jimenez et al., 1993; Reily et al., 1992). Specifically, we compared the ^{1}H chemical shift values and $^3J_{HNHA}$ coupling constants to "idealized" values expected from antiparallel β–strands (Wishart et al., 1991; Smith et al., 1996), β–turns (Wurthrich, 1986) and random

coil peptides (Wishart et al., 1995). Closer inspection of Figure 2.2 clearly shows how the β–sheet content changes periodically with the sequence length, with peptides of 6, 10 and 14 residues containing >70% β–sheet and peptides of 8, 12 and 16 residues containing <15% β–sheet. It is important to note the discrepancy between the chemical shift estimate and the J–coupling estimate of β–sheet content (Table 2.1). This is likely due to the intrinsic differences between how $^3J_{HNHA}$ coupling constants and ^1H chemical shifts vary with the ϕ dihedral angle. This difference is more exaggerated when the angle of interest is further from the 'idealized' antiparallel β–strand value (–139°) as in the case with this six residue analog.

β–sheet Periodicity and Cyclization Geometry. Initial results suggested that this length–dependent periodicity may be related to the ratio of hydrophobic and hydrophilic amino acids in each peptide, or possibly to the intrinsic β–sheet propensities of the residues in each strand. However, through the course of structure generation and modeling, it became obvious that the periodicity in β–sheet content had as much to do with cyclization geometry as with individual amino acid propensities. As seen in Figure 2.3, a linear peptide containing a β–strand with an odd number of amino acids bordered by two type II' β–turns will allow the N and C termini of the opposite strand to be optimally oriented for ring closure. We call this a "staple configuration" and, as might be expected, when the peptide is cyclized

through the N and C termini, it would lead to a stable β–sheet. This is exactly what is seen for the GS analogs containing 6, 10 and 14 residues. On the other hand, a β–strand with an even number of amino acids, bordered by the same type II' β–turns, will lead to the N and C termini of the opposite strand being oriented on opposite sides. We call this a "twisted staple configuration". This twisted staple configuration arises from the 180° rotation of the peptide bond each time an amino acid is inserted into an extended chain. Therefore, cyclization of a peptide in a "twisted staple" configuration would produce a twisted mobius–like ring. This sort of distortion prevents hydrogen bonds from forming and, as a result, leads to a disordered and somewhat more flexible structure typified by the GS analogs containing 8, 12 and 16 residues.

Confirmation of a Forty Year Old Prediction. Nearly forty years ago, a series of papers (Schwyzer, 1958; Schwyzer and Ludescher, 1969; Schwyzer et al., 1964) predicted that the number of amino acids within a cyclic peptide would influence the type of secondary structure adopted by that molecule. In particular, Robert Schwyzer (Schwyzer, 1958), on the basis of stereochemical considerations, hypothesized that cyclic peptides would form β–sheet structures if they contained 2(2n+1) residues (where n=1, 2, 3...). This is precisely what is seen for the GS analogs containing 6, 10 and 14 residues. We believe the results of this study represent the first detailed three–dimensional confirmation of Schwyzer's hypothesis.

However, it is important to note that the structural periodicity rules that Schwyzer predicted are not as universal nor as geometrically driven as originally suggested. Indeed, they are only valid under relatively limited conditions and, due to the results of this and other recent studies (Kumar et al., 1975; Patel and Tonelli, 1976; Blackledge et al., 1993; Bugess and Lim, 1996), we wish to propose some important refinements.

First, and most importantly, β–sheet formation in cyclic peptides can only take place in those molecules containing two — and only two — equally separated type I' or type II' β–turns. This is because only type I' and type II' β–turns have the required synperiplanar geometry necessary to correctly align the i and i+3 residues at both ends of a putative β–sheet (Muller, 1996). Therefore, if a cyclic peptide (that satisfies the 2(2n+1) rule) does not have the appropriate sequence or the appropriate placement of these very specific β–turns, it will not form a β–sheet.

Second, because of the positional requirement of type I' and type II' turns, β–sheet formation in cyclic peptides is dictated by the appropriate placement of D–amino acids and other "turn–forming" residues in the peptide sequence. Specifically, type II' β–turns have an absolute requirement for a D–amino acid (or glycine) in the i+1 position and a very strong preference for proline in the i+2 position (Kessler, 1982; Kessler et al., 1994). Likewise, type I' β–turns have an absolute requirement for D–amino acids in both the i+1 and i+2 positions

(Richardson and Richardson, 1987; Rose et al., 1985). Therefore, the sequence associated with the β–turn residues is exceedingly important for β–sheet formation. This observation also implies that cyclic peptides containing all L–amino acids, no matter what length or sequence, will never form stable β–sheets. Chapter 4 of this thesis describes in detail the stereochemical requirements for type II' β–turn formation and how type II' β–turns stabilize antiparallel β–sheet structure in GS analogs.

Third, the sequence and amino acid composition of both the turns and the β–strands is important for β–sheet periodicity. Substitutions of glycines or additional lysines into the β–strand region of GS (a peptide that satisfies the 2(2n+1) rule) have been shown, by CD and NMR spectroscopy, to disrupt the β–sheet and reduce the overall β–sheet content (Wishart et al., 1996; Kondejewski et al., 1996 b.). Similarly, the substitution of D–His in place of D–Tyr in the β–turn positions has also been shown to reduce the β–sheet content (Wishart et al., 1996). One would also expect that the substitution of a proline in the middle of either strand would substantially disrupt the β–sheet structure as well. This suggests that intrinsic secondary structural propensities of individual amino acids can play a significant role in the formation of β–sheets in cyclic peptides.

Fourth, cyclic peptides that satisfy the 2(2n+1) but which contain one or

more D–amino acids in one, or both, β–strands will not form β–sheets (Tamaki et al., 1988). This arises because the insertion of such an amino acid will disrupt the hydrogen bonding patterns typically associated with anti–parallel β–sheets. Therefore, the number and placement of D–amino acids, particularly in the β–strands, is also an important consideration in predicting β–sheet formation and β–sheet periodicity in cyclic peptides.

Fifth, as our data clearly show, cyclic peptides that do not contain 2(2n+1) residues will not form stable β–sheets. In other words, cyclic peptides containing two evenly spaced type I' or type II' turns will always form disordered or "random coil" structures if they contain 4n residues (where n =1, 2, 3...). Similarly, cyclic peptides containing an odd number of residues are also incapable of forming stable β–sheets (Morita et al., 1996; Morelli et al., 1991). These two amendments to Schwyzer's hypothesis are important since the original prediction failed to suggest what type of structure would be formed in cyclic peptides that did not contain 2(2n+1) residues.

While it is clear that geometrical and stereochemical considerations strongly dictate the formation of β–sheets in cyclic peptides, it is also clear that the amino acid sequence (i.e., the position of the D–amino acids and other turn–forming residues) and composition (i.e., the type and number of "turn–forming" and "β–sheet forming" residues) can play an equally important role in explaining β–sheet

periodicity. In other words, Schwyzer's hypothesis is correct insofar as it identifies a fundamental stereochemical issue that regulates cyclic peptide structure. However, a host of other conditions, ranging from appropriate stereochemistry, peptide geometry, electrostatic interactions, hydrogen bonding potential, residue position and intrinsic secondary structure propensities must be satisfied before this phenomenon of β–sheet periodicity can be observed. It is not surprising, then, that it has taken more than 40 years to observe this phenomenon experimentally.

2.4 Conclusion

To summarize, we have found strong evidence of a periodic sequence–length dependence on β–sheet content in a particular class of cyclic peptides. While such an observation was predicted 40 years ago, this is the first time that such a periodic variation in secondary structural content has been unequivocally confirmed on the basis of actual (NMR–derived) three–dimensional structures. Detailed model building, supplemented with additional experimental evidence from homologous peptides, also suggests that this periodicity is dependent not only on the geometric and stereochemical requirements of cyclization, but also on the sequence, composition and secondary structural propensities of the individual amino acids. Given the importance that cyclic peptides and artificial β–sheets now have in the creation of synthetic templates or template assembled synthetic proteins (TASPs) (Mutter et al., 1996; Tuchschere et al., 1994; Peng, 1999), artificial proteins (Richardson and Richardson, 1987; Richardson et al., 1992) and novel antibiotics (Kondejewski et al., 1996 b; Jelokhani–Niaraki et al., 2000; McInnes et al., 2000),

this unusual β–sheet periodicity may have important implications in the design of constrained β–sheet mimics as well as in our fundamental understanding of β–sheet formation.

References

Bax, A. and Davis, D.G. (1985) *J. Mag. Res.* 65:355–360.

Blackledge, M.J., Bruschweiler, R., Griesinger, C., Schmidt, J.M., Ping, X. and Ernst, R.R. (1993) *Biochemistry* 32:10960–10974.

Bothner–By, A.A., Stephens, R.L. and Lee, J. (1984) *J. Am. Chem. Soc.* 106:811–813.

Brunger, A.T. (1992) In *X–PLOR manual, version 3.1* Yale University Press, New Haven and London.

Bugess, K. and Lim, D. (1996) *J. Med. Chem.* 39:4520–4526.

Cartwright, H.M. (1993) In *Applications of Artificial Intelligence in Chemistry*, Oxford Chemistry Primers 11, Oxford Press.

Dodson, D.J., Woolfson, M.M., Main, P., Karlsson, R. and Hull, S.E. (1978) *Nature* 275:206–207.

Fahrner, R.L., Dieckmann, T., Harwig, S.S.L., Lehrer, R.I., Eisenberg, D. and Feigon, J. (1996) *Chemistry & Biology* 3:543–550.

Gibbons, W.A., Alms, H., Bockman, R.S. and Wyssbrod, H.R. (1972) *Biochemistry* 11:1721–1725.

Gellman, S.H. (1998) *Curr. Opin. Chem. Biol.* 2:717–725.

Guase, G.F. and Brazhnikova, M.G. (1944) *Nature* 154:703.

Hartman, R., Schawaner, R.C. and Hermans, J. B (1974) *J. Mol. Biol.* 90:415–429.

Hill, C.P., Anderson, D.H., Wesson, L., Degrado, W.F. and Eisenberg, D. (1990) *Science* 249:543–546.

Horovitz, A., Matthews, J.M. and Fersht, A.R. *J. Mol. Biol.* 227, 195–212 (1992).

Jelokhani–Niaraki, M., Kondejewski, L.H., Farmer, S.W., Hancock, R.E., Kay, C.M. and Hodges, R.S. (2000) *Biochem. J.* 349:747–755.

Jimenez, M.A., Bruix, M., Gonzalez, C., Blanco, F.J., Nieto, J.L., Herranz, J. and Rico, M. (1993) *Eur. J. Biochem.* 211:569–581.

Kemp, D.S. (1990) *Tibtech.* 8:249–255.

Kessler, H. (1982) *Angew. Chem. Int. Ed. Engl.* 21:512–523.

Kessler, H., Matter, H., Gemmecker, G., Diehl, H.-J., Isernia, C. and Mronga, S. (1994) *Int. J. Peptide Protein Res.* 43:47–61.

Kim, C.A. and Berg, J. M. (1993) *Nature* 362:267–270.

Kitagawa, T., Arita, J. and Nagahata, A. (1994) *Chem. Pharm. Bull.* 42:1655–1657.

Kondejewski, L.H., Farmer, S.W., Wishart, D.S., Hancock, R.E.W. and Hodges, R.S. (1996) a. *Int. J. Pept. Protein Res.* 47:460–466.

Kondejewski, L.H., Farmer, S.W., Wishart, D.S., Kay, C.M., Hancock, R.E.W. and Hodges, R.S. (1996) b. *J. Biol. Chem.* 271:25261–25268.

Kondejewski, L.H., Wishart, D.S., Sykes, B.D., Kay, C.M. and Hodges, R.S. (1996) c. In *Peptides: Chemistry, Structure and Biology* (P.T.P. Kaumoya and R.S. Hodges, Eds.) Mayflower Scientific Ltd. pp 68–70.

Krauss, E.M. and Chan, S.I. (1982) *J. Am. Chem. Soc.* 104:6953–6961.

Kumar, N.G., Izumiya, N., Miyoshi, M., Sugano, H. and Urry, D.W. (1975) *Biochemistry* 14:2179–2189.

Macura, S., Huang, Y., Suter, D. and Ernst, R.R. (1981) *J. Mag. Res.* 43:259–281.

McInnes, C., Kondejewski, L.H., Hodges, R.S. and Sykes, B.D. (2000) *J. Biol. Chem.* 275:14287–14294.

Minor, D.L. and Kim, P.S. (1994) *Nature* 367:660–663.

Morelli, M.A.C., Pastore, A., Pedone, C., Temussi, P.A., Zanotti, G. and Tancredi, T. (1991) *Int. J. Peptide Protein Res.* 37:81–89.

Morita, H., Kayashita, T., Takeya, K. and Itokawa, H. (1996) *Chem. Pharm. Bull.* 44:2177–2180.

Muller, G. (1996) *Angew. Chem. Int. Ed. Engl.* 35:2767–2769.

Mutter, M., Pascal, P., Garrouste, P., Lehmann, C., Mathieu, M., Peggion, C., Peluso, S., Razana, A. and Tuchschere, G. (1996) *Angew. Chem. Int. Ed. Engl.* 35:1482–1485.

Najbar, L.V., Craik, D.J., Wade, J.D., Salvatore, D. and McLeish, M.J. (1997) *Biochemistry* 36:11525–11533.

O'Neil, K.T. and DeGrado, W.F. (1990) *Science* 250:646–652.

Padmanabhan, S., Marquesee, S., Ridgeway,T., Laue, T.M. and Baldwin, R.L. (1990) *Nature* 344:268–270.

Peng, Z.H. (1999) *Biopolymers* 49:565–574.

Reily, M.D., Thanabal, V. and Omecinsky, D.O. (1992) *J. Am. Chem. Soc.* 114:6251–6252.

Richardson, J.S. and Richardson, D.C. (1987) In *Protein Engineering* (Oxender, D.L. and Fox C.F., eds.) Alan R. Liss pp. 149–163.

Richardson, J.S., Richardson, D.C., Tweedy, N.B., Gernert, K.M., Quinn, T.P., Hecht, M.H., Erickson, B.W., Yan, Y., McClain, R.D., Donlan, M.E. and Surles, M.C. (1992) *Biophys. J.* 63:1186–1209.

Rose, G.D., Gierasch, L.M. and Smith J.A. (1985) *Adv. Protein Chem.* 37:1–109.

Schmidt, G.M.J., Hodgkin, D.C. and Oughton, B.M. (1957) *Biochem. J.* 65:744–756.

Smith, C.K. and Reagan, L. (1997) *Acc. Chem. Res.* 30:153–161.

Smith, K., Withka, J.M. and Reagan, L. (1994) *Biochemistry* 33:5510–5517.

Patel, D.J. and Tonelli, A.E. (1976) *Biopolymers* 15:1623–1635.

Perczel, A., Park, K. and Fasman, G.D. (1992) *Proteins: Struct. Funct. Genet.* 13:57–69.

Perczel, A., Hollosi, M., Tusnady, G. and Fasman, G.D. (1991) *Protein Eng.* 4:669–679.

Prieto, J., Mattias, W., Jimenez, M.A., Rico, M. and Serrano, L. (1997) *J. Mol. Biol.* 268:760–778.

Schwyzer, R. (1958) *Chimia* 12:53–68.

Schwyzer, R. and Ludescher, U. (1969) *Helv. Chim. Acta* 52:2033–2040.

Schwyzer, R. Garrion, J.P. Gorup, B., Nolting, H. and Tun–Kyi, A. (1964) *Helv. Chim. Acta* 47:441–464.

Sefler, A.M., Lauri, G. and Bartlett, P.A. (1996) *Int. J. Peptide Protein Res.* 48:129–138.

Smith, L.J., Bolin, K.A., Schwalbe, H., MacArthur, M.W., Thornton, J.M. and Dobson, C.M. (1996) *J. Mol. Biol.* 255:494–506.

Tamaki, M., Takimoto, M. and Muramatsu, I. (1988) *Bull. Chem. Soc. Jpn.* 61:3925–3929.

Tuchschere, G., Steiner, V., Altmann, K.H. and Mutter, M. (1994) *Meth. Mol. Biol.* 36:261–285.

Viguera, A.R., Jimenez, M.A., Rico, M. and Serrano, L. (1996) *J. Mol. Biol.* 255:507–521.

Wishart, D.S., Sykes, B.D. and Richards, F.M. (1991) *J. Mol. Biol.* 222:311–333.

Wishart, D.S., Bigham, C.G., Holm, A., Hodges, R.S. and Sykes, B.D. (1995) *J. Biomol. NMR* 5:67–81.

Wishart, D.S., Sykes, B.D. and Richards, F.M. (1992) *Biochemistry* 31:1647–1651.

Wishart, D.S., Willard, L. and Sykes, B.D. (1997) VADAR, version 1.2 University of Alberta, Edmonton.

Wishart, D.S., Kondejewski, L.H., Semchuk, P.D., Kay, C.M., Hodges, R.S. and Sykes, B.D. (1995) In *Techniques in Protein Chemistry*, (Crabb, J.W., ed.) 4:451–457, Academic Press, San Diego.

Wishart, D.S., Kondejewski, L.H., Semchuck, P.D., Sykes, B.D. and Hodges, R.S. (1996) *Lett. Pep. Sci.* 3:53–60.

Wuthrich, K. (1986) In *NMR of Proteins and Nucleic Acids*, John Wiley & Sons, New York.

Zhou, N.E., Kay, CM. and Hodges, R.S. (1992) *J. Biol. Chem.* 267:2664–2670.

Table 2.1 Sequences and β-sheet Content of GS Analogs

Analog	Sequence[1]	% β-sheet ($\Delta\delta$)[2]	% β-sheet ($^3J_{HNHA}$)[3]	% β-sheet (Average)[4]
6-mer	KYPKYP	30	70	50
8-mer	KVYPLKYP	0	10	5
10-mer	VKLYPVKLYP	93	94	94
12-mer	VKLKYPKVKLYP	3	7	5
14-mer	VKLKVYPLKVKLYP	105	92	99
16-mer	VKLKVKYPKLKVKLYP	-	-	(15)[5]

1. The first and last residues are linked through the backbone (homodetic) to make the peptides cyclic. All tyrosine residues are of D-stereochemistry.
2. $\Delta\delta$ is the change in chemical shift. % β-sheet ($\Delta\delta$) = (average analog Lys $\Delta\delta$ – Lys random coil $\Delta\delta$)/(typical β-sheet $\Delta\delta$) x 100, where Lys random coil $\Delta\delta$ = 4.32 ppm, typical β-sheet $\Delta\delta$ = 0.4 ppm (Wishart et al., 1991).
3. % β-sheet ($^3J_{HNHA}$) = (average Lys $^3J_{HNHA}$ - average Tyr $^3J_{HNHA}$)/(ideal β-sheet $^3J_{HNHA}$ - ideal type II' β-turn $^3J_{HNHA}$) x 100, where ideal β-sheet $^3J_{HNHA}$ = 8.9 Hz, ideal type II' β-turn $^3J_{HNHA}$ = 4.1 Hz (Smith et al., 1996).
4. Average = average of % β-sheet ($\Delta\delta$) and % β-sheet ($^3J_{HNHA}$).
5. β-sheet content determined by CD spectroscopy.

Table 2.2 Structural Statistics for GS Analogs (20 structures each)

Analog	6–mer	8–mer	10–mer	12–mer	14–mer
Distance Restraints					
sequential	4	6	4	9	7
hydrogen bonds	4	0	8	0	12
Dihedral Restraints					
ϕ	6	8	10	12	14
ψ	6	8	10	12	14
ω	6	8	10	12	14
Total[1]	30	34	46	49	65
Mean Energies[2] (Kcal mol^{-1})					
$E_{coulomb}$	12.61±0.18	16.41±0.34	15.56±6.10	26.10±1.39	25.17±5.53
E_{vdW}	9.89±0.07	12.76±1.41	13.39±1.81	8.40±1.33	15.43±2.34
$E_{improper}$	0.02±0.00	0.24±0.10	0.05±0.01	0.18±0.01	0.12±0.05
E_{phi}	0.85±0.16	3.22±1.40	0.78±0.65	2.82±1.05	1.72±0.64
E_{theta}	9.23±0.22	12.54±0.80	12.35±0.41	21.65±3.90	18.37±1.20
E_{bond}	2.98±0.07	3.83±0.15	4.54±0.20	5.40±0.16	5.90±0.25
E_{total}	35.59±0.18	49.10±3.59	46.66±5.77	64.54±2.81	66.73±5.45
Ramachandran Analysis					
residues in favored regions	6	8	10	12	13
residues in allowed regions	0	0	0	0	1
residues in generous regions	0	0	0	0	0
residues in disallowed regions	0	0	0	0	0
Mean atomic RMSD[2] (Å)					
backbone	0.01±0.02	0.70±0.33	0.10±0.04	1.77±0.18	0.56±0.14

1. A cyclization restraint was added to force covalent ring closure, between the first and last residues.
2. Energies (Kcal mol^{-1}) and RMSD's (Å) reported with standard deviations.

Table 2.3 ^{1}H–NMR Assignments (ppm) for 6–mer

Amino Acid	HN	Hα	Hβ	Other	$^{3}J_{HNHA}$ (Hz)
Tyr1	8.48	4.67	2.91, 2.89	2,6H 7.17	5.12
				3,5H 6.87	
Pro2		4.30	1.92	γH 1.61, 1.61	
				δH 3.70, 2.88	
Lys3	7.46	4.44	1.75	γH 1.16, 1,25	8.42
				δH 1.25, 1.25	
				εH 2.97, 2.97	
				εNH3 7.51	
Tyr4	8.48	4.67	2.91, 2.89	2,6H 7.17	5.12
				3,5H 6.87	
Pro5		4.30	1.92	γH 1.61, 1.61	
				δH 3.70, 2.88	
Lys6	7.46	4.44	1.75	γH 1.16, 1,25	8.42
				δH 1.25, 1.25	
				εH 2.97, 2.97	
				εNH3 7.51	

Table 2.4 ^{1}H–NMR Assignments (ppm) for 8–mer

Amino Acid	HN	Hα	Hβ	Other	$^{3}J_{HNHA}$ (Hz)
Tyr1	8.45	4.97	2.99, 2.86	2,6H 7.12 3,5H 6.81	8.55
Pro2		4.37	2.15	γH 1.86, 1.86 δH 3.72, 3.31	
Lys3	8.06	4.47	1.69	γH 1.40, 1.40 δH 1.50, 1.50 εH 3.00, 3.00 εNH3 7.55	8.75
Val4	7.83	4.12	1.88	γH 0.89, 0.69	6.62
Tyr5	8.52	4.95	2.97, 2.91	2,6H 7.14 3,5H 6.84	7.80
Pro6		4.31	2.09	γH 1.86, 1.86 δH 3.72, 3.13	
Leu7	8.04	4.48	1.42	γH 0.87 δH 0.91, 0.85	8.20
Lys8	8.03	4.17	1.61	γH 1.21, 1.21 δH 1.50, 1.50 εH 2.95, 2.95 εNH3 7.55	8.55

Table 2.5 ^{1}H–NMR Assignments (ppm) for 10–mer

Amino Acid	HN	Hα	Hβ	Other	$^3J_{HNHA}$ (Hz)
Val1	7.53	4.16	2.13	γH 0.89	8.97
Lys2	8.41	4.69	1.86	γH 1.32, 1.32	8.79
				δH 1.63, 1.63	
				εH 3.15, 3.15	
Leu3	8.58	4.57	1.48	γH 1.40, 1.40	7.21
				δH 0.88, 0.88	
Tyr4	8.78	4.63	3.02,	2,6H 7.15	4.39
			2.92	3,5H 6.83	
Pro5		4.40	1.92	γH 1.65, 1.65	
				δH 3.68, 2.66	
Val6	7.53	4.16	2.13	γH 0.89	8.97
Lys7	8.41	4.69	1.86	γH 1.32, 1.32	8.79
				δH 1.63, 1.63	
				εH 3.15, 3.15	
Leu8	8.58	4.57	1.48	γH 1.40	9.15
				δH 0.88	
Tyr9	8.78	4.63	3.02,	2,6H 7.15	4.39
			2.92	3,5H 6.83	
Pro10		4.40	1.92	γH 1.65, 1.65	
				δH 3.68, 2.66	

Table 2.6 ^{1}H–NMR Assignments (ppm) for 12–mer

Amino Acid	HN	Hα	Hβ	Other	$^{3}J_{HNHA}$ (Hz)
Val1	7.96	3.98	2.08	gH 0.92	7.21
Lys2	8.38	4.39	1.83	γH 1.41, 1.41	7.45
				δH 1.71, 1.71	
				εH 3.00, 3.00	
Leu3	7.96	4.38	1.55	γH 1.31, 1.31	7.21
				δH 0.93, 0.93	
Lys4	7.98	4.24	1.53	γH 1.09, 1.09	6.98
				δH 1.29, 1.29	
				εH 2.91, 2.91	
Tyr5	8.47	4.96	3.04,	2,6H 7.04	6.59
			2.87	3,5H 6.78	
Pro6		4.34	2.19	γH 1.87	
				δH 3.68, 3.34	
Lys7	8.27	4.30	1.78	γH 1.44, 1.44	7.08
				δH 1.69, 1.69	
				εH 3.00, 3.00	
Val8	7.84	4.20	2.08	γH 0.88	8.18
Lys9	8.32	4.39	1.77	γH 1.38, 1.38	7.45
				δH 1.68, 1.68	
				εH 2.98, 2.98	
Leu10	7.96	4.38	1.55	γH 1.31, 1.31	7.21
				δH 0.93, 0.93	
Tyr11	8.47	4.96	3.04,	2,6H 7.16	7.21
			2.87	3,5H 6.80	
Pro12		4.41	2.06	γH 1.87, 1.87	
				δH 3.72, 3.21	

Table 2.7 ^{1}H–NMR Assignments (ppm) for 14–mer

Amino Acid	HN	Hα	Hβ	Other	$^{3}J_{HNHA}$ (Hz)
Val1	7.58	4.19	2.12	γ0.88,0.88	8.54
Lys2	8.33	4.74	1.65	γ1.25, δ1.40 ε 2.93	9.15
Leu3	8.69	4.57	1.53	γ1.53, δ0.83, 0.83	9.16
Lys4	8.41	4.77	1.86	γ1.37, 1.37 δ1.67, ε3.00	7.81
Val5	8.50	4.18	1.94	γ0.87, 0.80	8.91
dTyr6	8.89	4.62	3.06,2.91	2,6H 6.91 3,5H 6.63	4.06
Pro7		4.41	1.89	γ1.62, 1.62 δ3.59, 2.55	
Leu8	7.69	4.44	1.69	γ1.50, δ0.89, 0.81	8.06
Lys9	8.29	4.79	1.64	γ1.28, δ1.41 ε2.95	9.77
Val10	8.65	4.31	1.98	γ0.85, 0.85	9.40
Lys11	8.47	4.66	1.87	γ1.37, δ1.67 ε3.01	7.93
Leu12	8.58	4.54	1.46	γ1.36, δ0.85, 0.85	9.16
dTyr13	8.74	4.66	3.02,2.92	2,6H 6.88 3,5H 6.60	4.64
Pro14		4.40	1.92	γ1.67, 1.67 δ3.66, 2.71	

Table 2.8 Amide Temperature Coefficients (ppb/K)

6mer	Tyr1	Lys3	Tyr4	Lys6						
	7.60	4.10	7.60	4.10						
8mer	Tyr5	Tyr1	Lys3	Leu7	Lys8	Val4				
	6.45	7.10	6.00	5.90	5.10	6.55				
10mer	Tyr4	Leu3	Lys2	Val1	Tyr9	Leu8	Lys7	Val6		
	9.30	0.96	6.80	4.60	9.30	0.96	6.80	4.60		
12mer	Tyr5	Tyr11	Lys2	Lys9	Lys7	Lys4	Val1	Leu3	Leu10	Val3
	7.50	8.50	7.20	5.96	6.55	4.50	5.70	6.30	6.30	7.40
14mer	Tyr6	Tyr13	Leu3	Val10	Leu12	Val5	Lys11	Lys4	Lys2	Lys9	Leu8	Val1
	7.80	3.70	5.30	4.40	2.60	2.50	5.20	5.00	5.80	5.30	1.60	3.40

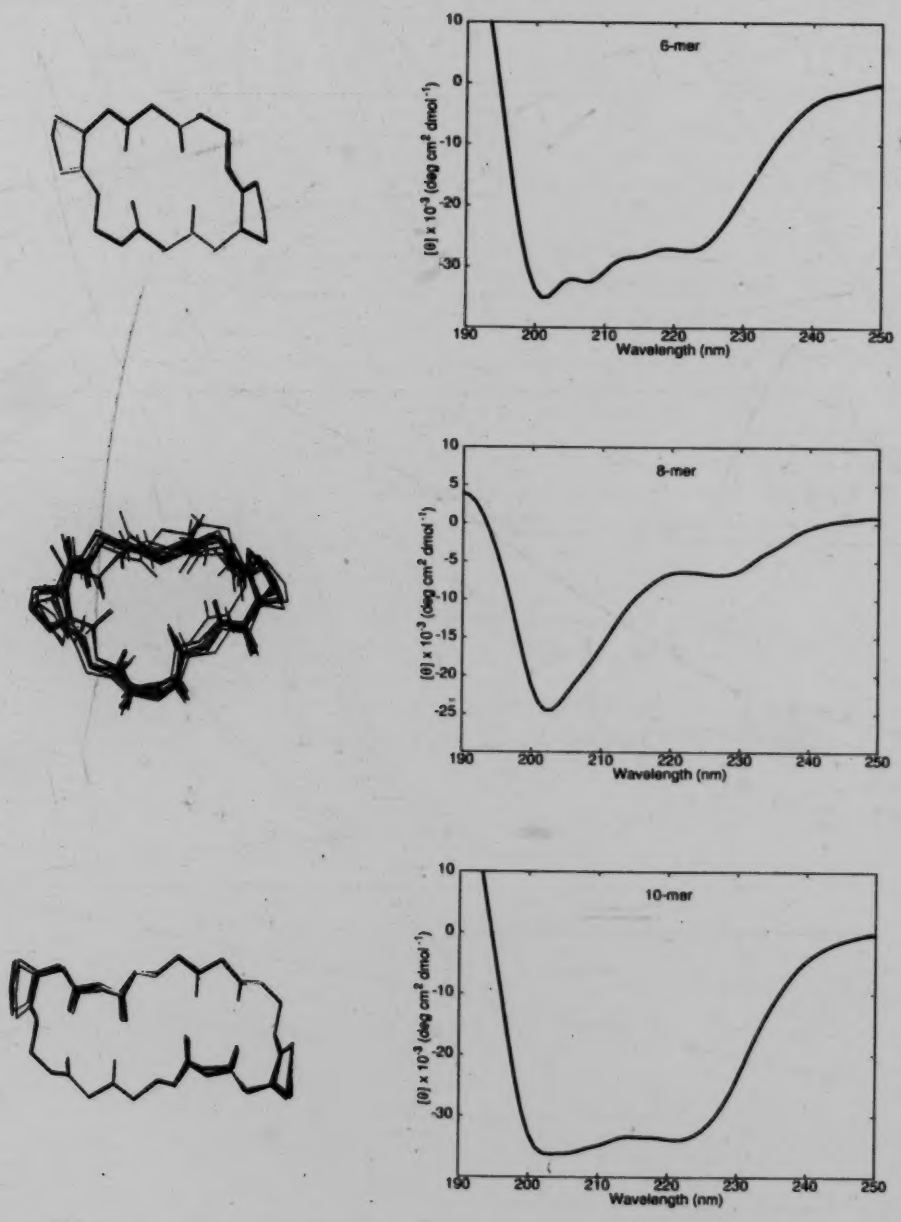

Figure 2.1. Solution structures of the five GS analogs with corresponding CD spectra. Each ensemble includes twenty structures superimposed to fit over the backbone average structure. The CD spectrum of the 16 residue analog is shown separately.

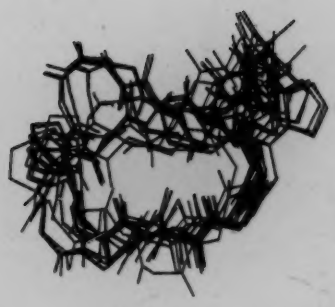

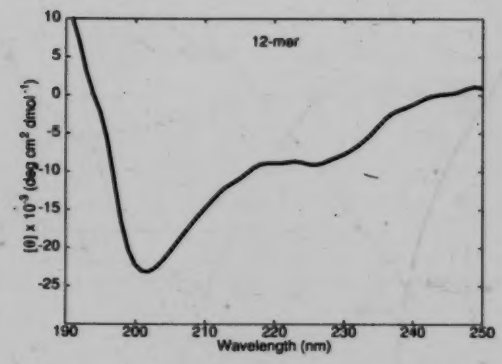

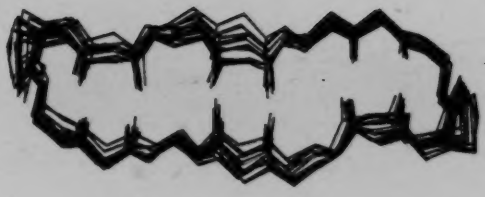

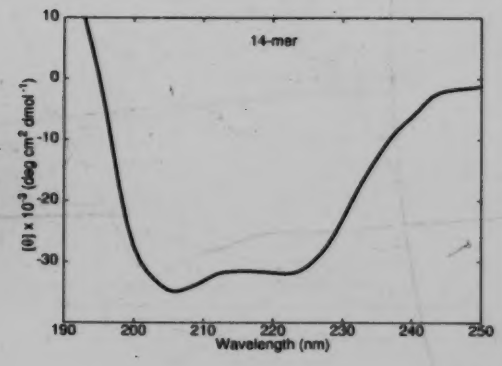

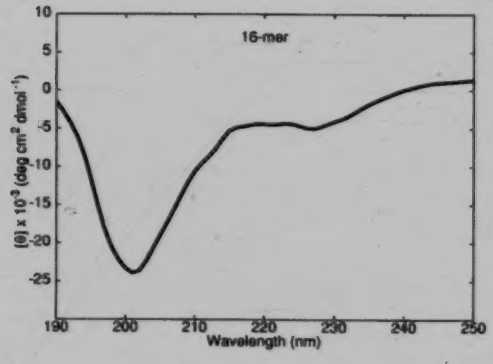

Figure 2.1 continued.

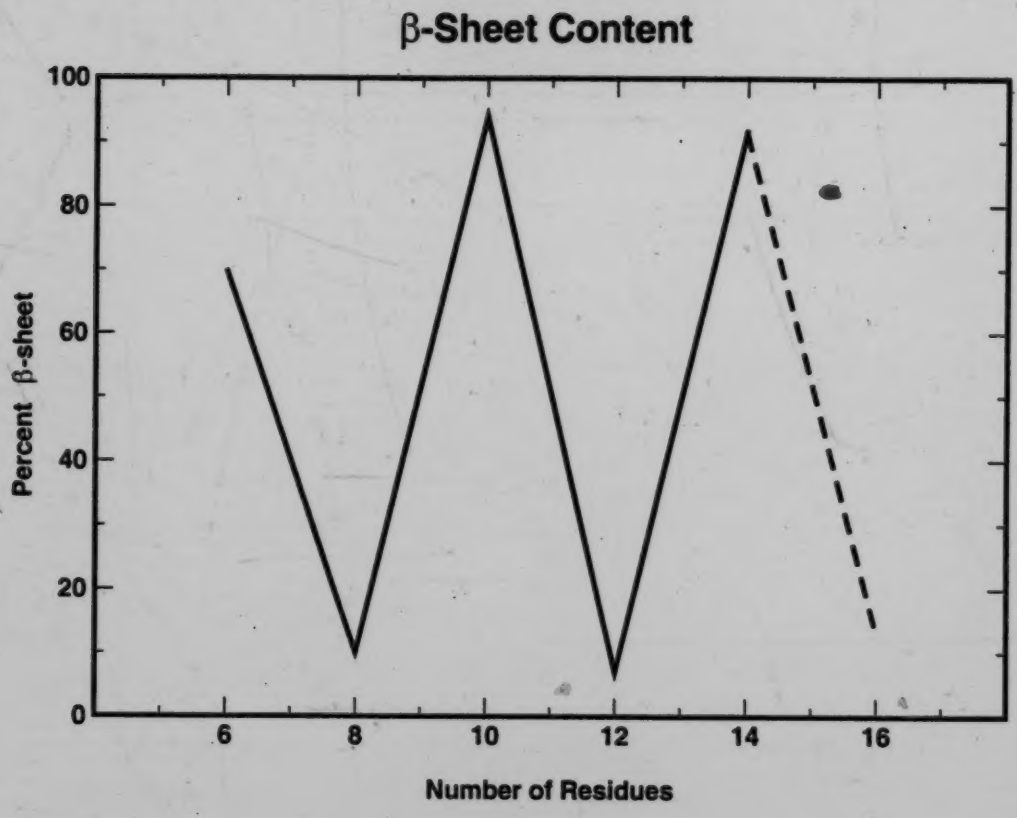

Figure 2.2. β–sheet content of all six GS analogs. The β–sheet content of the 6, 8, 10, 12 and 14 residue analogs (solid line) was determined by NMR ($^3J_{HNHA}$) data (See Table 2.1). β–sheet content (dashed line) for the 16 residue analog was determined by CD analysis.

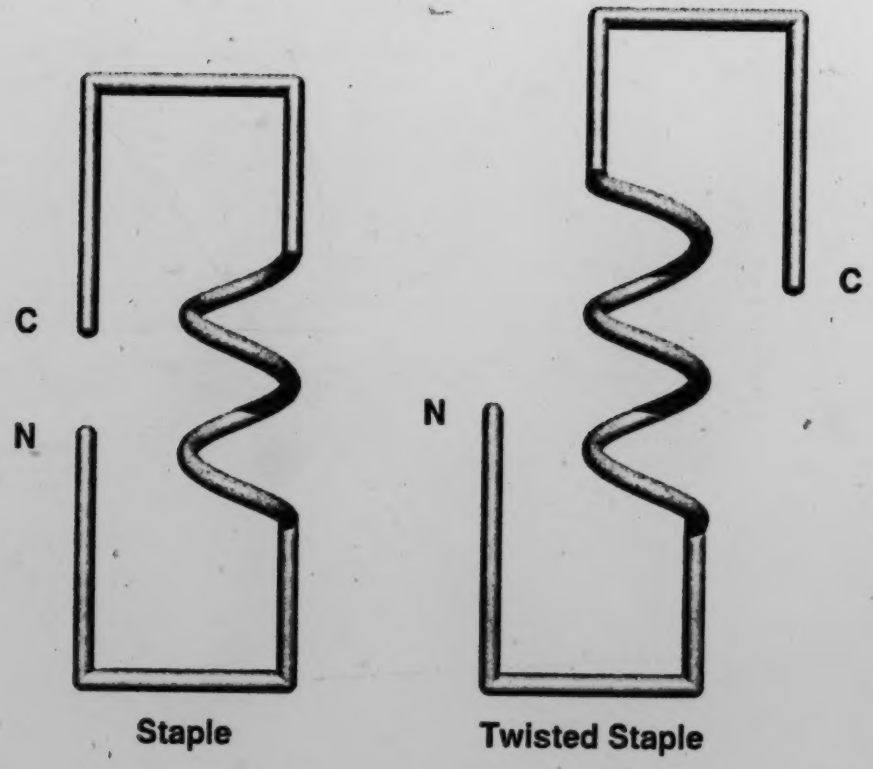

Figure 2.3. The Staple and Twisted Staple configurations. The left 'molecule' has a 'staple configuration', produced when an odd number of amino acids are bordered by two type II' β–turns. An even number of amino acids between two type II' β–turns causes a 180° rotation of the peptide bond leading to a 'twisted staple configuration' as shown with the right 'molecule'. The 'screw' portion is used to illustrate how the addition of one amino acid leads to a ½ turn rotation in the screw (peptide) axis.

Chapter 3*

Bacteriocin Analogs: Antibacterial Activity and Interactions of Leucocin A with its Enantiomer, Carnobacteriocin B2 and Truncated Derivatives

3.1 Introduction

Many antibacterial peptides exert their bacteriocidal effects by interacting with the bacterial cell membrane (see Figure 1.4). These membrane active antibacterial peptides follow one of two primary mechanistic routes. Route 1: membrane disruption (barrel–stave model, carpet model etc.), known to disturb the protonmotive force (Δp) or cytoplasmic homeostasis and route 2) peptide–membrane translocation, where the peptide after translocating into the cytoplasm, influences a cytoplasmic target. Although the former mechanistic route is most prevalent, recent studies have corroborated the latter route for certain peptides (Wu et al., 1999). It has also been observed that certain antibacterial peptides require relatively high concentrations to cause leakage in membranes. This suggests that at lower physiologically relevant concentrations, interaction with other cellular targets may be the dominant mechanism of action (Wu et al., 1999). Furthermore, cellular targets have been implicated with mersacidin and nisin A antibacterial activity. These peptides inhibit cell wall synthesis by binding to lipid II, the precursor for peptidoglycan synthesis. (Brötz et al., 1998; Breukink et al., 1999). It is likely, in

---

*This Chapter was published as a paper by Yan, L.Z., Gibbs, A.C., Stiles, M.E., Wishart, D.S. and Vederas, J.C. (2000) in *J. Med. Chem.* 43:4579–4581.

certain cases, the binding of a chiral cell wall precursor or protein receptor by an antibacterial peptide may initiate membrane disruption or peptide–membrane translocation, as well as possibly inactivating the function of the target.

Enantiomeric (optical antipode) syntheses are a common method to study whether a chiral recognition/discrimination is a necessary feature of a particular mechanism of action (Eliel and Wilen, 1994). It was on this basis that enantiomers of antibacterial peptides have been previously synthesized and studied. Examples of enantiomers that display equal antibacterial activity to their all–L–enantiomers include: gramicidin S (Izumiya et al., 1979), temporin A (Wade et al., 2000), plantaricin A (Hauge et al., 1998), cecropin A, mellitin (Wade et al., 1990), cecropin B (Bland et al., 2001), magainin (Bessalle et al., 1990), adroctonin (Hetru et al., 2000) and mastoparan M (Li et al., 2000). Interestingly, there are no examples of all–D–amino acid enantiomers of cationic, amphipathic α–helical antibacterial peptides that do not have antibacterial activity. In contrast to the bacteriocidal D–enantiomer peptides, only a few all–D–amino acid antibacterial peptides have been shown to be devoid of activity: polymyxin B (Tsubery et al., 2000), drosocin (Bulet et al., 1996) and apidaecine (Casteels and Tempst, 1994). Based on these studies, one may hypothesize that polymyxin B, drosocin and apidaecines antibacterial effects are mediated through some type of chiral recognition.

Recently, the solution structure of the 37–residue, antibacterial peptide

leucocin A (LeuA) was determined by NMR spectroscopy (Gallagher et al., 1997; Wang et al., 1999). These studies indicate LeuA contains a C–terminal cationic, amphipathic α–helix with an N–terminal three–stranded antiparallel β–sheet. Although detailed solution structures of LeuA have been determined, its mechanism of action still remains unclear. In order to help elucidate LeuA's mechanism of action, we have synthesized its all–D–amino acid enantiomer (D–LeuA) then subsequently assayed for bioactivity against a number of bacterial strains. In addition, various fragments of LeuA were prepared in an attempt to determine the residues and secondary structural elements necessary for antibacterial activity. This study represents the first synthesis of an all–D–amino acid enantiomer of a type IIa bacteriocin antibacterial peptide.

3.2 Materials and Methods

Synthesis, purification and characterization of D–LeuA. The synthesis, purification and characterization of D–LeuA, was carried out with the assistance of Dr. Liang Zeng Yan. D–LeuA was manually synthesized by stepwise solid phase synthesis (Bodanszky, 1993) using all D–amino acids with Fmoc α–amine protection. Orthogonal protection was as follows: Arg (Pmc); Asn (Trt); Cys (Trt); Glu (OtBu); His (Trt); Lys (Boc); Ser (tBu); Thr (tBu); Trp (Boc); Tyr (tBu). Initially, Fmoc–Trp–Boc (C–terminal amino acid) was coupled to 0.3 mmoles of Wang resin using DCC as the activating agent in the presence of catalytic amount of DMAP in DMF. The peptide chain was assembled in a stepwise manner with deprotection, activation and coupling cycles, as shown in Figure 1.6. All steps were

followed by washing sequentially with DMF, DCM, isopropanol, DCM and DMF, to remove excess reagents and protecting groups. Fmoc deprotection was catalyzed by 20% piperidine in DMF. Amino acid activation was carried out by using HBTU in DMF and N–methylmorpholine and a four–fold excess of the Fmoc protected amino acid was used to maximize yield of the HOBt–amino acid ester. The extent of coupling was monitored by using a ninhydrin assay to check for residual free α–amine (Sarin et al., 1981). The amount of residual α–amine present after coupling determined whether or not another coupling step was required, capping with acetic anhydride was needed or if the next amino acid should be added. To help drive the coupling reaction for amino acids that failed to couple completely, a combination of the activating agent HATU and heat was employed. Following synthesis, peptide cleavage from the resin was carried out in a mixture of 90% TFA, 5% thioanisole, 3% DTT and 2% anisole for 2 h. The TFA catalyzes the hydrolysis of peptide from resin and the thioanisole, DTT and anisole act as protecting group scavengers.

The peptide was purified to homogeneity (see Figure 3.1) using preparative reversed phase HPLC with a Zorbax 300 SB C–8 column and a water/acetonitrile gradient. Following lyophylization, the peptide was tested for homogeneity with an HP1100, LC–MSD electrospray mass spectrometer and determined to have a molecular weight of 3932.11 ± 0.35 Da (see Figure 3.2). The oxidation state of the two cysteine residues was checked via an iodoacetamide reaction. The peptide was stirred under O_2, to promote oxidation, until no iodoacetamide derivatization was observed. The molecular weight of the oxidized peptide was determined to be

3929.95 ± 0.59 Da. Purified D–LeuA was further characterized by amino acid sequencing, HPLC co–injection with L–LeuA and circular dichroism (CD) spectroscopy. Amino acid analysis using standard Edman degradation with a Applied Biosystems model 470A gas phase sequencer was used to confirm the peptide sequence. Figure 3.3, an analytic HPLC co–injection of D–LeuA and L–LeuA further confirmed the constitution of D–LeuA, as shown by the enantiomers overlapping retention times. Since enantiomers absorb left and right circularly polarized light opposite to each other, CD spectroscopy is a common method to differentiate optical antipodes. CD spectra were collected on a Jasco J–500C spectropolarimeter at 25°C. The CD spectra were averages of four scans collected between 190–250 nm, with D– and L–LeuA concentrations of 0.1 mM (see Figure 3.4). The spectra were recorded in the following solvents: 90% trifluoroethanol (TFE) in 0.1% TFA; aqueous dodecylphosphocholine (DPC) in 0.1% TFA (1:40 ratio of LeuA:DPC); and 0.1% aqueous TFA.

The two L–LeuA peptide fragments (residues 18–32 and residues 18–37, see Table 3.1) were synthesized (Fmoc chemistry) and characterized at BioTools Inc. (Edmonton, AB).

Antibacterial activity of D–LeuA. Antibacterial activity studies were carried out by Dr. Liang Zeng Yan. The antibacterial activity of the peptides was determined by the spot–on–lawn test (Quadri et al., 1997). The following cultures were screened: *Carnobacterium divergens* LV13, *Carnobacterium piscicola* N5,

Carnobacterium piscicola LV17A, *Carnobacterium piscicola* LV17B (Bac^+ and Bac^-), *Enterococcus faecium* BFE 900, *Leuconostoc gelidum* UAL187, *Leuconostoc gelidum* UAL187.13, *Lactococcus messenteroides* 23386, *Lactobacillus sake* 20017, and *Listeria monocytogenes* LI0502. Agonistic and antagonistic effects of mixtures of D– and L–LeuA were also measured. Solutions to test for agonistic or antagonistic activity were prepared with different molar ratios of L– to D–LeuA ranging from 0.1 to 100 (Solution A, 0.004 : 0.04 μg/μL; Solution B, 0.04 : 0.04 μg/μL; Solution C, 0.4 : 0.04 μg/μL; Solution D, 0.4 : 0.004 μg/μL).

Fragment inhibition studies were also carried out by Dr. Liang Zeng Yan. Bacteriocin activity was measured via 96–well microtiter plates. L–LeuA solution at two–fold dilutions, various concentrations of the 15–mer or 20–mer peptide fragments, and 2 μL of 16 h culture (indicator strain, *Carnobacterium divergens* LV13 or *Lactobacillus sake* 20017) were added to each microtiter plate well containing 200 μL of APT broth. The microtiter plates were then incubated for 16 h at 25°C, after which the growth of the indicator strain was measured spectrophotometrically at 650 nm. The culture absorbance was then plotted against the peptide concentration and the minimum inhibitory concentration (MIC) was determined directly from the graph. MIC was defined as the bacteriocin concentration that inhibited the growth of the indicator strain by 50% (i.e. 50% of the absorbance of the control culture without bacteriocin at 650 nm). All tests were repeated at least once.

Induction tests towards *C. Piscicola* LV17B (Bac⁻). Induction studies were performed by Dr. Liang Zeng Yan. Bac⁻ cells of *Carnobacterium piscicola* LV17B were prepared from Bac⁺ cells by serial one tenth dilutions (Saucier et al., 1995). The Bac⁻ cells were subcultured before use and no bacteriocin was found in the supernatant. The medium was added to different concentrations of L–LeuA or D–LeuA, concentrations of the peptides in the culture medium ranged from 10 μg/mL to $10x2^{-10}$ μg/mL. After the culture reached full growth, the inhibitory activity of the heat–treated supernatant (100°C for 15 min) was assayed by the spot–on–lawn technique, on a bacterial lawn of *Carnobacterium divergens* LV13. Background bacteriocin activity, from the bacteriocin added to the culture medium, was taken into account when determining induction at high concentrations. The supernatant of Bac⁺ culture, which induces the production of bacteriocin, was included as a positive control and the subculture of Bac⁻ cells was included as a negative control.

3.3 Results and Discussion

The Bacteriocins. Over the last few years ribosomally synthesized antibacterial peptides produced by gram positive bacteria, in particular lactic acid bacteria (LAB), have attracted considerable interest as more than fifty of these so–called bacteriocins have been characterized (Jack et al., 1995; Nes and Holo, 2000). The bacteriocins of LAB usually contain between 20 and 60 residues, are cationic, hydrophobic and often amphipathic. The inhibitory spectrum of bacteriocins is limited to gram–positive bacteria and usually to strains closely related to the producer. These

peptides have very potent bacteriocidal activity, common inhibitory concentrations are typically in the nanomolar range. LAB bacteriocins are classified into three families (Kaenhammer 1993): class I – the lantibiotics (Guder et al., 2000), class II – heat stable unmodified bacteriocins (Nes and Holo, 2000) and class III – large heat labile bacteriocins. Class II, the largest class, is further divided into at least three subclasses, a, b and c (van Belkum and Stiles, 2000). Class IIa bacteriocins (Ennahar et al., 2000) produced by LAB possess considerable potential as nontoxic food–preserving agents (Vandenbergh, 1993) due to their effectiveness against the food pathogen *Listeria monocytogenes*. In addition to food preservation these antibacterial peptides show therapeutic promise in the treatment of antibiotic resistant bacteria (Nissen–Meyer, 1997; Tannock, 1999) and gastrointestinal infections (Stiles, 1996; Konings, et al. 1999).

LeuA is isolated from the fermentation supernatant of the LAB *Leuconostoc gelidum* UAL187 (Hastings et al., 1991; Hastings and Stiles, 1991) and belongs to the class IIa bacteriocins. Class IIa bacteriocins are distinguished from other bacteriocins by a conserved YGNGV motif at their N–terminal ends (see Table 3.1) (Klaenhammer, 1993). The YGNGV motif has been coined the *Listeria* active part of class IIa bacteriocins because it is thought to be involved in the recognition of *Listeria monocytogenes* membranes (Bhugaloo–Vial et al., 1996; Ennahar et al., 2000). Many type IIa bacteriocins are thought to self associate, form pores and subsequently disrupt bacterial cell membranes (Moll et al., 1999; Ennahar et al., 2000). However, obvious differences in bacteriocin antibacterial spectrum of action suggests a more specific mechanism of action (Eijsink et al., 1998). A more specific

(or chiral) mechanism of action is supported by the observation that differences in spectrum of action exist despite a high sequence homology between the type IIa bacteriocins. Therefore, high sequence homology does not necessarily imply a similar mode of action (Fleury, 1996; Gallagher et al., 1997; Chikindas et al., 1993; Jack et al., 1995) and in the case of class IIa bacteriocins, recognition of a chiral target may be a necessary step in the mechanism of action.

If chiral recognition is a necessary step in bacteriocin mechanism of action, it is safe to assume three–dimensional structure is implicated in bacteriocidal spectrum of action. This assumption has basis in that LeuA and the closely related class IIa bacteriocin carnobacteriocin B2 (CbnB2), not only have different antibacterial spectra of action but different three–dimensional solution structures as well. Figure 3.5 contains a superimposition of LeuA and CbnB2. These structures, as solved in low–dielectric solvents (Gallagher et al., 1997; Wang et al., 1999), clearly show similarities and differences. The peptides have very different N–terminal structures. LeuA contains a well defined N–terminal three–strand, antiparallel β–sheet (residues 2–16) fixed by a disulfide bond whereas the disulfide bond in CbnB2 resides in a random coil region and does not stabilize a β–sheet. On the other hand, the C–terminal sections of these peptides are structurally very similar. Their amphipathic α–helices superpose with low backbone RMSD (as is evident with Trp 18 and Phe 22 side–chains), despite a relatively lower sequence homology than the N–terminal regions.

In order to further elucidate structure–activity correlations among type IIa bacteriocins a series of recent experiments have produced interesting, but not always complimentary, results. Studies on chimeric bacteriocins where the N– and C–terminal sections are interchanged, indicate the C–terminus (helix) determines antibacterial specificity (Fimland et al., 1996). Other studies show the integrity of the entire sequence, including oxidized cysteines and the C–terminal tryptophan of mesentericin Y 105^{37}, are all essential for full antibacterial activity (Fleury et al., 1996). Incidentally, mesentericin Y 105^{37} has 95% sequence homology with LeuA (see Table 3.1). Chemical modifications to divercin V41 (Table 3.1) that neutralize the overall net positive charge, do not effect its antibacterial activity (Bhugaloo–Vial et al., 1999). This result suggests electrostatic interactions may be of limited importance to divercin V41's mechanism of action. Similar to mesentericin Y 105^{37}, divercin V41 also showed a significant loss in antibacterial activity concomitant to a loss (reduction) of the disulfide bond. In contrast to divercin V41, it has been determined that electrostatic interactions govern pediocin PA–1's (Table 3.1) binding of the target membrane (Chen et al., 1997). Furthermore, the study ruled out the possibility that the conserved YGNGV motif mediates pediocin PA–1's binding of the target membrane. It is important to mention, although pediocin PA–1 is a class IIa bacteriocin, it contains a second disulfide bond that is not only essential to its bacteriocidal activity (Chikindas et al., 1993) but also likely destabilizes a putative C–terminal helix. Moreover, the Chikindas study also suggests a chiral recognition step may be necessary for pediocin PA–1 to initiate its bacteriocidal effects.

D–Leucocin A. Following synthesis, D–LeuA was tested for antibacterial activity and for possible agonist/antagonist effects with L–LeuA against ten different strains of bacteria. With similar concentrations to L–LeuA, D–LeuA showed no antibacterial activity against any of the strains tested. This result clearly demonstrates that interaction with a chiral receptor molecule is a critical feature of the mechanism of action of this class IIa bacteriocin. D–LeuA was not able to antagonize the antibacterial effect of L–LeuA at any concentration tested. These results contrast a similar study on plantaricin A, a 26 residue bacteriocin (deficient in the YGNGV motif and disulfide bond – i.e. not class IIa, see Table 3.1) isolated from *Lactobacillus plantarum* (Diep et al., 1994). Plantaricin A, similar to LeuA and CbnB2, adopts an α–helical conformation in low dielectric solvents. Synthetic D– and L–enantiomers of plantaricin A, truncated by four N–terminal residues, both have full and equal antibacterial activity (Hague et al., 1998). The plantaricin A study mirrors results from enantiomer and truncation studies on cecropin A, magainin 2 and melittin (Merrifield, 1994; Wade et al., 1990). The truncated peptides and their D–enantiomers retain equal potency relative to the native peptides. In addition, the natural all–L–amino acid plantaricin A has a dual function, in that it also acts as a pheromone, i.e. induction of bacteriocin production. Interestingly, the D–enantiomer of plantaricin A does not show similar pheromone activity, but it does have the ability to inhibit the pheromone induction caused by the L–enatiomer. This result indicates pheromone activity is a chiral receptor–mediated function.

Production of bacteriocins is accomplished either through a dedicated regulator (induction factor) or is self–regulated by the bacteriocin itself (Saucier et al., 1995). Interestingly, previous studies have shown CbnB2 and several structural variants are able to re–establish a Bac^+ phenotype in Bac^- cultures (Quadri et al., 1997). However in the present study, we found both enantiomers of LeuA were unable to re–establish bacteriocin production in Bac^- cultures of *Carnobacterium piscicola* LV17B.

Bacteriocin Fragments. Recently, a 15 residue fragment (residues 20–34) of pediocin PA1, was found not to show antibacterial activity but significantly inhibited the activity of the parent pediocoin PA1 (20–fold increase in MIC) (Fimland et al., 1998). These results suggest that the 15–mer interacts with a chiral receptor, a receptor that normally binds the same sequence on the parent bacteriocin. On this basis, we synthesized (with L amino acids) the following L–LeuA fragments: residues 18–32, 18–37 and N–Acetyl 18–37, all corresponding to the amphipathic, α–helical region (Table 3.1). Also, a CbnB2 fragment (1–22) was synthesized. None of these fragments displayed antibacterial activity by themselves. A slight inhibition in LeuA activity was observed when equal amounts of LeuA fragments were mixed with LeuA, however, very little inhibition as compared to the pediocin PA1 fragment study. Similarly, the CbnB2 fragment did not inhibit the antibacterial activity of mature CbnB2. Because LeuA and CbnB2 have somewhat overlapping antibacterial spectra, we examined whether or not they could inhibit each other. Combining a 10–fold molar excess of CbnB2 with LeuA increased the

specific activity of LeuA 2– to 4–fold against *Leuconostoc mesenteroides* 23386 and *Lactobacillus sakei* 20017 (two strains that are insensitive to CbnB2). On the other hand, a 1000–fold molar excess of CbnB2 to LeuA, reduced the specific activity of LeuA towards *Carnobacterium piscicola* UAL26/8B by 16–fold. Since these bacteriocin fragments are devoid of activity, in contrast to the plantaricin A fragments, these findings reinforce the requirement of a chiral receptor for class IIa bacteriocins. Whereby a putative receptor may recognize the amphipathic, α–helical C–terminal section of the peptide and this chiral recognition accounts for the potent but relatively narrow antibacterial spectrum.

Putative Bacteriocin Receptor. The data from this study supports involvement of a chiral interaction. Similarly, other indirect evidence points to a chiral interaction as well. Bacteriocin immunity maybe indirectly related to a putative bacteriocin receptor. Immunity proteins are co–transcribed with bacteriocins. They range in size from 80–120 amino acids and have low sequence homology (Eijsink et al., 1998). In contrast to sequence homology, secondary structure predictions have shown a high α–helical homology between the proteins (Eijsink et al., 1998). However, secondary structure predictions indicate the sequences do not have transmembrane helices, suggesting the immunity proteins are either secreted or remain in the cytoplasm (Bukhtiyarova et al., 1994). Evidence suggests the immunity proteins for CbnB2 and mesentericin Y105[37], remain in the cytoplasm. It has been shown, that expression of the CbnB2 immunity protein within the cell provides immunity, however, the immunity protein applied externally does not

confer immunity (Quadri et al., 1995). The study also indicated CbnB2 to have no binding affinity for its immunity protein, thereby implicating a 'third party'. Similarly, immunofluorescence and electron microscopy techniques have shown the mesentericin $Y105^{37}$ immunity protein is found only in the cytoplasm (Abdel–Dayem et al., 1996). These studies point towards a cytoplasmic immunity protein that must protect the producer from inside the cell, a scenario suggested for the class II bacteriocin lactococcin A immunity protein (Venema et al., 1994). Since bacteriocins are not active until they are exported from the cell, one can assume the immunity protein interacts with a membrane–bound protein, more than likely the putative bacteriocin receptor (whose primary biological function may be unrelated).

3.4 Conclusion

Although the antibacterial spectra of LAB bacteriocins is limited, these peptdies show considerable promise because they are nontoxic to mammals (i.e. they are not hemolytic) and are much more potent than conventional antibacterial compounds. This study supports earlier studies that show the entire peptide is necessary for the full antibacterial activity of class IIa bacteriocins. More importantly, by way of the unnatural D–enantiomer of LeuA (see Figure 3.6), we have demostrated a requirement for interaction with a chiral receptor molecule is a key step in LeuA mechanism of action. This affords a unique possibility for future antibiotic development. Incidentally, recent genetic experiments on bacteriocin resistance provide circumstantial evidence that the protein components of the sugar phosphotransferase systems (PTS) may be the target of these peptides (Gravesen et

al., 2000; Ramnath et al., 2000).

References

Abdel-Dayem, M., Fleury, Y., Devilliers, G., Chaboisseau, E., Girard, R., Nicolas, P. and Delfour, A. (1996) *FEMS Microbiol. Lett.* 138:251–259.

Casteels, P. and Tempst, P. (1994) *Biochem. Biophys. Res. Commun.* 199:339–345.

Bessalle, R., Kapitokovsky, A., Gorea, A., Shalit, I. and Fridkin, M. (1990) *FEBS Lett.* 274, 1,2:151–155.

Bhugaloo-Vial, P., Dousset, X., Metivier, A., Sorakine, O., Anglade, P., Boyaval, P. and Marion, D. (1996) *Appl. Environ. Microbiol.* 62:4410–4416.

Bland, J.M., De Lucca, A.J., Jacks, T.J. and Vigo, C.B. (2001) *Mol. Cell. Biochem.* 218:105–111.

Bodanszky, M. (1993) In *Principles of Peptide Synthesis* Springer Verlag: Berlin.

Brötz, H., Bierbaum, G., Leopold, K., Reynolds, P.E. and Sahl, H.G. (1998) *Antimicrob. Agents Chemother.* 42:154–160.

Brukink, E., Wiedemann., I., van Kraaij, C., Kuipers, O.P., Sahl, H.G. and de Kruijff, B. (1999) *Science* 286:2361–2364.

Bukhtiyarova, M., Yang, R. and Ray, B. (1994) *Appl. Environ. Microbiol.* 60:3405–3408.

Bulet, P., Urge, L., Ohresser, S., Hetru, C. and Otvos, L. Jr. (1996) *Eur. J. Biochem.* 238:64–69.

Chikindas, M. L., Garcia-garcera, M. J., Driessen, A. J. M., Ledeboer, A. M., Nissen-Meyer, J., Nes, I.F., Abee, T., Konings, W.N. and Venema G. (1993) *Appl. Environ. Microbiol.* 59:3577–3584.

Diep, D.B., Håvarstein, L.S., Nissen-Meyer, J. and Nes, I.F. (1994) *Appl. Environ. Microbiol.* 60:160–166.

Eijsink, V.G.H., Skeie, M., Middelhoven, P.H., Brurberg, M.B. and Nes, I.G. (1998) *Appl. Environ. Microbiol.* 64:3275–3281.

Eliel, E.L. and Wilen, S.H. (1994) In *Stereochemistry of Organic Compounds*, John Wiley and Sons, Inc., New York, NY.

Ennahar, S., Sashihara, T., Sonomoto, K. and Ishizaki, A. (2000) *FEMS Microbiol. Rev.* 24:85–106.

Fimland, G., Blingsmo, O., Sletten, K., Jung, G., Nes, I.F. and Nissen-Meyer J. (1996) *Appl. Environ. Microbiol.* 62:3313–3318.

Fleury Y., Dayem, M. A., Montagne, J. J., Chaboisseau, E., Le Caer, J. P., Nicolas, P. and Delfour, A. (1996) *J. Biol. Chem.* 271:14421–14429.

Fregeau Gallagher, N. L., Sailer, M., Niemczura, W.P., Nakashima, T.T., Stiles, M.E., and Vederas, J.C. (1997) *Biochemistry* 36:15062–15072.

Gravesen, A., Warthoe, P., Knochel, S. and Thirstrup, K. (2000) *Microbiology* 146:1381–1389.

Guder, A., Wiedemann, I. and Sahl, H.G. (2000) *Biopolymers* 55:62–73.

Hastings, J. W., Sailer, M., Johnson, K., Roy, K.L., Vederas, J.C. and Stiles M.E. (1991) *J. Bacteriol.* 173:7491–7500.

Hastings, J. W., and Stiles M.E. (1991) *J. Appl. Bacteriol.* 70:127–134.

Hauge, H.H., Mantzilas, D., Moll, G.N., Konings, W.N., Driessen, A.J.M., Eijsink, V.G.H. and Nissen-Meyer, J. (1998) *Biochemistry* 37:16026–16032.

Hetru, C., Letellier, L., Oren, Z., Hoffmann, J.A. and Shai, Y. (2000) *Biochem. J.* 345:653–664.

Izumiya, N., Kato, T., Aoyaga, H., Waki, M. and Kondo, M. (1979) In *Synthetic Aspects of Biologically Active Peptides: Gramicidin S and Tyrocidines*, New York.

Jack, R. W., Tagg, J.R. and Ray B. (1995) *Microbiol. Rev.* 59:171–200.

Klaenhammer, T. R. (1993) *FEMS Microbiol. Rev.* 12:39–85.

Konings, W.N. and Kuipers, O.P. (1999) In *Lactic Acid Bacteria: Genetics, Metabolism and Applications*, Kluwer Academic Publishers. Norwell, MA.

Li, M., Liao, R., Qiu, J., Wang, Z. and Wu, T. (2000) *Int. J. Antimic. Agents* 13:203–208.

Merrifield, R. B., Merrifield, E.L., Juvvadi, P., Andreu, D. and Boman H.G. (1994) *Antimicrobial Peptides.* Wiley, Chichester (Ciba Foundation Symposium 186), p5–26.

Moll, G.N., Konings, W.N. and Driessen A.J. (1999) *Antonie Van Leeuwenhoek* 76:185–198.

Nes, I.F. and Holo, H. (2000) *Biopolymers* 55:50–61.

Nissen-Meyer, J. and Nes, I.F. (1997) *Arch. Mirobiol.* 167:67–77.

Quadri, L.E., Sailer, M., Terebiznik, M.R., Roy, K.L., Vederas, J.C. and Stiles, M.E. (1995) *J. Bacteriol.* 177:1144–1151.

Ramnath, M., Beukes, M., Tamura, K. and Hastings, J.W. (2000) *Appl. Environ. Microbiol.* 66:3098–3101.

Sarin, V. K., Kent, S. B. H., Ram, J. P. and Merrifield, R.B. (1981) *Anal. Biochem.* 117:147–157.

Saucier, L., Poon, A. and M. E. Stiles. (1995) *J. Appl. Bacteriol.* 78:684–690.

Stiles, M.A. (1996) *Antonie van Leeuwenhoek* 70:331–345.

Tannock, G. W. (1999) In *Probiotics: A Critical Review.* Horizon Scientific Press. Norfolk, England.

Tsubery, H., Ofek, I., Cohen, S. and Fridkin, M. (2000) *Biochemistry* 39:11837–11844.

van Belkum, M.J. and Stiles, M.E. (2000) *Nat. Prod. Rep.* 17:323–335.

Vanderbergh, P. A. (1993) *FEMS Microbiol. Rev.* 12:221–238.

Venema, K., Haverkort, R.W., Abee, T., Haandrikman, A.J., Leenhouts, K.H., Venema, G. and Kok, J. (1994) *Mol. Microbiol.* 14:521–533.

Wade, D., Boman, A., Wahlin, B., Drain, C.M., Andreu, D., Boman, H.G. and Merrifield, R.B. (1990) *Proc. Natl. Acad. Sci. USA* 87:4761–4765.

Wade, D., Silberring, J., Soliymani, R., Heikkinen, S., Kilpeläinen, I., Lankinen, H. and Kuusela, P. (2000) *FEBS Lett.* 479:6–9.

Wang, Y., Henz, M.E., Fegeau Galagher, N.L., Chai, S., Gibbs, A.C., Yan, L.Z., Stiles, M.E., Wishart, D.S. and Vederas, J.C. (1999) *Biochemistry* 38:15438–15447.

Wu, M., Maier, E., Benz, R. and Hancock, R.E.W. (1999) *Biochemistry* 38:7235–7242.

Table 3.1 Sequences of Bacteriocins and Peptide Fragments

Peptide[1]	---------- Sequence[2] ----------		
CbnB2	VN YGNGV	SCSKTKCSVN	WGQAFQERYTAGINSFVSGVASGAGSIRRRP
Frag. 1	VN YGNGV	SCSKTKCSVN	WGQAF
LeuA	KY YGNGV	HCTKSGCSVN	WGEAFSAGVHRLANGGNGFW
Frag. 2			WGEAFSAGVHRLANGGNGFW
Frag. 3			WGEAFSAGVHRLANG
MesY105	KY YGNGV	HCTKSGCSVN	WGEAASAGIHRLANGGNGFW
PedPA-1	KY YGNGV	TCGKHSCSVD	WGKATTCIINNGAMAWATGGHQGNHK
DivV41	TKY YGNGV	YCNSKKCWVD	WGQASGCIGQTVVGGWLGGAIPGKC
PlntA			KLLAYSLEMGATAIKEVKKLFKKWGW

1. CbnB2 = carnobacteriocin B2; Frag. 1 = 1-22 of carnobacteriocin B2; LeuA = leucocin A; Frag. 2 = 18-37 of leucocin A (note: an N-terminally acetylated variant was also tested); Frag. 3 = 18-32 of leucocin A; MesY105 = mesentericin Y105[37]; PedPA-1 = pediocin PA-1; DivV41 = divercin V41 and PlntA = plantericin A.
2. Sequences are aligned by the common YGNGV motif.

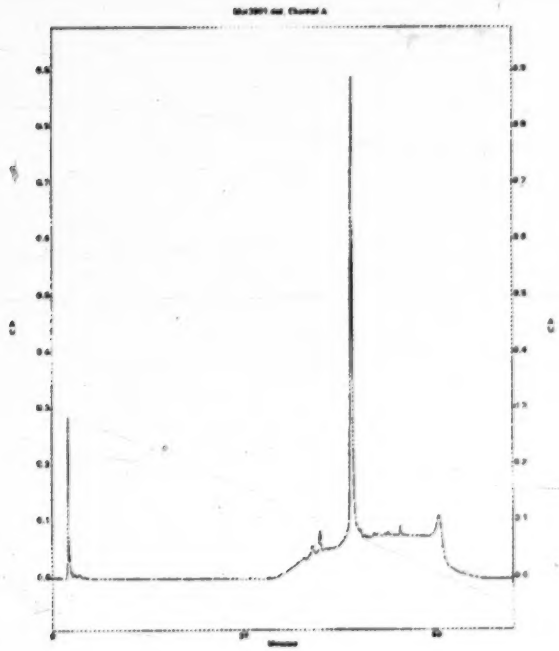

Figure 3.1. D-LeuA HPLC trace

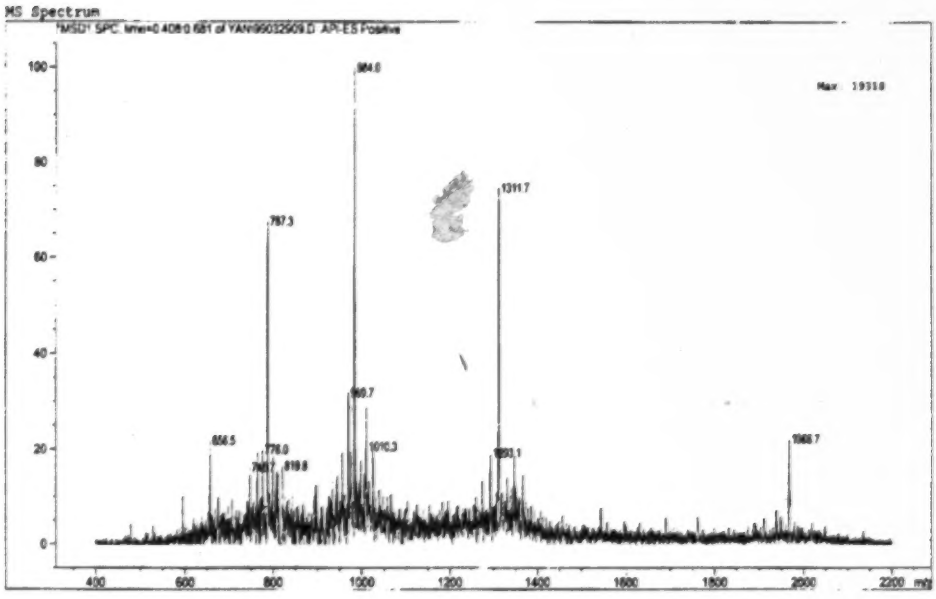

Figure 3.2. D–LeuA electrospray mass spectrum

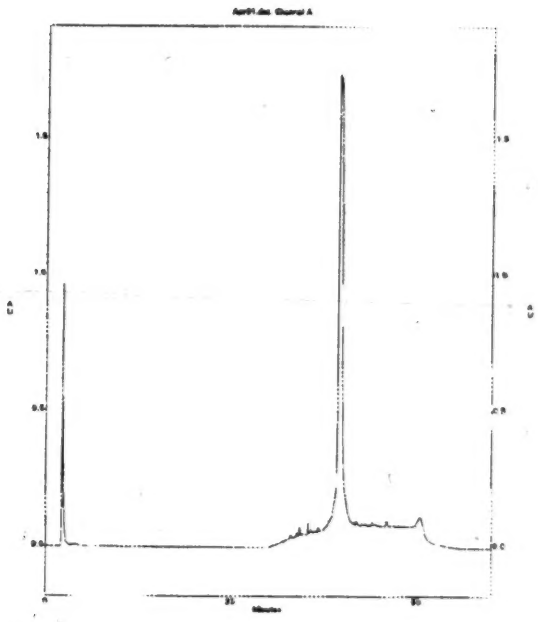

Figure 3.3. HPLC trace of a 1:1 mixture of L–LeuA and D–leuA

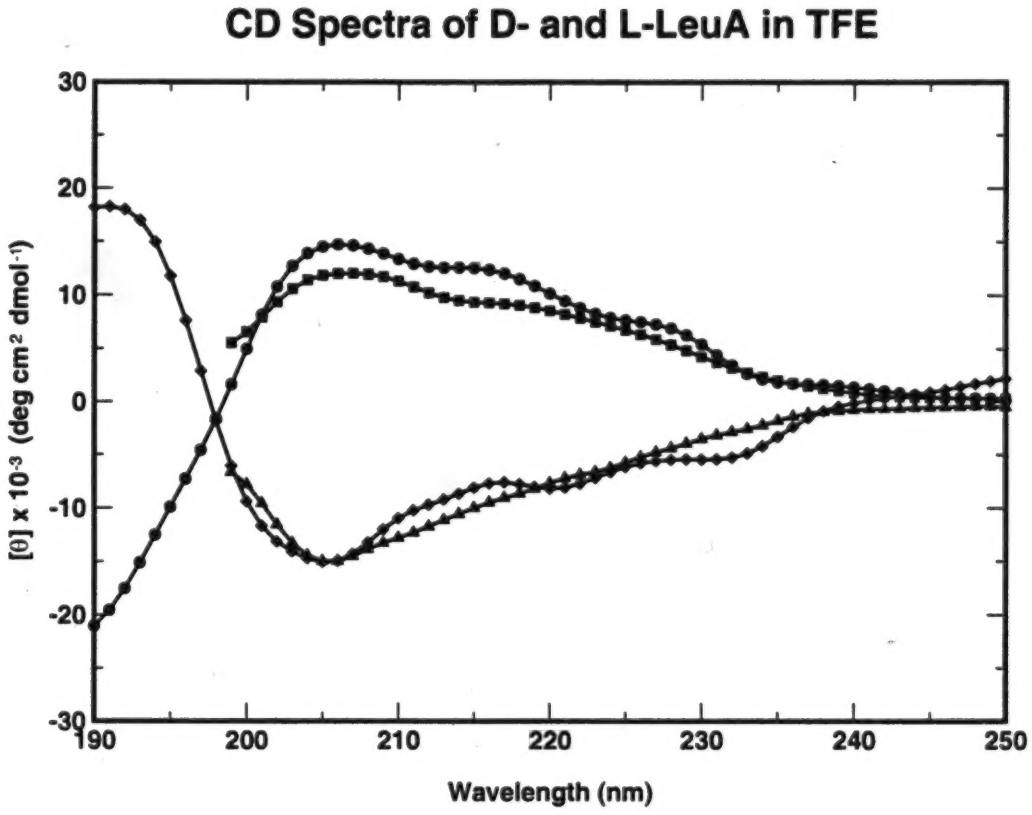

Figure 3.4. CD spectra of D- and L-Leu A in 90% TFE/10% H2O. ● = 0.1 mM D-LeuA; ■ = 0.5 mM D-LeuA; ♦ = 0.1 mM L-LeuA and ▲ = 0.5 mM L-LeuA.

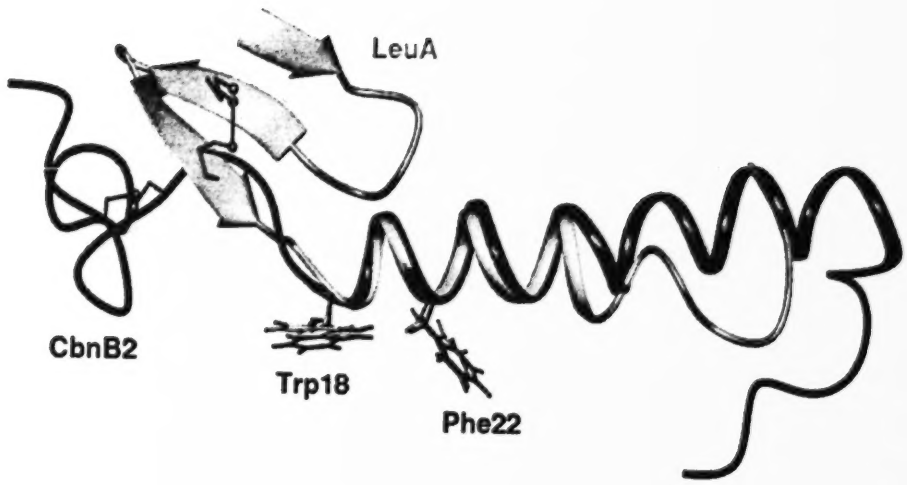

Figure 3.5. LeuA and CbnB2 superimposition. Clearly visible are the differences in N–terminal structures.

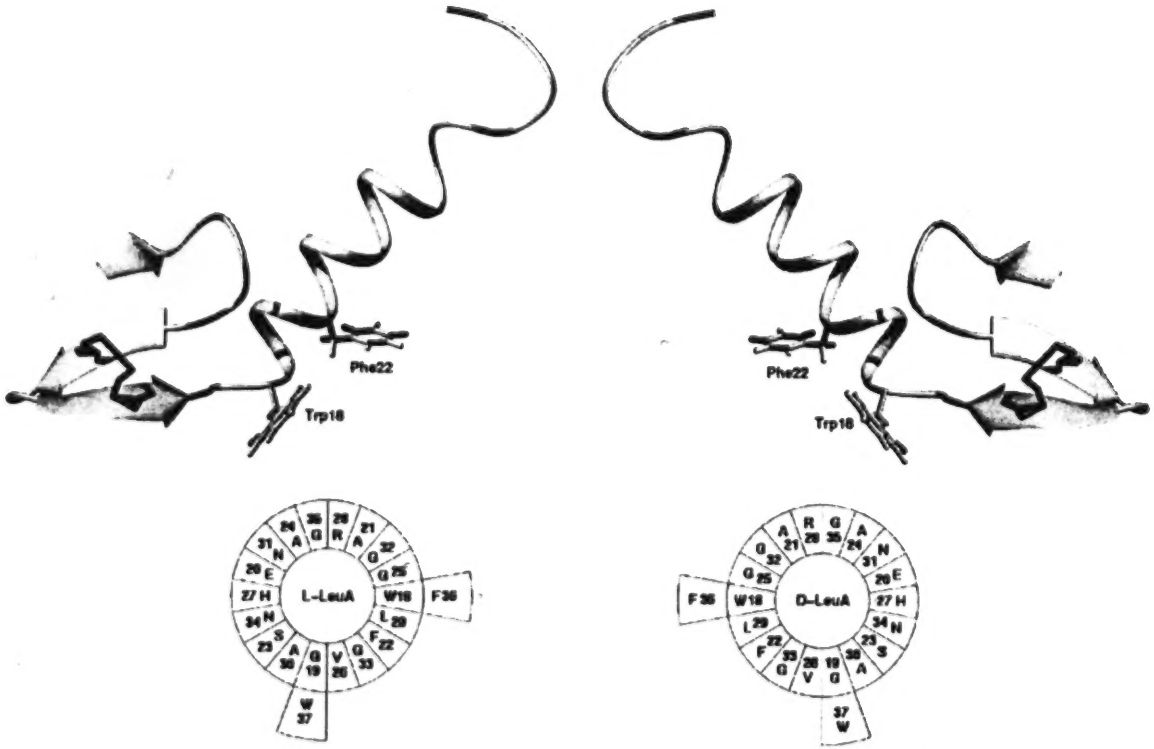

Figure 3.6. Hypothetical structure of D-LeuA (right) and the solution structure of L-LeuA (left). The helical wheels illustrate opposite amphipathic faces.

Chapter 4*

Probing the Structural Determinants and Conformational Space of Type II' β–turns

4.1 Introduction

β–turns were first recognized in the late 1960's by Venkatachalam (Venkatachalam, 1968). They are now known to be common structural motifs comprising up to 25% of all residues in folded proteins and peptides (Mattos et al., 1994; Wilmont and Thornton, 1988; Kabsch and Sander, 1983). β–turns also appear to play important roles in stabilizing tertiary structure, initiating folding and in facilitating intermolecular recognition (Wilmont and Thornton, 1988). Because of their critical importance in protein structure there has been considerable interest in designing β–turns and β–turn mimetics that may improve biological activity or enhance bioavailibility.

Simply stated, a β–turn causes a reversal in direction of the peptide backbone. The β–turn itself is usually the product of a strategically placed four–residue sequence (denoted i to i+3), between two secondary structural elements. The residues that make up a β–turn are typically amino acids with strong turn–forming propensity that allow the polypeptide backbone to adopt a conformation

*This chapter has been submitted as a paper by Gibbs, A.C., Hodges, R.S. and Wishart, D.S.

where the $C\alpha_i$ to $C\alpha_{i+3}$ distance is less than 7.0 Å (Richardson, 1981; Lewis et al., 1973). Turn–forming propensity involves a number of intra– and inter–residue (local) interactions, the details of which are not yet fully understood (Rose et al., 1985). Depending on the classification used, up to 10 different types of β–turns have been identified and classified. Lewis (Lewis et al., 1973) classified β–turns into 10 distinct types I, I', II, II', III, III', IV, V, VI, and VII, while Richardson (Richardson, 1981) later reclassified β–turns into 6 distinct types I, I', II, II', VIa, VIb and a random category IV. With each type of β–turn having a distinctly different influence on local β–sheet properties such as: hydrogen–bond register, β–sheet twist, β–sheet stability and β–sheet nucleation rates.

In order to systematically study the influence of β–turns on β–hairpin formation and stability, a well–defined and preferably small β–hairpin model is essential. Unlike the α–helix, where various peptide models have revealed much about the energetics and dynamics of this structure (Zhou et al., 1992; Chakrabartty and Baldwin, et al., 1995; Muñoz and Serrano, 1995; O'Neil and Degrado, 1990; Rothemund et al., 1995; Kohn et al., 1998; Lavigne et al., 1996), β–hairpin models have not been as readily forthcoming (Gellman, 1998). Recently, several β–hairpin and β–sheet models have emerged including: peptide mimetics (Kemp, 1990; Diaz et al., 1993; Nowich et al., 1996; Ripka et al., 1993), natural occurring small proteins (Smith et al., 1994), artificial proteins (Richardson and Richardson, 1987),

protein fragments (Blanco et al., 1994; Maynard et al., 1998) and model β–hairpin peptides (Blanco et al., 1993; Sharman and Searle, 1998; Dortemme et al., 1998; Schenck and Gellman, 1998; Das et al., 1998). One particularly appealing β–hairpin model is based on gramicidin S (GS) and its synthetic analogs (see Chapter 1 and 2). In GS the type II' β–turns are composed of residues LdFPV (i to i+3 respectively). This peptide model has several important advantages in that GS analogs can be readily synthesized, the β–hairpin structure is highly populated and this structure is largely solvent and solute independent. Furthermore, GS peptides are highly water soluble and exhibit a low propensity to aggregate (i.e., they are monomeric) (Wishart et al., 1996). These favorable properties have allowed us to systematically investigate, via NMR and CD spectroscopy, the influence of amino acid substitutions on β–hairpin formation and β–sheet periodicity on a series of variable length (6, 8, 10, 12 and 14 residue) analogs (Gibbs et al., 1998).

To extend our studies on β–hairpin formation and stability, we have chosen to explicitly examine the role of the β–turn. More specifically, we wish to investigate the role of amino acid substitutions in type II' β–turn propensity and β–hairpin propensity using various substituted GS analogs. The type II' β–turn is also known as a 'mirror image' turn or a diastereomer of the more common type II β–turn. Due to this diastereotopic relationship, type II' and type II turns have identical ϕ and ψ angles but with opposing signs. It is important to note, that while type II and type II' β–turns are mirror image equivalents, they are not energetically

equivalent – especially if they are composed of chiral amino acids (Rose et al., 1985). As it turns out, type I' and type II' β–turns have a much higher propensity for β–sheet nucleation than either type I or type II β–turns. This different propensity may result from the fact that the natural twist of these turns is more compatible with the left handed twist of an antiparallel β–sheet composed of L–amino acids (Wilmont and Thornton, 1998).

For this study we selected a 14 residue cyclic analog of GS (the naming scheme used for the peptides in this study is based on the i+1 and i+2 residues – Table 4.1), which has previously shown to exhibit a very stable β–hairpin structure with two 'ideal' type II' β–turns. Ten different analogs were synthesized with amino acid substitutions being limited to the i+1 and/or i+2 positions of just one of the turns (designated as Turn 1). These substitutions were specifically chosen to answer questions about the effects of chirality, side chain steric interactions and side–chain/side–chain interactions on type II' β–turn formation. All peptides were characterized by CD and ^{1}H–NMR spectroscopy and the solution structures fully determined using conventional NMR and computational methods (Wurthrich, 1986). The results of these structural studies show some very clear and somewhat expected trends which should help broaden our understanding of the local interactions that determine type II' β–turn stability and β–hairpin formation.

4.2 Materials and Methods

Peptide Synthesis. All peptides listed in Table 4.1 were synthesized either manually or with an Applied Biosystems 430A automated peptide synthesizer. Standard solid phase peptide synthetic techniques using t–butyloxycarbonyl (Boc) chemistry and Boc–Pro–phenylacetamidomethyl resin were used as previously described for other GS analogs (Wishart et al., 1996). Following cleavage from the resin with anhydrous hydrogen flouride, the linear 14 residue peptides were subsequently purified via reversed–phase HPLC using a Zorbax C–8 preparative column. The solvent system used in all purifications was a linear 0.33%/min acetonitrile/water gradient in the presence of 0.05% trifluoroacetic acid as a counter ion. C to N terminal cyclizations were performed with orthogonally protected formyl lysine, at peptide concentrations of 1–2 mg/ml in N,N–dimethylformamide. Cyclization was driven by using three equivalents of: benzotriazole–1–yloxytrisphosphonium hexafluorophosphate (BPO), 1–hydroxbenzotriazole hydrate (HOBT) and diisopropylethylamine (DIEA). After completion of the cyclization reaction (3 hours), the formyl protecting groups were removed using 10% hydrochloric acid in methanol at 310 K (16 hours). The peptides were identified and tested for homogeneity with a Fisons VG Quattro triple quadrupole electrospray mass spectrometer and a Beckman–System Gold analytical reversed–phase HPLC, following a final reversed–phase HPLC purification.

NMR Spectroscopy. All NMR experiments were performed using a Varian VXR–500 or a Unity INOVA 500 MHz NMR spectrometer. The peptides were dissolved

in 500 µl of 90% H_2O/10% D_2O yielding solutions having 1–2 mM concentrations. All peptide samples were subsequently sonicated with a Branson 2210 sonicator for 2–5 minutes to ensure maximum solubility. 0.1 mM 3–(Trimethylsilyl)–1–propanesulfonic acid (DSS) was added as an internal chemical shift reference. The sample pH was maintained between 4.5–5.5. All spectra were collected at 298 K, unless otherwise stated. Individual residue spin systems were assigned using TOCSY (Bax and Davis, 1985) and spectra were collected with spin–lock (MLEV–17) mixing times ranging from 30–60 ms. Sequential residue assignments were made from NOESY (Jeener et al., 1979; Kumar et al., 1980) and ROESY (Bothner–By et al., 1984; Kessler et al., 1987) experiments collected with mixing times of 150 ms and 250 ms respectively. All 2–D ^{1}H–NMR spectra were collected with 256 t_1 increments and 6000 Hz spectral widths. Shifted sinebell squared weighting and zero filling to 2K x 2K was applied before Fourier transformation. J–View, an in–house curve fitting program, was used to measure $^3J_{HNHA}$ coupling constants from 1–D ^{1}H–NMR spectra. Amide proton temperature coefficients were measured from 1–D ^{1}H–NMR spectra collected in 10 K increments from 298 K to 318 K.

Structure Generation. Interproton distance restraints were derived from through–space interactions observed in the NOESY and ROESY spectra. Assigned resonances were grouped into three families and given upper–distance bounds of 1.8–3.0 Å (strong), 1.8–4.0 Å (medium) and 1.8–5.0 Å (weak), based on crosspeak intensity. Amide proton temperature coefficients were used to identify hydrogen bond donors. NH–O distances were calculated from secondary shifts measured for

amide protons using a 1/r relationship (Wishart et al., 1991). The NH–O distances provided an additional 6 intra–strand HN–O and 6 N–O distance restraints for peptides exhibiting some β–sheet content as judged by the Chemical Shift Index (Wishart et al., 1992) and amide temperature coefficients (<5 ppb/K) (Wuthrich, 1986). The $^3J_{HNHA}$ coupling constants determined from 1–D ^{1}H–NMR spectra were converted to ϕ angles via a recently re–parameterixed version of the Karplus equation (Wang et al., 1997). The Chemical Shift Index (CSI) was used to determine ψ angle restraints. CSI values of +1, 0, –1 corresponding to ψ ranges of 120° +/– 30°, –40° +/– 180° and –60° +/– 40° respectively were used. Backbone ω angle restraints were set to 180°. An additional aromatic side chain restraint was added to peptides that showed significant (> 0.2 ppm) ring current anisotropy on the neighboring imino acid in the type II' β–turn region. Specifically a χ_1 restraint of 130° +/– 20 was added to all tyrosine residues that exhibited this anisotropy. The tyrosine χ_1 restraint was determined by calculating the i+2 residue chemical shifts using both emperical and *ab initio* (magnetic shielding tensors) methods. By calculating the chemical shifts at 5° intervals, it was possible to determine the position (+/– 20°) of the aromatic ring (χ_1) relative to the i+2 residue.

Substructure embedding was used to generate an initial ensemble of distance geometry, energy minimized atomic coordinates as implemented in X–PLOR v3.8.5 (Brunger, 1992). Following generation of the embedded ensemble of 20 structures, simulated annealing regularization and refinement was performed using 8,000 high–

temperature steps followed by 4000 cooling steps. Structures having no interproton distance restraint violations greater than 0.5 Å and no torsion angle violations greater than 5° were used as input for further refinement against proton chemical shifts (Kuszewski et al., 1995) and $^3J_{HNHA}$ coupling constants. During this final refinement stage, 500 steps of Powell energy minimization was performed with $^3J_{HNHA}$ coupling constant and ^1H chemical shift force constants of 1.0 Kcal/mol/Hz and 7.5 Kcal/mol/ppm, respectively. Average structures were calculated from a final ensemble of 20 accepted structures, after chemical shift and $^3J_{HNHA}$ coupling constant refinement.

Molecular Dynamics. Representative structures of dPRO–PRO (high β–sheet content), dPHG–PRO (moderate β–sheet content) and GLY–GLY (low β–sheet content) were individually solvated in rectangular boxes with an average of 700 SPC (Berendsen et al., 1981) water molecules. 10 nanosecond unrestrained molecular dynamics simulations were performed using GROMACS v2.0 (Berendsen et al., 1995) with the following parameters: Weak individual coupling of peptide and solvent to a bath of constant temperature (300 K) with a coupling time τ_T of 0.1 picoseconds. Pressure coupling to a pressure bath (reference pressure 1 bar) with a coupling time τ_P of 1.0 ps. The SETTLE (Miyamoto and Kollman, 1992) algorithm was used to constrain water bond lengths and angles.

Structure Evaluation. The structure validation program VADAR v3.0 (Wishart et al., 1997) was used to examine the quality of the final ensembles. MolMol v2k

(Koradi et al., 1996) was used to visualize, superimpose and calculate root–mean–square deviation (RMSD) values for all structural ensembles.

Circular Dichroism Spectroscopy. CD spectra were recorded at 298 K on a Jasco J–500C spectropolarimeter using 0.02 cm path length quartz cells. The CD spectra are averages of four scans, collected at 0.1 nm intervals between 190 and 250 nm. The peptides were prepared at concentrations of 1 mg/ml with pH ranging from 4.5–5.5. Ellipticity is reported as mean residue ellipticity [θ], with approximate errors of +/– 10% at 220 nm.

4.3 Results and Discussion

Rationale for GS model. The study of β–turns and β–turn propensity is particularly challenging because it is often difficult to separate distal effects from proximal or local effects. Looking at the statistical preferences of residues involved in β–turns in proteins does not allow one to ascertain whether the absence or abundance of certain residues in β–turns is a consequence of the secondary or tertiary structural preferences of neighboring residues or of the entire protein. The only way to remove these distal or context–dependent influences from β–turns is to look at β–turns (and β–hairpins) in isolation. The ideal way to do this would be to prepare a synthetic β–hairpin in which the hairpin portion (i.e., the β–sheet) is always preserved (for this peptide model, we will use the terms β–hairpin and β–sheet interchangeably). Our approach has been to create a constrained β–hairpin

peptide model in which the N and C terminus of the β–hairpin have been covalently linked and the two β–strands brought into proper register.

An advantage to creating a permanent β–hairpin is that we greatly increase the number of compact or 'folded' states available to the peptide. This allows us to detect and measure structural properties (β–sheet content, ϕ and ψ angles, NOE's, hydrogen–bonds, etc.) that might otherwise be too poorly populated or to fleeting to detect in an unrestrained peptide. As we will show (*vide infra*) by preferentially populating structured states we make the model far more sensitive to perturbations in β–turn propensity and consequently, β–sheet content. In other words, the range of β–sheet content in these peptide models extends from ~5% to 90% (ie: a 20 fold difference) as opposed to ~10% to 20% (2 fold) in unrestrained linear peptides (Blanco et al., 1993; Sarman and Searle, 1998; Dortemme et al., 1998).

The use of a covalent constraint to force a chain reversal is not new to peptide engineering (DeGrado et al., 1999). Disulfide bonds are frequently used to bring two distal peptide segments in close proximity. However, disulfide bonds do not necessarily favor nor do they ensure the formation of antiparallel β–strands. Indeed the geometry of disulfide bonds strongly disfavors the alignment and backbone orientation necessary for hydrogen bond formation and consequently β–sheet stabilization. In contrast, type II' β–turns always provide the appropriate geometry, topological twist and in–register peptide alignment to consistently form

β–hairpins (Rose et al., 1985). In this regard the substitution of a type II' β–turn in place of a disulfide bond essentially acts as a 'covalent hydrogen bond' that strongly favors β–hairpin formation. With its two type II' β–turns, GS (and its synthetic analogs) offers the opportunity to systematically investigate β–turn formation and β–turn propensity by changing only one of the two turns. By choosing to modify only a single turn in these peptide constructs we were able to preserve the 'pseudo–hydrogen bond' constraint provided by the second type II' β–turn, thus mimicing an extended β–sheet. This constraint ensures that the two strands in the hairpin would always be in close proximity and that if a hydrogen bonding network or antiparallel β–sheet were even remotely capable of forming that it would have a high probability of doing so.

Design of peptide constructs. We designed our β–hairpin peptides such that a systematic series of substitutions at the i+1 and i+2 residues of Turn 1 (residues 6 and 7, see Table 4.1) could be made to maximize synthetic and comparative efficiency. In particular we used the second turn (Turn 2) as a within–peptide control (and structural anchor) while the first turn (Turn 1) served as the variable. In order to answer questions regarding the influence of side–chain steric restriction, chirality and side–chain/side–chain interactions on type II' β–turn formation and stability, we used a variety of coded and non–coded amino acids (see Figure 4.1). Specifically, D–proline (at i+1) and two other proline analogs, 3,4–dehydroproline and pipecolic acid (at i+2) were used to study N–alkylation and steric restriction.

Glycine, sarcosine, D/L–tyrosine and D/L–proline were used to study achiral, homochiral and heterochiral backbone effects. And, finally, side–chain/side–chain interactions were explored with D–threonine, D–tyrosine, D–proline and D–phenylglycine substitutions (at i+1).

Assessing β–sheet content and stability. In evaluating the influence of various amino acid substitutions on β–turn stability, we hypothesized that total β–sheet content would serve as a good proxy for measuring the stabilizing influence that each residue or combination of residues would have on the type II' β–turn. In particular, residues that strongly stabilized the type II' β–turn would likely reinforce the β–sheet structure and increase the β–sheet content while residues that destabilized the type II' β–turn would likely disrupt or destroy the antiparallel β–sheet structure. In this regard, small changes in stabilization energy or residue geometry at the type II' β–turn of interest would be expected to be amplified throughout the length of the peptide and be detectable as measurable changes in overall β–sheet content. We chose to assess β–sheet content both qualitatively and quantitatively using CD, NMR and measurable molecular dynamics parameters. These are summarized in Table 4.1.

CD spectra were recorded for all GS analogs then divided into three groups (based on ^{1}H–NMR β–sheet content measurements); high, moderate and low β–sheet content (Figure 4.2). Peptides with high (> 67%) β–sheet content include,

dTYR–PRO, dTYR–DHP, dTYR–PIP, dPRO–PRO and dTHR–PRO. The moderate (30% – 36%) β–sheet content peptides include SAR–SAR and dPHG–PRO while the GS analogs with low (< 12%) β–sheet content include, TYR–PRO, GLY–GLY and dTYR–dPRO. The low β–sheet content peptides exhibit the characteristic random coil CD spectra with a single strong minimum at 200 nm (Brahms and Brahms, 1980). The peptides with high β–sheet have the characteristic double minimum (205 nm and 223 nm) of native GS (Izumiya et al., 1979). While this is sometimes mistaken for a helical CD spectrum, the GS spectrum is dominated by a strong absorption band at 205 nm arising from its type II' β–turn and probable aromatic side–chain interactions (Rose et al., 1985). Note that this 205 nm band is somewhat reduced for the two peptides (dPRO–PRO and dTHR–PRO) with one less aromatic side–chain. The other minimum at 223 nm is characteristic of peptides with β–sheet content. As seen in the middle panel, the peptides with moderate β–sheet content exhibit a reduced 223 nm band relative to the 205 nm band. Because of the complex influence of side–chain interactions and the unconventional β–sheet CD spectrum seen for these peptides we did not attempt to quantify their β–sheet content through detailed CD spectral analysis.

^{1}H–NMR is a much more accurate method for quantitatively measuring peptide secondary structure and conformation (Wishart et al., 1991; Wishart et al., 1992). To more fully characterize their β–sheet content and three–dimensional solution structures, all 10 GS analogs were assigned and a near complete set of

through space $^1H-^1H$ coupling (NOE) data and $^3J_{HNHA}$ coupling constants collected, see Tables 4.3–4.12. Dihedral and distance–restrained structural ensembles were further refined against proton chemical shifts to produce 'fit' structures with low (< 0.5 Å) backbone RMSD's for the high β–sheet content peptides (see Figure 4.3 for a typical high β–sheet content analog). Table 4.13 contains the structural statistics for all 10 GS analogs. Chemical shift refinement was justified as a strong correlation between experimental and empirically calculated (Case, 1995) lysine α proton chemical shifts was observed.

In order to provide internal consistency two ^1H–NMR parameters were used in the calculation of β–sheet content (Table 4.1), lysine α proton chemical shifts and lysine $^3J_{HNHA}$ coupling constants. These parameters where chosen because it is well recognized that α proton chemical shifts and $^3J_{HNHA}$ coupling constants are sensitive indicators of backbone dihedral and secondary structure (Wishart et al., 1991; Wishart et al., 1992). Lysine residues were used for β–sheet content measurements as these residues are the only residues not associated with either Turn 1 or Turn 2 and they are solely in the 'strand' regions comprising four of the six 'strand' residues. By using a parametric average, internal consistency is maintained by limiting the effects of inaccuracies such as the inherently lower precision of $^3J_{HNHA}$ coupling constant measurements (Ramirez–Alvarado et al., 1999).

Our ^1H–NMR derived classification of high, moderate and low β–sheet

content accurately describes the peptides with high and low percent β–sheet content, i.e., β–sheet and random coil conformations, respectively. However, the meaning of a moderate (30% – 36%) class is a little more nebulous. What is meant by moderate (~30%) β–sheet content? Does it mean that the peptide has a full length β–sheet that is present only 30% of the time? Or does it mean that the peptides have a very stable β–sheet that is half as long as expected? Or is it a combination of both? One way to answer these questions is to monitor the motions of these peptides over a sufficiently long period of time to assess when, where and how the β–sheet changes (if at all). Using our NMR structures for the initial set of atomic coordinates, we calculated relatively long (10 nanosecond), fully solvated, unrestrained molecular dynamics trajectories on representatives from the high (dPRO–PRO), moderate (dPHG–PRO) and low (GLY–GLY) β–sheet classes. Figure 4.4 compares the number of intramolecular hydrogen bonds over time (left panels), derived from molecular dynamics trajectories, with snapshots of typical structures for the representative peptides (right panels). Only the final 8 nanoseconds of the molecular dynamics simulations are shown as the first 2 nanoseconds are required for system equilibration. By quantitating the number of intramolecular hydrogen bonds over this length of time we clearly see that there is a significant difference between the (temporal) average number of hydrogen bonds between the high, low and moderate β–sheet classes. In particular, we see an average of 5.4 hydrogen bonds in the dPRO–PRO construct, 4.2 hydrogen bonds in the dPHG–PRO construct and just 2.6 hydrogen bonds in the GLY–GLY construct.

Furthermore, the hydrogen bonds in the GLY–GLY analog are not well correlated nor are they necessarily sequential (a requirement for β–sheet formation) so they do not likely indicate the formation of any detectable β–sheet. Based on these molecular dynamics data, we can conclude that those peptides with a moderate amount of β–sheet content exhibit a dynamic cycling of roughly half the maximum number of intramolecular hydrogen bonds. While most of the β–sheet is limited to the region around Turn 2, this hydrogen bond network is both dynamic and extensible and so we are led to conclude that the β–sheet values we obtain from our NMR studies are actually a combination of both temporal and conformational averages.

Effects of backbone chirality. It has been known for some time that backbone chirality plays an important role in defining the conformational space for β–turn formation (Rose et al., 1985). However, it has only been relatively recently that good inroads have been made into characterizing the detailed effects of chirality on β–turn formation (Gibbs et al., 1998; Aubry et al., 1985; Haque et al., 1994, 1995, 1996; Gardner et al., 1995; Stranger and Gellman, 1998; Raghothama, 1998). These studies have established the principle of backbone heterochirality as a driving force for specific types of turn nucleation. Furthermore, the degree to which backbone chirality helps define a turn depends on the type of turn. For example most 'non mirror–image' turns readily form with homochiral (all L or all D amino acids in the i+1 and i+2 positions) backbones. Mirror–image turns, on the other had, require

backbone torsion angles which are most easily adopted by heterochiral backbones (a D, L or L, D combination of amino acids at the i+1 and i+2 positions). This is shown by the fact that D amino acids at the i+1 position are known to increase type II' β–turn propensity. No doubt backbone chirality does not act alone in defining the allowed conformational space for all types of turns. Properties indirectly related to chirality which may also participate in turn formation include: side–chain/side–chain interactions, side–chain/backbone interactions and backbone/backbone interactions, where these interactions may be electrostatic or hydrophobic in nature.

We studied the effects of backbone chirality by substituting various D, L and achiral amino acids at positions i+1 and/or i+2 of Turn 1. Two analogs in particular led to an achiral modification at Turn 1, the GLY–GLY and SAR–SAR peptides. Glycine is conformationally the least restricted of all the amino acids. It was our intention to measure whether or not this conformational freedom was, in itself, enough to allow torsion angles for a type II' β–turn at Turn 1. The expectation was that if conformational freedom alone was indeed enough for type II' β–turn formation then a peptide with a high percent β–sheet content would be formed.

As shown in Table 4.1, the GLY–GLY analog actually has the lowest percent β–sheet of all the peptides. This is further illustrated by backbone conformational data in Table 4.2, where the GLY–GLY Turn 1 and Turn 2 torsion angles are found to be far from the idealized values for type II' β–turns (where three

angles are allowed to deviate by up to 30° and one angle up to 45°). The $C\alpha_i$ to $C\alpha_{i+3}$ distances in the GLY–GLY peptide are all greater than 7 Å, which is substantially different than distances of 4.6 Å typical for type II' β–turns. Interestingly, based on empirical data (Hutchinson and Thornton, 1994), the glycine–glycine sequence has the highest propensity of the coded amino acids for forming type I' β–turns. However, a type I' β–turn was not detected in this GLY–GLY analog, possibly due to Turn 2's opposing synperiplanar geometry (Muller, 1996). Synperiplanar turn geometry would direct sheet twisting in opposing directions.

Sarcosine, the N–subsituted non–coded amino acid, occupies positions i+1 and i+2 of Turn 1 in the SAR–SAR analog. The conformational freedom of sarcosine is somewhat hindered by steric interactions of its N–methyl group and the presence of this methyl group renders sarcosine devoid of an HN donor for secondary structure stabilization. Conformational analysis via quantum chemical calculations performed on di– and tri–peptides containing sarcosine (Mohle and Hofmann, 1998), have shown that type II and type VIa turns are stabilized while type I β–turns are destabilized. Our results suggest a sarcosine–sarcosine sequence does not promote type II' β–turn stabilization, as indicated by SAR–SAR's very low β–sheet content (Table 4.1). SAR–SAR's slightly higher β–sheet content over GLY–GLY may be due to transient hairpin formation around Turn 2. Average torsion angles in Turn 2 (Table 4.2), are much closer to idealized type II' β–turn

values than those of Turn 1.

Other peptides showing low β–sheet content are the two homochiral analogs, dTYR–dPRO and TYR–PRO. These analogs are the only diastereomeric isomers of the model dTYR–PRO peptide, each differing only at one chiral center. This difference clearly illustrates the necessity for heterochiral i+1 and i+2 residues in order to fulfill type II' –turn torsional angle requirements as only those peptides with two heterochiral turns have significant β–sheet content.

The apparent necessity for heterochirality for type II' β–turn stabilization is directly related to side chain orientation. Rose (Rose et al., 1985) points out that β–turns are essentially quasi 10 membered rings (see Figure 4.5). The i+1 and i+2 side chains orient either axially or equatorially on the 10 membered ring, with respect to the plane of the turn, depending on chirality. The configuration of the i+1 and i+2 residues will direct the axial (up or down) or equatorial disposition of the side chains. Interestingly, for type I, I', II and II' β–turns the i+1 residue side chains adopt an equatorial orientation and the i+2 residue side chains adopt an axial orientation. With i+1 and i+2 configurations of L–L, D–D, L–D and D–L amino acids one can direct the formation of type I, I', II and II' β–turns, respectively. The peptides in this study with high β–sheet content all exhibit D–L heterochirality with i+1 equatorial and i+2 axial side chain orientation. A representative β–turn from the dTYR–PRO ensemble is shown in Figure 4.5, where the characteristic equatorial

i+1 and axial i+2 side chain orientation is quite pronounced.

Effects of backbone steric restriction by N–substitution. Amide N–substitution has been shown to affect the allowed torsional space of peptide backbones and, more specifically, secondary structural forming propensities of amino acids (Hohle and Hofmann, 1998; Chalmers and Marshall, 1995; Takeuchi and Marshall, 1998). Proline (the only N–substituted coded amino acid) has arguably the strongest turn–forming propensity of all amino acids and has been statistically shown to occupy, to a large degree, both the i+1 and i+2 position of various turns (Hutchinson and Thornton, 1994). This high turn–forming propensity is due to the restricted conformational space of its ϕ and ψ angles which, in turn, is a product of its intra–residue 5 member pyrrolidine ring. L–proline typically adopts ϕ angles of approximately -65° +/– 15°, making it ideal for type I and type II turns whose ϕ_{i+1} angles are close to -60°. A similar rationale can be developed for the use of L–proline at position i+2 for type II' β–turns as ϕ angles of approximately -80° are preferred.

Due to the restricted torsion angle propensities of proline, we believed it would be desirable to investigate the effects of ring size and ring strain on type II' β–turn stabilization. Consequently, we made substitutions at i+2 using different sized/strained proline analogs in order to observe intra–residue ring strain on allowed torsional space and assess the affects on type II' β–turn formation. The proline ring analogs used in this study are pipecolic acid and the relatively strained

3,4–dehydroproline (Figure 4.1). With a six–membered ring, pipecolic acid was expected to have slightly more conformational freedom than proline because of its three allowable puckering modes (chair, boat, chair) and very low angle strain. 3,4–dehydro proline on the other hand, with a near planar five–membered ring, should be more sterically restricted as it is unable to pucker to the same degree as proline. Therefore, it should have a much smaller ϕ range.

Previous studies using pipecolic acid and 3,4–dehydroproline as proline homologs to probe the roles of ring size on protein function have been reported (Zhao et al., 1996). Pipecolic acid derivatives have also found roles as β–turn mimetics (Chung et al., 1998; Wu and Raleigh, 1998, 1998). Takeuchi and Marshall report strong nucleation of reverse turns when using pipecolic acid at position i+2 of model tetrapeptides based on Monte Carlo conformational searches using AMBER (Takeuchi and Marshall, 1998). Thermodynamic data highlight the differences in local conformational propensities of proline and pipecolic acid and indicate that pipecolic acid can have significant structural and kinetic differences. Our results support this conclusion as we found pipecolic acid, when substituted at position i+2, to have high β–turn nucleation propensity.

Among the sterically restricted substitutions, the dPRO–PRO analog has the highest β–sheet content of all ten GS analogs. As might be expected, the D–proline–L–proline sequence rigidly fixes the backbone dihedral angles to type II' β–turn space. By contrast, the ϕ and ψ torsional angles adopted by the dTYR–PIP

analog (Table 4.2) exhibit far–from–ideal type II' β–turn values. In fact, the angles are closer to that of a type III β–turn which has typical values of $\phi_{i+1} = -60°$, $\psi_{i+1} = -30°$, $\phi_{i+2} = -60°$ and $\psi_{i+2} = -30°$. Interestingly, this torsional preference allows for a close–to–ideal $C\alpha_i$ to $C\alpha_{i+3}$ distance of 5.2 Å, thus leading to a very stable 14 residue β–hairpin. This dTYR–PIP analog is the only example in our study which accommodated a non type II' β–turn at Turn 1. dTYR–DHP, containing 3,4–dehydroproline at position i+2 of Turn 1, also displays high β–sheet content. It appears (Table 4.2) that the conformational restriction in 3,4–dehydroproline leads to very similar ϕ and ψ angle limits as proline, regardless of its higher ring strain. The RMSD of the 3,4–dehydroproline residue over the twenty lowest energy dTYR–DHP conformers is very low (0.13 Å) indicating little puckering and inherently rigid torsional space (see Figure 4.6). As for 3,4–dehydroproline, it appears ring pucker has negligible affect on restricting the ϕ angle space. These data indicate that 3,4–dehydroproline acts as a good type II' β–turn constraint and pipecolic acid, unexpectedly, acts as a good type III β–turn constraint.

The only N–alkylated non–proline homolog (not alkylated by its own side chain) used in this study was sarcosine. As mentioned above, the SAR–SAR analog contains two sarcosine amino acids in Turn 1. The ϕ torsion angles adopted by SAR–SAR do not approach those of proline's so it can safely be assumed that side chain N–alkylation restricts torsional space much more than simple N–methylation.

This suggests that N–methylation of i+1 and i+2 cannot be used as a type II' β–turn constraint.

Effects of side chain interactions. One of the more interesting observations to arise from this work was the detection of an aromatic side–chain/side–chain interaction between the i+1 and i+2 residues among those turns with a stable type II' conformation (Figure 4.7). This interaction, which could not be detected through NOE measurements or earlier X–ray studies is manifested as a strong ring current effect arising from the phenolic tyrosine ring (i+1) coming in close proximity to the proline (or proline analog) side chain (i+2). Proline and proline analog δ proton shifts are the most dramatically affected, followed by the γ and β protons. These protons show a definite upfield shift compared to random coil proline chemical shifts (Wishart et al., 1992) and the degree of shielding observed depends on the distance from and angle to the plane of the aromatic ring.

This is the first description of an aromatic–proline interaction associated with type II' β–turns, although a similar interaction with i–1 proline–aromatic sequences has been observed for type VIa turns (Nardi et al., 2000; Nardi et al., 1997; Demchuk et al., 1997). It was hypothesized that this interaction stabilizes a cis peptide bond and may also offer an explanation behind type VIa to type VIb β–turn interconversion (Demchuk et al., 1997). The local interaction observed in our peptides may play a similar role in stabilizing the tight torsion angles of the turn. The interaction may be a consequence of van der Waals forces, and/or electrostatic

attraction between the partial charges on the aromatic ring and pyrrolidine/piperidine rings. Electrostatic interactions between the aromatic ring and the imide nitrogen may also participate in some way (Wu and Raleigh, 1998 a; 1998 b).

Although Turn 1 contained the variable sequence in this family of peptides and dictated the formation (or deformation) of the cyclic β–hairpin, we also notice a strong correlation with the unmodified Turn 2 and β–sheet content, see Figure 4.8. More specifically, a correlation with β–sheet content and Turn 2 δ2–δ3 proton chemical shift separation (anisotropy arising from the ring current) is evident. It is apparent that if Turn 1 causes a deformation of the β–sheet, there is subsequent disruption of the aromatic–proline interaction at Turn 2, to varying degrees.

4.4 Conclusions

There can be little doubt that local sequence effects are the primary causal factor for β–hairpin formation (Alba et al., 1997, 1999). To elucidate some of the structural details that determine type II' β–turn formation, we chose to examine the roles of chirality, side chain effects and N–substitution on type II' β–turn formation. Although it is obvious from our results that no single physical property is independently responsible for type II' β–turn formation, we can draw some important conclusions about the primary contributing factors.

It is clear that chirality, namely heterochirality, is an essential requirement

for type II' β–turn formation. The achiral GLY–GLY analog, with its free rotational barriers, is not able to adopt or stabilize type II' β–turn. This is also true for the achiral SAR–SAR analog. Homochirality, as shown by the low β–sheet content found with the dTYR–dPRO and TYR–PRO analogs, is also not conducive to type II' β–turn stabilization. Our results clearly support the 'equatorial–axial rule' first postulated by Rose (Rose et al., 1985) that suggested only heterochiral backbones are able to adopt side chain orientations of equatorial (for the i+1 residue) and axial (for the i+2 residue) necessary for type II' β–turn formation. According to our β–sheet content measurements, the heterochiral Turn 1 analogs have at least 67% β–sheet content. The difference between the 'background' β–sheet content of ~12% (average β–sheet content of achiral and homochiral analogs) and the minimum β–sheet content formed from the heterochiral analogs, is ~60%. Therefore, we can conclude that proper heterochirality accounts for ~60% of type II' β–turn stabilization.

Side chain steric interactions and side chain orientation also influence type II' β–turn stabilization. The dTHR–PRO analog contains proper heterochirality at Turn 1, however it lacks the aromatic side chain. dPHG–PRO on the other hand, has an aromatic side chain and proper Turn 1 heterochirality. However both analogs lack the favorable aromatic/proline interaction. Obviously threonine is unable to accommodate an aromatic side chain interaction with proline due to its lack of an aromatic ring. Nevertheless, the differences with the dPHG–PRO analog are more

subtle. Phenylglycine contains a β, as opposed to γ (as in tyrosine), aromatic ring which is surprisingly insufficient for an aromatic/proline interaction. Because these two analogs lack the favorable aromatic/proline interaction in both turns, a certain degree of β–hairpin destabilization exists. The difference between the maximum (76%) β–sheet content of these two constructs from the minimum β–sheet content aromatic/proline construct (67%) is ~10%. Based on the percent β–sheet content of these two analogs, it appears proper side chain interactions accounts for ~10% type II' β–turn stabilization.

Free rotational barriers are not a contributing factor to type II' β–turn stabilization. On the contrary, rigid, static rotational barriers are. Side chain steric restriction (through N–alkylation) is a convenient way to minimize ϕ angle rotational space. Unequivocally, proline is the best example of this. Our results indicate the proline homologs, pipecolic acid and 3,4–dehydroproline, are equivalent to proline in torsion angle space and thus are as good as proline for type II' β–turn stabilization. Analogs with L–proline (or a proline analog) at position i+2 of the turn and/or D–proline at position i+1, have a predisposition to form a β–turn. The dPRO–PRO analog indicates that D–proline is even better than an aromatic amino acid at the i+1 position for type II' β–turn stabilization. However, it is important to mention N–methylation (as in SAR–SAR) does not appear to be a strong type II' β–turn promoter. Instead N–methylation seems to enhance type II and type VIa β–

turn formation (Mohle and Hofmann, 1998). The percent β–sheet difference between dTHR–PRO (lowest of the high β–sheet content peptides) and the all proline dPRO–PRO construct, is ~20%. These results show that D–proline (i+1), pipecolic acid and 3,4–dehydroproline act as excellent type II' β–turn promoters and may account for up to 20% type II' β–turn stability (assuming that proper chirality restrictions are fulfilled). Overall these results provide one of the first detailed analysis of type II' β–turn formation. We believe this information could be particularly useful for the de novo design of peptides, proteins and peptidyl mimetics.

References

Alba, E. de, Jimenez, M.A. and Rico, M. (1997) *J. Am. Chem. Soc.* 119:175–183.

Alba, E. de, Rico, M. and Jimenez, M.A. (1999) *Protein Sci.* 8:2234–2244.

Aubry, A.; Cung, M.T. and Marraud, M. (1985) *J. Am. Chem. Soc.* 107:7640–7647.

Bax, A. and Davis, D.G. (1985) *J. Magn. Reson.* 65:355–360.

Berendsen, H.J.C., Postma, J.P.M., van Gunsteren, W.F. and Hermans, J. (1981) *Intermolecular forces; B.* Pullman: Dordrecht.

Berendsen, H.J.C., van der Spoel, D. and van Drunen, R. (1995) *Comp. Phys. Comm.* 91:43–56.

Blanco, F.J., Rivas, G. and Serrano, L. (1994) *Nat. Struct. Biol.* 1:584–590.

Blanco, F.J., Jimenez, M.A., Herranz, J., Rico, M., Santoro, J. and Nieto, J.L. (1993) *J. Am. Chem. Soc.* 115:5887–5888.

Bothner–By, A.A., Stephans, R.L., Lee, J. Warren, C.D. and Jeanloz, R.W. (1984) *J. Am. Chem. Soc.* 106:811–813.

Brahms, S. and Brahms, J. (1980) *J. Mol. Biol.* 138:149–178.

Brunger, A. (1992) *X–PLOR Version 3.1. A system for X–ray crystallography and NMR,* New Haven.

Case, D.A. The program SHIFTS 3.0 was used for empirical chemical shift calculations. SHIFTS 3.0 was obtained at http://www.scripps.edu/case/casegroup.html

Chakrabartty, A. and Baldwin, R.L. (1995) *Adv. Protein Chem.* 46:141–176.

Chalmers, D.K. and Marshall, G.R. (1995) *J. Am. Chem. Soc.* 117:5927–5937.

Chung, Y.J., Christianson, L.A., Stanger, H.E., Powell, D.R. and Gellman, S.H. (1998) *J. Am. Chem. Soc.* 120:10555–10556.

Cung, M.T., Vitoux, B. and Marraud, M. (1987) *New. J. Chem.* 11:503–510.

Das, C., Raghothama, S. and Balaram, P. (1998) *J. Am. Chem. Soc.* 120:5812–5813.

DeGrado, W.F., Summa, C.M., Pavone, V., Nastri, F. and Lombardi, A. (1999) *Annu. Rev. Biochem.* 68:779–819.

Demchuk, E., Bashford, D. and Case, D.A. (1997) *Fold. Des.* 2:35–46.

Diaz, H., Tsang, K.Y., Choo, D., Espina, J.R. and Kelly, J.W. (1993) *J. Am. Chem. Soc.* 115:3790–3791.

Dortemme, T., Ramirez–Alvarado, J. and Serrano, L. (1998) *Science* 281:253–256.

Gardner, R.R., Liang, G. and Gellman, S.H. (1995) *J. Am. Chem. Soc.* 117:3280–3281.

Gellman, S.H. (1998) *Curr. Opin. Chem. Biol.* 2:717–725.

Gibbs, A.C., Kondejewski, L.H., Gronwald, W., Nip, A.M., Hodges, R.S., Sykes, B.D. and Wishart, D.S. (1998) *Nat. Struct. Biol.* 5:284–288.

Haque, T.S., Little, J.C. and Gellman, S.H. (1994) *J. Am. Chem. Soc.* 116:4105–4106.

Haque, T.S., Little, J.C. and Gellman, S.H. (1996) *J. Am. Chem. Soc.* 118:6975–6985.

Haque, T.S. and Gellman, S.H. (1997) *J. Am. Chem. Soc.* 119:2303–2304.

Hutchinson, E.G. and Thornton, J.M. (1994) *Protein Sci.* 3:2207–2216.

Izumiya, N., Kato, T., Aoyaga, H., Waki, M. and Kondo, M. (1979) *Synthetic Aspects of Biologically Active Peptides: Gramicidin S and Tyrocidines*, New York.

Jeener, J., Meier, B.H., Bachmann, P. and Ernst, R.R. (1979) *J. Chem. Phys.* 71:4546–4553.

Kabsch, W. and Sander, C. (1983) *Biopolymers* 22:2577–2637.

Kang, Y.K., Jhon, J.S. and Han, S.J. (1999) *J. Peptide Res.* 53:30–40.

Kemp, D.S. (1990) *TIBTECH* 8:249–255.

Kessler, H., Griesingerm R., Kerssebaum, R., Wagner, K. and Ernst, R.R. (1987) *J. Am. Chem. Soc.* 109:607–609.

Kohn, W.D., Kay, C.M., Sykes, B.D. and Hodges, R.S. (1998) *J. Am. Chem. Soc.* 120:1124–1132.

Kondejewski, L.H., Farmer, S.W., Wishart, D.S., Hancock, R.E.W. and Hodges, R.S. (1996) *J. Pept. Protein Res.* 47:460–466.

Kondejewski, L.H., Farmer, S.W., Wishart, D.S., Kay, C.M., Hancock, R.E. and Hodges, R.S. (1996) *J. Biol. Chem.* 271:25261–25268.

Koradi, R., Billeter, M. and Wuthrich, K. (1996) *J. Mol. Graphics* 14:51–55.

Kumar, A., Ernst, R.R. and Wuthrich, K. (1980) *Biochem. Biophys. Res. Comm.* 95:1–6.

Kuszewski, J., Gronenborn, A.M. and Clore, G.M. (1995) *J. Magn. Reson. B* 107:293–297.

Lavigne, P., Sonnichsen, F.D., Kay, C.M. and Hodges, R.S. (1996) *Science* 271:1136–1138.

Lewis, P.N., Momany, F.A. and Scheraga, H.A. (1973) *Biochim. Biophys. Acta.* 303:211–229.

Mattos, C., Petsko, G.A. and Karplus, M. (1994) *J. Mol. Biol.* 238:733–747.

Maynard, A.J., Sharman, G.J. and Searle, M.S. (1998) *J. Am. Chem. Soc.* 120:1996–2007.

Miyamoto, S. and Kollman, P.A. (1992) *J. Comp. Chem.* 13:952–962.

Mohle, K. and Hofmann, H. (1998) *J. Peptide Res.* 51:19–28.

Muller, G. (1996) *Angew. Chem. Int. Ed. Engl.* 35:2767–2769.

Muñoz, V. and Serrano, L. (1995) *Curr. Opin. Biotech.* 6:382–386.

Nowich, J.S., Smith, E.M. and Pairish, M. (1996) *Chem. Soc. Rev.* 401–415.

Nardi, F., Kemmink, J., Sattler, M. and Wade, R.C. (2000) *J. Biomol. NMR* 17:63–77.

Nardi, F., Worth, G.A. and Wade, R.C. (1997) *Fold. Des.* 2:S62–S68.

O'Neil, K.T. and DeGrado, W.F. (1990) *Science* 250:645–652.

Raghothama, S.R., Awasthi, S.K. and Balaram, P. (1998) *J. Chem. Soc., Perkin Trans. 2* 137–143.

Ramirez–Alvarado, M., Kortemme, T., Blanco, F.J. and Serrano, L. (1999) *Bioorg. Med. Chem.* 7:93–103.

Richardson, J.S. and Richardson, D.C. (1987) *Prot. Engng.* (eds Oxender, D.L.; Fox, C.F), 149–163.

Richardson, J.S. (1981) *Adv. Protein Chem.* 34:167–339.

Ripka, W.C., De Lucca, G.V., Bach II, A.C., Pottorf, R.S. and Blaney, J.M. (1993) *Tetrahedron* 17:3609–3628.

Rose, G.D., Gierasch, L.M. and Smith, J.A. (1985) *Adv. Protein Chem.* 37:1–109.

Rothemund, S., Beyermann, M., Krause, E., Krause, G., Bienert, M., Hodges, R.S., Sykes, B.D. and Sonnichsen, F.D. (1995) *Biochemistry* 34:12954–12962.

Schenck, H.L. and Gellman, S.H. (1998) *J. Am. Chem. Soc.* 120:4869–4870.

Schwyzer, R. (1958) *Chimia* 12:53–68.

Schwyzer, R., Garrion, J.P., Gorup, B., Nolting, H. and Tun–Kyi, A. (1964) *Helv. Chim. Acta* 47:441–464.

Smith, K., Withka, J.M. and Regan, L. (1994) *Biochemistry* 33:5510–5517.

Sharman, G.J. and Searle, M.S. (1998) *J. Am. Chem. Soc.* 120:5291–5300.

Stanger, H.E. and Gellman, S.H. (1998) *J. Am. Chem. Soc.* 120:4236–4237.

Takeuchi, Y. and Marshall, G.R. (1998) *J. Am. Chem. Soc.* 120:5363–5372.

Wang, Y., Nip, A.M. and Wishart, D.S. (1997) *J. Biomol. NMR* 10:373–382.

Wilmont, C.M. and Thornton, J.M. (1988) *J. Mol. Biol.* 203:221–232.

Wishart, D.S., Sykes, B.D. and Richards, F.M. (1991) J. *Mol. Biol.* 222:311–333.

Wishart, D.S., Sykes, B.D. and Richards, F.M. (1992) *Biochemistry* 31:1647–1651.

Wishart, D.S., Willard, L. and Sykes, B.D. (1997) VADAR v1.2 (University of Alberta, Edmonton, Canada).

Wishart, D.S., Kondejewski, L.H., Semchuck, P.D., Sykes, B.D. and Hodges, R.S. (1996) *Lett. Pep. Sci.* 3:53–60.

Wu, W. and Raleigh, D.P. (1998) a. *J. Org. Chem.* 63:6689–6698.

Wu, W. and Raleigh, D.P. (1998) b. *Biopolymers* 45:381–394.

Wuthrick, K. (1986) *NMR of Proteins and Nucleic Acids*; New York.

Venkatachalam, C.M. (1968) *Biopolymers* 6:1425–1436.

Zhao, Z., Liu, X., Shi, Z., Danley, L., Huang, B., Jiang, R.-T. and Tsai, M.D. (1996) *J. Am. Chem. Soc.* 118:3535–3536.

Zhou, N.E., Kay, C.M. and Hodges, R.S. (1992) *J. Biol. Chem.* 267:2664–2670.

Table 4.1 Sequence and Percent β–Sheet Content of GS analogs

Analog[2]	Sequence														% β–sheet		
	——Turn 1——							——Turn 2——							Δδ[3]	$^3J_{HNHA}$[4]	Average[5]
dTYR–PRO	Val	dTyr	Pro	Leu	Lys	Val	Lys	Leu	dTyr	Pro	Val	Lys	Leu	Lys	74	78	76
dTYR–DHP[6]	Val	dTyr	Dhp	Leu	Lys	Val	Lys	Leu	dTyr	Pro	Val	Lys	Leu	Lys	75	63	69
dTYR–PIP[6]	Val	dTyr	Pip	Leu	Lys	Val	Lys	Leu	dTyr	Pro	Val	Lys	Leu	Lys	100	72	86
dPHG–PRO[6]	Val	dPhg	Pro	Leu	Lys	Val	Lys	Leu	dTyr	Pro	Val	Lys	Leu	Lys	37	34	36
dPRO–PRO	Val	dPro	Pro	Leu	Lys	Val	Lys	Leu	dTyr	Pro	Val	Lys	Leu	Lys	79	100	90
dTHR–PRO	Val	dThr	Pro	Leu	Lys	Val	Lys	Leu	dTyr	Pro	Val	Lys	Leu	Lys	72	61	67
GLY–GLY	Val	Gly	Gly	Leu	Lys	Val	Lys	Leu	dTyr	Pro	Val	Lys	Leu	Lys	12	0	6
SAR–SAR[6]	Val	Sar	Sar	Leu	Lys	Val	Lys	Leu	dTyr	Pro	Val	Lys	Leu	Lys	21	39	30
dTYR–dPRO	Val	dTyr	dPro	Leu	Lys	Val	Lys	Leu	dTyr	Pro	Val	Lys	Leu	Lys	0	23	12
TYR–PRO	Val	Tyr	Pro	Leu	Lys	Val	Lys	Leu	dTyr	Pro	Val	Lys	Leu	Lys	0	0	0
Residue Number	1	2	3	4	5	6	7	8	9	10	11	12	13	14			
Turn Position	i	i+1	i+2	i+3				i	i+1	i+2	i+3						

1. All peptides are cyclic. Cyclized through N and C termini, residues 1 and 14.
2. The peptides are named after the modified i+1 and i+2 residues of turn 1.
3. % β–sheet (Δδ) = (average Lysine α proton chemical shift – Lysine random coil α proton chemical shift) / (maximum Lysine α proton chemical shift – random coil α proton chemical shift) x 100.
4. % β–sheet ($^3J_{HNHA}$) = (average Lysine $^3J_{HNHA}$ – Lysine random coil $^3J_{HNHA}$) / (maximum Lysine $^3J_{HNHA}$ – average Lysine $^3J_{HNHA}$) x100.
5. % β–sheet (Average) = β–sheet (Δδ) + β–sheet ($^3J_{HNHA}$) / 2.
6. DHP = 3,4 dehydro proline, PIP = pipecolic acid, PHG = phenylglycine, SAR = sarcosine.

Table 4.2 Turn Torsion Angles[1]

Analog		ϕ (i + 1)	ψ (i +1)	ϕ (i +2)	ψ (i +2)	Cα i – Cα i+3 Distance
Type II' turn[2]		60	–120	–80	0	4.6
dTYR–PRO	Turn 1	38	–118	–77	25	5.1
	Turn 2	44	–101	–60	–15	4.9
dTYR–DHP	Turn 1	42	–123	–83	22	5.3
	Turn 2	32	–90	–54	–39	5.0
dTYR–PIP	Turn 1	–12	–74	–55	–38	5.2
	Turn 2	40	–101	–93	–8	5.2
dPHG–PRO	Turn 1	54	–110	–66	–9	4.9
	Turn 2	36	–96	–60	–15	4.9
dPRO–PRO	Turn 1	29	–130	–87	16	5.3
	Turn 2	36	–103	–89	–10	5.1
dTHR–PRO	Turn 1	48	–145	–60	–5	5.5
	Turn 2	43	–100	–63	–26	5.0
GLY–GLY	Turn 1	90	70	28	–92	8.5
	Turn 2	171	–127	–64	147	7.3
SAR–SAR	Turn 1	132	158	164	110	8.2
	Turn 2	45	–177	–60	–17	6.9
dTYR–dPRO	Turn 1	–45	78	56	–117	7.0
	Turn 2	81	–154	–54	–108	7.2
TYR–PRO	Turn 1	–71	–151	–49	176	7.8
	Turn 2	141	–148	–65	–126	7.8

1. Values derived from the average structure of a 20 peptide ensemble.
2. Idealized type II' β–turn phi and psi angles (Lewis et al., 1973). Cutoffs of 30° deviation from these angles with one angle allowed to deviate by 45° constitutes a type II' β–turn.

Table 4.3. ^{1}H–NMR Assignments (ppm) for dTYR–PRO

Amino Acid	HN	Hα	Hβ	Other	$^3J_{HNHA}$ (Hz)
Val1	8.50	4.18	1.94	γ0.87, 0.80	8.91
dTyr2	8.89	4.62	3.06,2.91	2,6H 6.91	4.06
				3,5H 6.63	
Pro3		4.41	1.89	γ1.62, 1.62	
				δ3.59, 2.55	
Leu4	7.69	4.44	1.69	γ1.50, δ0.89,	8.06
				0.81	
Lys5	8.29	4.79	1.64	γ1.28, δ1.41	9.77
				ε2.95	
Val6	8.65	4.31	1.98	γ0.85, 0.85	9.40
Lys7	8.47	4.66	1.87	γ1.37, δ1.67	7.93
				ε3.01	
Leu8	8.58	4.54	1.46	γ1.36, δ0.85,	9.16
				0.85	
dTyr9	8.74	4.66	3.02,2.92	2,6H 6.88	4.64
				3,5H 6.60	
Pro10		4.40	1.92	γ1.67, 1.67	
				δ3.66, 2.71	
Val11	7.58	4.19	2.12	γ0.88,0.88	8.54
Lys12	8.33	4.74	1.65	γ1.25, δ1.40	9.15
				ε 2.93	
Leu13	8.69	4.57	1.53	γ1.53, δ0.83,	9.16
				0.83	
Lys14	8.41	4.77	1.86	γ1.37, 1.37	7.81
				δ1.67, ε3.00	

Table 4.4. ^{1}H–NMR Assignments (ppm) for dTHR–PRO

Amino Acid	HN	Hα	Hβ	Other	$^3J_{HNHA}$ (Hz)
Val1	8.56	4.26	2.00	γ0.90, 0.83	7.32
dThr2	8.67	4.44	4.06	γ1.25	7.33
Pro3		4.56	2.25, 2.09	γ1.91, 1.91	
				δ3.98, 3.78	
Leu4	7.73	4.45	1.71	γ1.56, δ0.91,	8.43
				0.86	
Lys5	8.27	4.76	1.67	γ1.27, δ1.42	8.74
				ε2.93	
Val6	8.60	4.30	1.97	γ0.85, 0.85	8.79
Lys7	8.38	4.74	1.84	γ1.35, δ1.63	7.87
				ε2.96	
Leu8	8.54	4.54	1.47	γ1.35, δ0.83,	7.33
				0.83	
dTyr9	8.70	4.66	3.01, 2.92	2,6H 7.14	
				3,5H 6.86	
Pro10		4.43	1.96, 1.89	γ1.75, 1.69	
				δ3.67, 2.72	
Val11	7.57	4.18	2.14	γ0.89, 0.89	8.61
Lys12	8.28	4.76	1.63	γ1.27, δ1.42	8.44
				ε2.93	
Leu13	8.65	4.55	1.50	γ1.35, δ0.84,	
				0.84	
Lys14	8.44	4.65	1.86	γ1.36, δ1.66	7.70
				ε3.01	

Table 4.5. ^{1}H–NMR Assignments (ppm) for dTYR–DHP

Amino Acid	HN	Hα	Hβ	Other	$^{3}J_{HNHA}$ (Hz)
Val1	8.60	4.53	1.51	γ0.81, 0.81	7.69
dTyr2	8.82	4.62	3.01, 2.94	2,6H 7.12	3.00
				3,5H 6.84	
Deh3		5.03	5.86	γ5.75, δ4.33,	
				3.52	
Leu4	7.67	4.37	1.63	γ1.48, δ0.86,	8.24
				0.75	
Lys5	8.23	4.29	1.66	γ1.25, δ1.40	8.97
				ε2.92	
Val6	8.55	4.28	1.96	γ0.83, 0.83	8.06
Lys7	8.41	4.60	1.82	γ1.34, δ1.63	7.59
				ε2.99	
Leu8	8.51	4.50	1.42	γ1.33, δ0.82,	
				0.82	
dTyr9	8.66	4.65	2.98, 2.90	2,6H 7.12	3.19
				3,5H 6.80	
Pro10		4.41	1.93, 1.89	γ1.74, 1.68	
				δ3.66, 2.75	
Val11	7.57	4.16	2.10	γ0.87, 0.87	8.42
Lys12	8.29	4.31	1.63	γ1.23, δ1.38	8.60
				ε2.91	
Leu13	8.50	4.17	2.10	γ1.91, δ0.86,	
				0.75	
Lys14	8.38	4.68	1.83	γ1.35, δ1.63	7.87
				ε2.98	

Table 4.6. ^{1}H–NMR Assignments (ppm) for dPHG–PRO

Amino Acid	HN	Hα	Hβ	Other	$^3J_{HNHA}$ (Hz)
Val1	8.28	4.10	1.88	γ0.73,0.73	
dPhg2	8.88	5.60		2,6H 7.03	2.77
				3,5H 7.35	
				4H 6.75	
Pro3		4.38	2.07, 1.93	γ1.83, 1.83,	
				δ3.85, 3.38	
Leu4	8.31	4.37	1.48	γ1.32, δ0.77,	
				0.73	
Lys5	8.31	4.45	1.73	γ1.28, δ1.55	
				ε2.85	
Val6	8.32	4.18	1.90	γ0.77,0.77	
Lys7	8.16	4.56	1.61	γ1.21, δ1.34	7.69
				ε2.88	
Leu8	7.83	4.36	1.65	γ1.48, δ0.84,	7.69
				0.76	
dTyr9	8.48	4.74	2.86, 2.86	2,6H 7.04	3.29
				3,5H	
Pro10		4.31	1.86, 1.66	γ1.66, 1.66	
				δ3.59, 2.78	
Val11	7.56	4.04	2.00	γ0.79,0.79	8.06
Lys12	8.20	4.56	1.58	γ1.18, δ1.31	7.32
				ε2.85	
Leu13	8.40	4.39	1.44	γ1.44, δ0.74,	7.69
				0.74	
Lys14	8.25	4.53	1.77	γ1.29, δ1.56	7.33
				ε2.88	

Table 4.7. ^{1}H–NMR Assignments (ppm) for dPRO–PRO

Amino Acid	HN	Hα	Hβ	Other	$^3J_{HNHA}$ (Hz)
Val1	8.61	4.38	1.87	γ0.78, 0.71	10.26
dPro2		4.37	2.21,2.03	γ1.93, 1.78	
				δ3.77, 3.44	
Pro3		4.41	2.15, 1.99	γ1.80, 1.80	
				δ3.86, 3.62	
Leu4	7.70	4.38	1.66	γ1.44, δ0.80,	8.79
				0.73	
Lys5	8.21	4.80	1.59, 1.51	γ1.17, δ1.31	10.62
				ε2.82	
Val6	8.68	4.23	1.84	γ0.74, 0.74	8.98
Lys7	8.41	4.72	1.77	γ1.26, δ1.51	8.24
				ε2.93	
Leu8	8.59	4.48	1.41	γ1.24, δ0.82,	9.70
				0.74	
dTyr9	8.71	4.51	2.93, 2.78	2,6H 7.03	3.12
				3,5H 6.76	
Pro10		4.31	1.76, 1.86	γ1.63, 1.57	
				δ3.58, 2.51	
Val11	7.39	4.10	2.03	γ0.77,0.77	8.79
Lys12	8.19	4.78	1.53	γ1.12, δ1.28	10.43
				ε2.79	
Leu13	8.75	4.49	1.40	γ1.21, δ0.71,	8.61
				0.71	
Lys14	8.31	4.76	1.73	γ1.21, 1.29	7.88
				δ1.53, ε2.86	

Table 4.8. ^{1}H–NMR Assignments (ppm) for dTYR–dPRO

Amino Acid	HN	Hα	Hβ	Other	$^{3}J_{HNHA}$ (Hz)
Val1	8.73	3.91	1.76	γ0.59, 0.59	7.51
dTyr2	8.11	4.18	3.03, 2.70	2,6H 7.04	6.41
				3,5H 6.73	
dPro3		4.34	2.18, 1.91	γ1.78, 1.78	
				δ3.72, 3.47	
Leu4	8.17	4.19	1.72	γ1.27, δ0.62,	9.15
				0.62	
Lys5	8.20	4.31	1.70	γ1.56, δ1.35,	7.15
				1.26, ε2.85	
Val6	7.97	4.26	1.82	γ0.74, 0.74	
Lys7	7.94	4.26	1.67	γ1.26, δ1.56	7.32
				ε2.87	
Leu8	8.46	4.32	1.57	γ1.44, δ0.76,	8.79
				0.76	
dTyr9	8.27	4.23	2.91, 2.79	2,6H 7.06	8.14
				3,5H 6.74	
Pro10		4.30	1.96, 1.79	γ1.71, 1.71	
				δ3.58, 3.09	
Val11	7.51	4.00	1.87	γ0.77,0.77	8.24
Lys12	8.02	4.22	1.48	γ1.05, δ1.24	6.96
				ε2.87	
Leu13	8.54	4.26	1.67	γ1.50, 1.28	7.87
				δ0.74, 0.74	
Lys14	8.20	4.25	1.64	γ1.27, δ1.53	7.15
				ε2.78	

Table 4.9. ^{1}H–NMR Assignments (ppm) for GLY–GLY

Amino Acid	HN	Hα	Hβ	Other	$^{3}J_{HNHA}$ (Hz)
Val1	8.17	4.09	1.92	γ0.82, 0.82	
Gly2	8.70	3.89, 3.77			
Gly3	8.36	3.89, 3.80			
Leu4	7.88	4.36	1.59	γ1.48, δ0.81 0.79	7.88
Lys5	8.27	4.26	1.70	γ1.33, δ1.49 ε2.89	
Val6	8.19	4.15	1.93	γ0.78, 0.78	
Lys7	8.19	4.39	1.86	γ1.27, δ1.67 ε2.91	
Leu8	8.19	4.33	1.67	γ1.27, δ0.73, 0.73	
dTyr9	8.42	3.90	2.89	2,6H 7.06 3,5H 6.77	6.04
Pro10		4.34	1.86, 1.67	γ1.67, 1.23 δ3.59, 2.91	
Val11	7.68	4.01	2.00	γ0.82, 0.82	7.88
Lys12	8.25	4.49	1.64	γ1.24, δ1.56 ε2.87	6.14
Leu13	8.23	4.26	1.58	γ1.32, δ0.81, 0.78	
Lys14	8.28	4.41	1.66	γ1.27, δ1.57 ε2.89	

Table 4.10. ^{1}H–NMR Assignments (ppm) for dTYR–PIP

Amino Acid	HN	Hα	Hβ	Other	$^{3}J_{HNHA}$ (Hz)
Val1	8.52	4.07	1.83	γ0.82, 0.74	9.34
dTyr2	9.07	4.86	3.04,2.82	2,6H 7.08	2.50
				3,5H 6.80	
Pip3		5.01	2.13,1.38	γ1.24, 1.11	
				δ0.93, 0.02	
				ε3.58,2.82	
Leu4	7.67	4.43	1.63	γ1.49, δ0.82	9.34
				δ0.78	
Lys5	8.26	4.93	1.60	γ1.17, δ1.33	8.79
				ε2.83	
Val6	8.71	4.22	1.88	γ0.76, 0.76	
Lys7	8.41	4.74	1.8	γ1.28, δ1.54	7.96
				ε2.93	
Leu8	8.59	4.41	1.43	γ1.27, δ0.74,	8.97
				0.74	
dTyr9	8.70	4.54	2.95, 2.82	2,6H 7.06	2.95
				3,5H 6.78	
Pro10		4.37	1.89, 1.80	γ1.65,1.57	
				δ3.59,2.57	
Val11	7.43	4.07	2.06	γ0.82, 0.79	8.97
Lys12	8.21	4.95	1.59	γ1.33, 1.16	9.34
				δ1.55	
Leu13	8.71	4.45	1.44	γ1.23, δ0.82	
				δ0.78	
Lys14	8.32	4.95	1.73	γ1.21, δ1.54	7.90
				ε2.89	

Table 4.11. ^{1}H–NMR Assignments (ppm) for SAR–SAR

Amino Acid	HN	Hα	Hβ	Other	$^3J_{HNHA}$ (Hz)
Val1	8.38	4.23	1.99	γ0.84, 0.84	10.45
Sar2		4.24, 4.01		N–Me 3.22	
Sar3		4.24, 4.12		N–Me 3.15	
Leu4	7.87	4.42	1.69	γ1.60, δ0.90, 0.90	
Lys5	8.08	4.27	1.67	γ1.27, δ1.38 ε2.99	7.10
Val6	8.24	4.00	2.04	γ0.93, 0.89	8.45
Lys7	8.31	4.54	1.70	γ1.29, δ1.42 ε2.96	8.65
Leu8	8.40	4.40	1.67	γ1.38, δ0.84, 0.80	
dTyr9	8.55	4.48	3.15, 2.84	2,6H 7.13 3,5H 6.84	5.35
Pro10		4.40	1.93	γ1.78, 1.72 δ3.67, 2.87	
Val11	7.68	4.14	2.08	γ0.92, 0.88	8.35
Lys12	8.35	4.53	1.72	γ1.31, δ1.43 ε2.95	8.25
Leu13	8.47	4.44	1.55	γ1.38, δ0.85, 0.82	
Lys14	8.25	4.42	1.78	γ1.35, δ1.68	6.50

Table 4.12. ^{1}H–NMR Assignments (ppm) for TYR–PRO

Amino Acid	HN	Hα	Hβ	Other	$^{3}J_{HNHA}$ (Hz)
Val1	7.70	4.05	2.00	γ0.79, 0.79	
Tyr2	8.32	4.10	2.87	2,6H 7.04	
				3,5H 6.72	
Pro3		4.36	2.14, 1.88	γ1.72, 1.72	
				δ3.65, 3.42	
Leu4	7.64	4.11	1.69	γ1.39, δ0.69,	8.61
				0.63	
Lys5	8.04	4.17	1.71, 1.65	γ1.28, 1.32	
				δ1.43 ε2.84	
Val6	7.76	4.06	1.99	γ0.84, 0.84	7.51
Lys7	8.18	4.27	1.73, 1.63	γ1.30, δ1.34	
				ε2.88	
Leu8	8.04	4.34	1.56	γ1.43, δ0.77,	7.51
				0.73	
dTyr9	7.71	4.40	2.80	2,6H 7.02	7.33
				3,5H 6.72	
Pro10		4.26	1.91, 1.81	γ1.67, 1.62	
				δ3.56, 2.92	
Val11	7.91	3.93	1.89	γ0.80, 0.80	7.32
Lys12	8.10	4.12	1.65, 1.58	γ1.23, δ1.31	6.34
				ε2.86	
Leu13	7.92	4.27	1.65	γ1.36, δ0.78,	
				0.73	
Lys14	8.31	4.40	1.68, 1.55	γ1.21, δ1.28	5.77
				ε2.80	

Table 4.13 Structural Statistics for GS analogs

	dPRO–PRO	dTYR–PIP	dTYR–PRO	dTYR–DHP	dTHR–PRO
Ebond[1]	4.31 +/– 0.56	3.74 +/– 0.74	1.21 +/– 0.32	10.03 +/– 0.6	4.34 +/– 0.50
Eangle[1]	22.78 +/– 1.99	28.79 +/– 3.07	12.01 +/– 1.36	70.8 +/– 1.71	24.17 +/– 3.05
Eimproper[1]	3.84 +/– 0.86	4.85 +/– 0.62	1.13 +/– 0.29	67.91 +/– 0.99	5.56 +/– 0.94
Ecdih[1]	1.20 +/– 0.52	2.19 +/– 0.78	0.29 +/– 0.28	1.82 +/– 0.24	1.84 +/– 0.55
Enoe[1]	17.99 +/– 5.60	18.82 +/– 4.12	8.29×10^{-2} +/– 9.56×10^{-2}	11.13 +/– 1.51	31.59 +/– 3.91
RMSD–bond[2]	4.07×10^{-3} +/– 2.58×10^{-4}	3.71×10^{-3} +/– 3.61×10^{-4}	2.11×10^{-3} +/– 2.7163×10^{-4}	6.15×10^{-3} +/– 1.83×10^{-4}	4.09×10^{-3} +/– 2.40×10^{-4}
RMSD–angle[2]	0.55 +/– 2.37×10^{-2}	0.61 +/– 3.20×10^{-2}	0.39 +/– 2.24×10^{-2}	0.97 +/– 1.17×10^{-2}	0.57 +/– 3.59×10^{-2}
RMSD–improper[2]	0.46 +/– 5.07×10^{-2}	0.49 +/– 3.18×10^{-2}	0.24 +/– 3.03×10^{-2}	1.54 +/– 1.25×10^{-2}	0.55 +/– 4.73×10^{-2}
RMSD–cdih[2]	0.78 +/– 0.12	0.94 +/– 0.16	0.29 +/– 0.15	0.86 +/– 5.76×10^{-2}	0.87 +/– 0.13
RMSD–noe[2]	6.18 +/– 9.41×10^{-3}	5.93×10^{-2} +/– 6.28×10^{-3}	7.46 +/– 5.63×10^{-3}	7.63×10^{-2} +/– 5.19×10^{-3}	9.84×10^{-2} +/– 6.06×10^{-3}
Evdw ave.[1]	66.99 +/– 9.39	151.50 +/– 9.24	64.47 +/– 6.48	98.39 +/– 11.18	105.71 +/– 10.91
NOEviol. > 0.2 Å	2.85 +/– 0.73	2.50 +/– 0.98	0	1.70 +/– 0.71	5.00 +/– 1.26
NOEviol. > 0.5 Å	5.00×10^{-2} +/– 0.22	0.10 +/– 0.30	0	0	5.00×10^{-2} +/– 0.22
NOEviol. > 1.0 Å	0	0	0	0	0
RMSD[2] (heavy)	0.67	0.77	1.11	0.77	1.03
RMSD[2] (backbone)	0.37	0.34	0.48	0.28	0.56

1. Energies are reported in Kcal mol^{-1} plus or minus the standard deviation.
2. RMSD's are reported in Å plus or minus the standard deviation.

Table 4.13 Structural Statistics for GS analogs

	dPHG–PRO	SAR–SAR	GLY–GLY	dTYR–dPRO	TYR–PRO
Ebond[1]	7.82 +/– 0.51	5.52 +/– 1.09	12.77 +/– 3.58	2.99 +/– 0.58	2.29 +/– 0.71
Eangle[1]	61.76 +/– 1.58	28.61 +/– 3.67	60.34 +/– 6.02	23.69 +/– 4.11	15.37 +/– 3.44
Eimproper[1]	7.52 +/– 0.76	3.27 +/– 0.96	13.98 +/– 6.41	3.62 +/– 1.05	1.79 +/– 0.88
Ecdih[1]	1.89 +/– 0.41	0.56 +/– 0.52	0.11 +/– 0.27	3.80×10^{-2} +/– 0.11	3.44×10^{-2} +/– 0.12
Enoe[1]	8.49 +/– 2.17	12.86 +/– 2.17	2.53 +/– 3.13	17.97 +/– 3.67	6.93 +/– 7.78
RMSD–bond[2]	5.45×10^{-3} +/– 1.75×10^{-4}	4.68×10^{-3} +/– 4.42×10^{-4}	7.16×10^{-3} +/– 9.98×10^{-4}	3.33×10^{-3} +/– 3.36×10^{-4}	2.89×10^{-3} +/– 4.30×10^{-4}
RMSD–angle[2]	0.91 +/– 1.16×10^{-2}	0.64 +/– 3.95×10^{-2}	0.93 +/– 4.75×10^{-2}	0.56 +/– 4.74×10^{-2}	0.45 +/– 4.89×10^{-2}
RMSD–improper[2]	0.64 +/– 3.31×10^{-2}	0.45 +/– 5.87×10^{-2}	0.88 +/– 0.20	0.42 +/– 6.09×10^{-2}	0.30 +/– 6.55×10^{-2}
RMSD–cdih[2]	0.89 +/– 0.10	0.69 +/– 0.29	0.17 +/– 0.28	8.59×10^{-2} +/– 0.18	7.57×10^{-2} +/– 0.18
RMSD–noe[2]	6.10×10^{-2} +/– 7.10×10^{-2}	0.13 +/– 1.04×10^{-2}	5.83×10^{-2} +/– 5.42×10^{-2}	0.21 +/– 2.19×10^{-2}	8.96×10^{-2} +/– 5.94×10^{-2}
Evdw[1] ave.	205.66 +/– 9.78	176.15 +/– 16.23	152.56 +/– 38.30	98.83 +/– 20.29	85.45 +/– 12.08
NOEviol. > 0.2 Å	1.35 +/– 0.48	1.30 +/– 0.56	0.35 +/– 0.48	2.45 +/– 0.59	0.70 +/– 0.71
NOEviol. > 0.5 Å	0	0	0	0	0.15 +/– 0.36
NOEviol. > 1.0 Å	0	0	0	0	0
RMSD[2] (heavy)	0.81	2.62	3.11	3.02	3.08
RMSD[2] (backbone)	0.31	1.41	2.04	1.59	1.68

1. Energies are reported in Kcal mol^{-1} plus or minus the standard deviation.
2. RMSD's are reported in Å plus or minus the standard deviation.

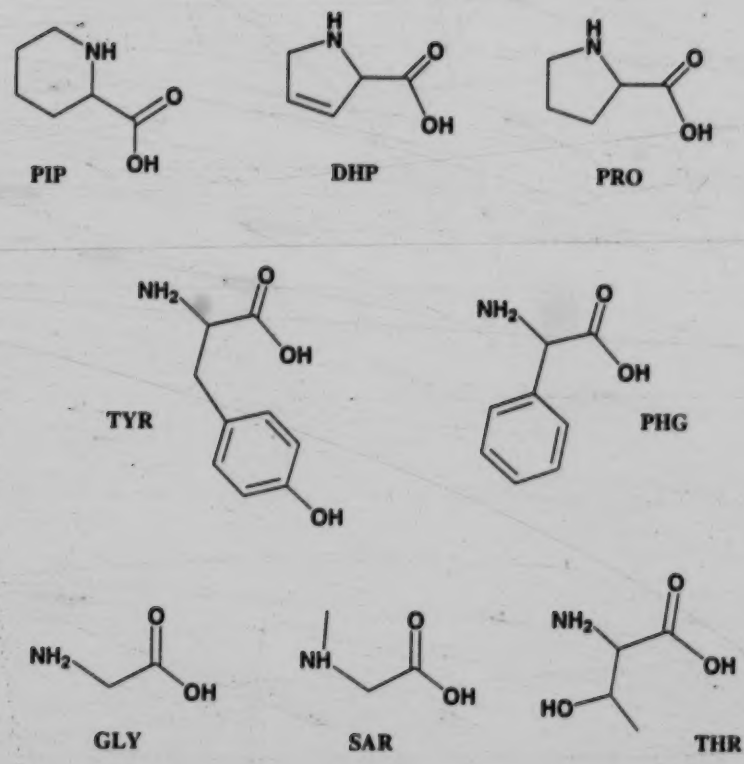

Figure 4.1. Amino acids at positions i+1 and i+2 in both Turn 1 and Turn 2. PIP = pipecolic acid, DHP = 3,4 dehydroproline, PRO = proline, TYR = tyrosine, PHG = phenylglycine, GLY = glycine, SAR = sarcosine and THR = threonine.

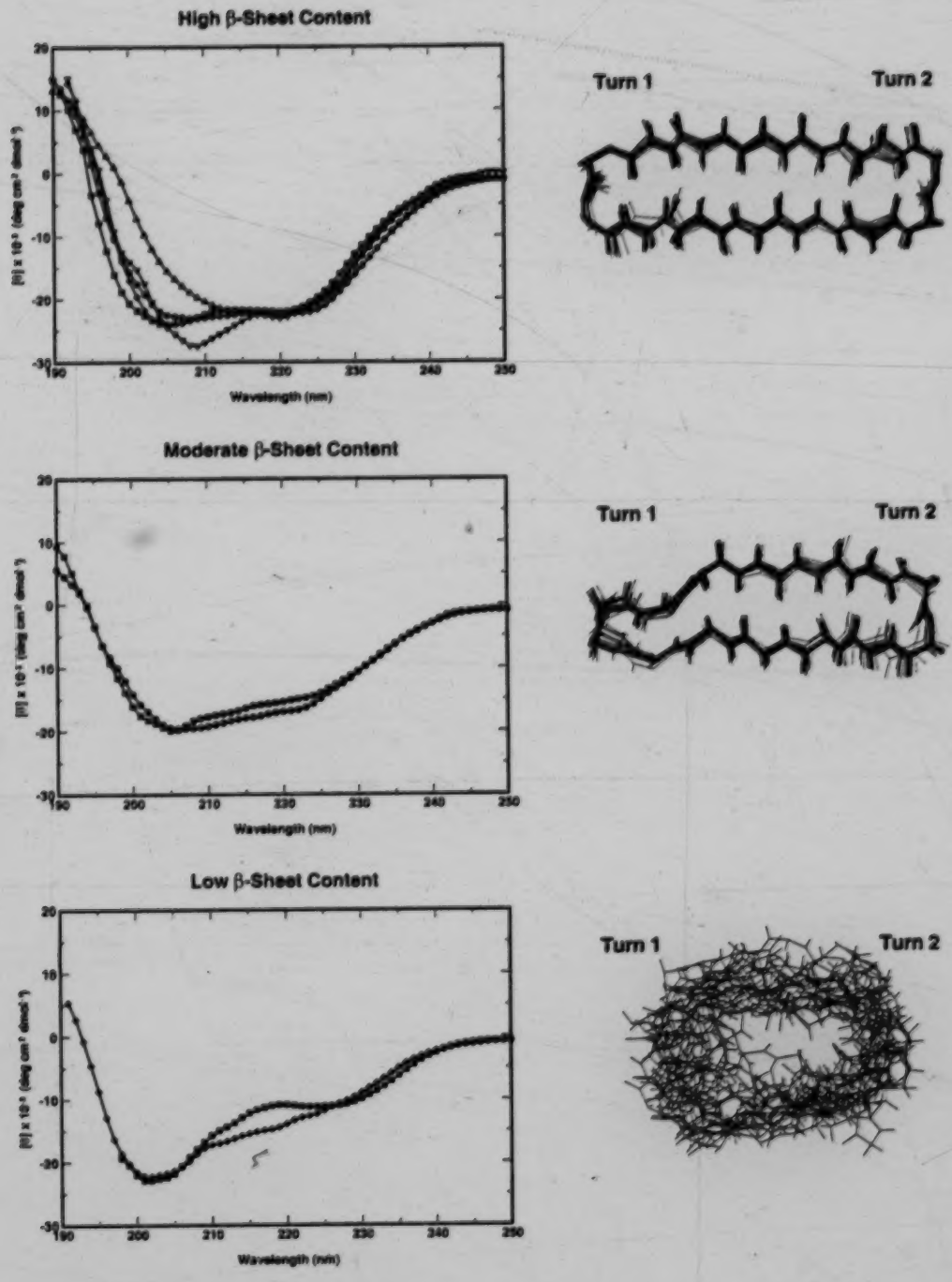

Figure 4.2. See next page.

Figure 4.2. The panels on the left contain CD spectra for the high (>67%) β-sheet content peptides. ♦ = dTYR-DEH, ▲ = dPRO-PRO, ● = dTYR-PIP, ■ = dTYR-PRO, ▼ = dTHR-PRO. These curves contain a second maxima between 220-225 nm. Note: the two 'irregular' shaped curves belong to the Turn 1 aromatic-less constructs, dPRO-PRO and dTHR-PRO. The middle panel contains CD for the moderate (30 – 36%) β-sheet content peptides. ● = dPHG-PRO, ■ = SAR-SAR. The bottom panel conatins CD spectra for the low (< 12%) β-sheet content peptides. ■ = dTYR-PRO, ♦ = TYR-PRO, the far UV wavelengths were unattainable for the GLY-GLY construct. The panels on the right contain the NMR derived ensemble (20 structures) for the corresponding high (dPRO-PRO), moderate (dPHG-PRO) and low (GLY-GLY) β-sheet structures.

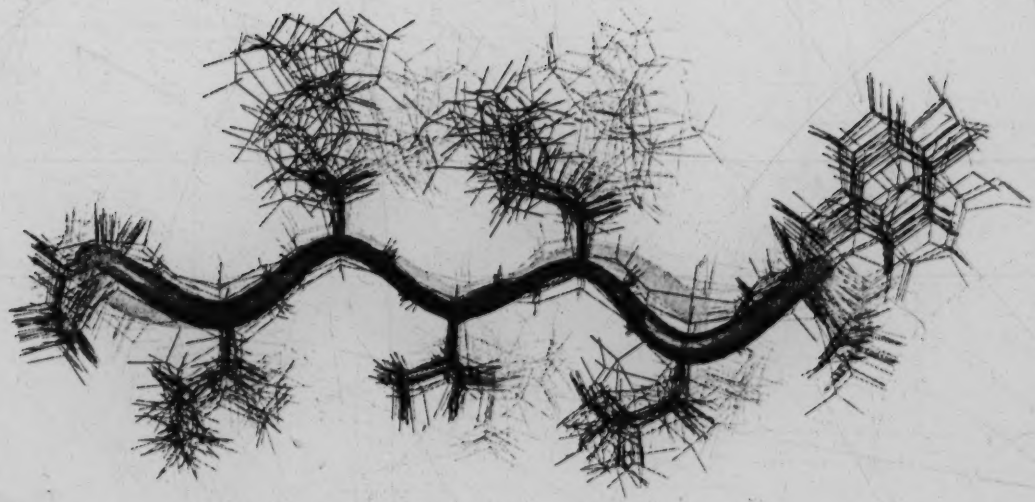

Figure 4.3. A typical low backbone RMSD of a high β–sheet content peptide. A 20 structure ensemble of dPRO–PRO is shown.

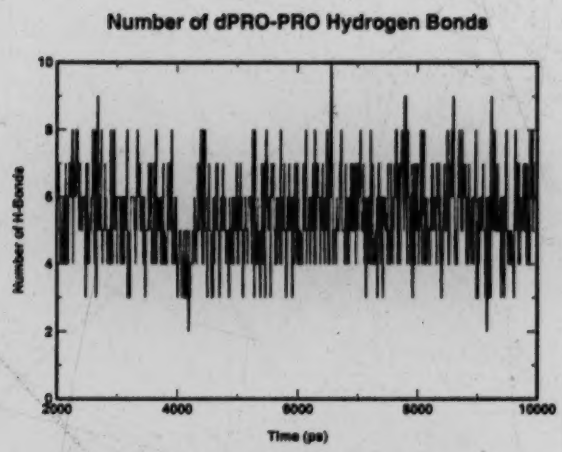

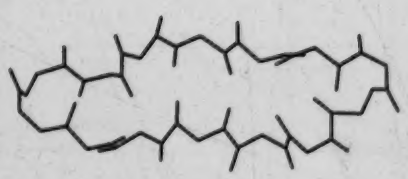

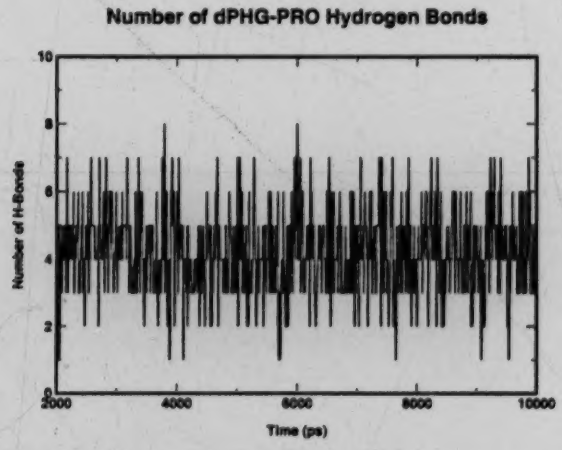

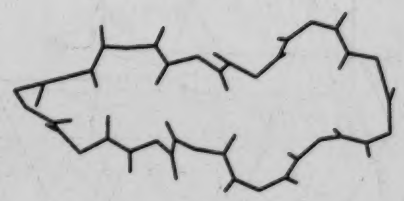

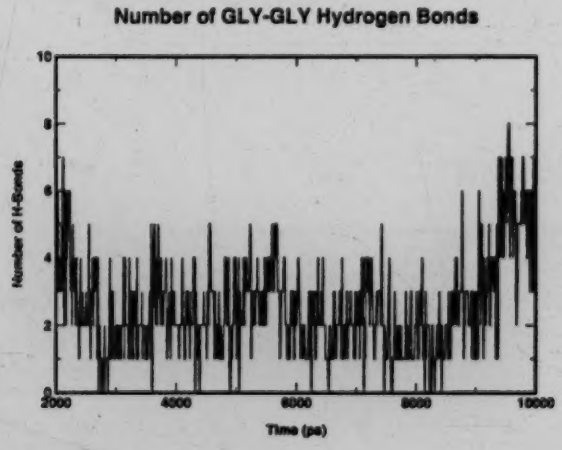

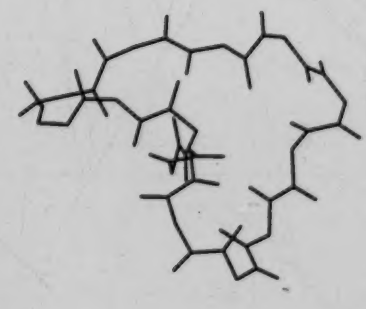

Figure 4.4. See next page.

Figure 4.4. The panels on the left contain molecular dynamics trajectories for representative high (dPRO–PRO), moderate (dPHG–PRO) and low (GLY–GLY) β–sheet content peptides. The trajectories show the number of intramolecular hydrogen bonds formed (every 10 picoseconds) over the last 8 nanoseconds (8000 picoseconds). The first 2 nanoseconds are not shown as this is the equilibration time for these peptides. The panels on the right are atomic coordinate 'snapshots' at 5580 picoseconds. A twisted β–sheet is clearly visible for the dPRO–PRO construct along with a random coil structure for the GLY–GLY construct.

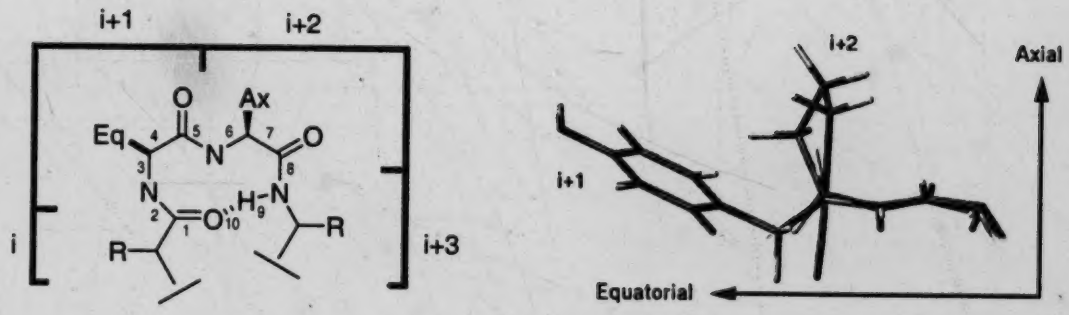

Figure 4.5. On the left, the β–turn illustrating the pseudo 10 membered ring and the **Eq**uatorial (i+1) and **Ax**ial (i+2) side chains. The panel on the right shows a side view of a turn from a representative dTYR–PRO structure. The equatorial tyrosine (i+1) and the axial proline (i+2) side chain orientations are very distinct.

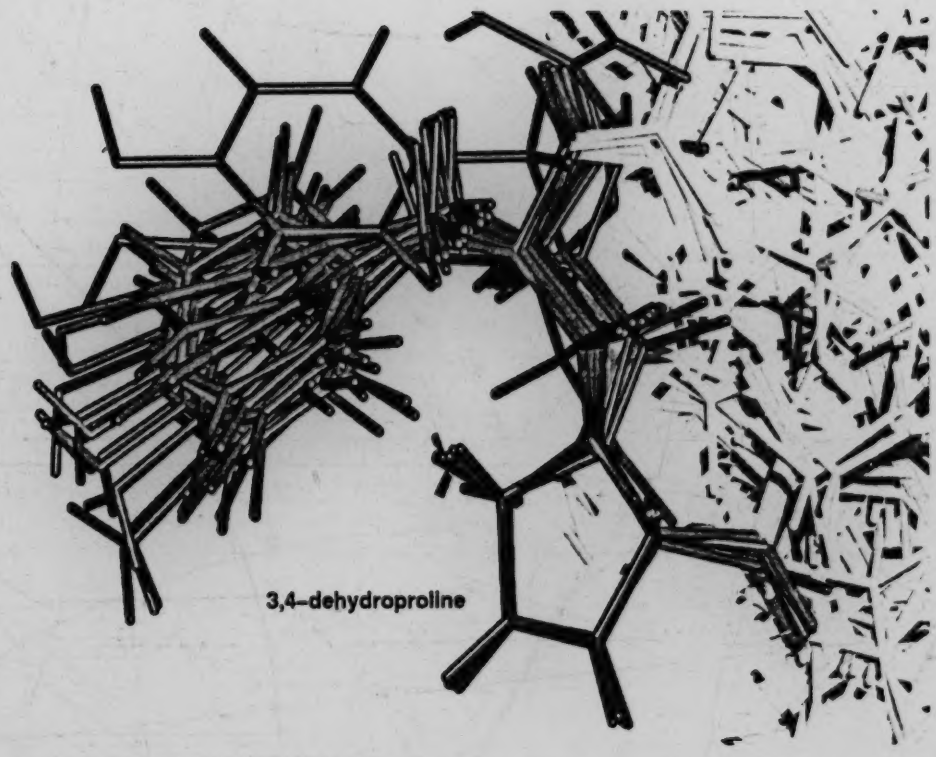

Figure 4.6. A side–chain superimposition of the minimal 3,4–dehydroproline ring pucker, imparted from the 3,4 unsaturation.

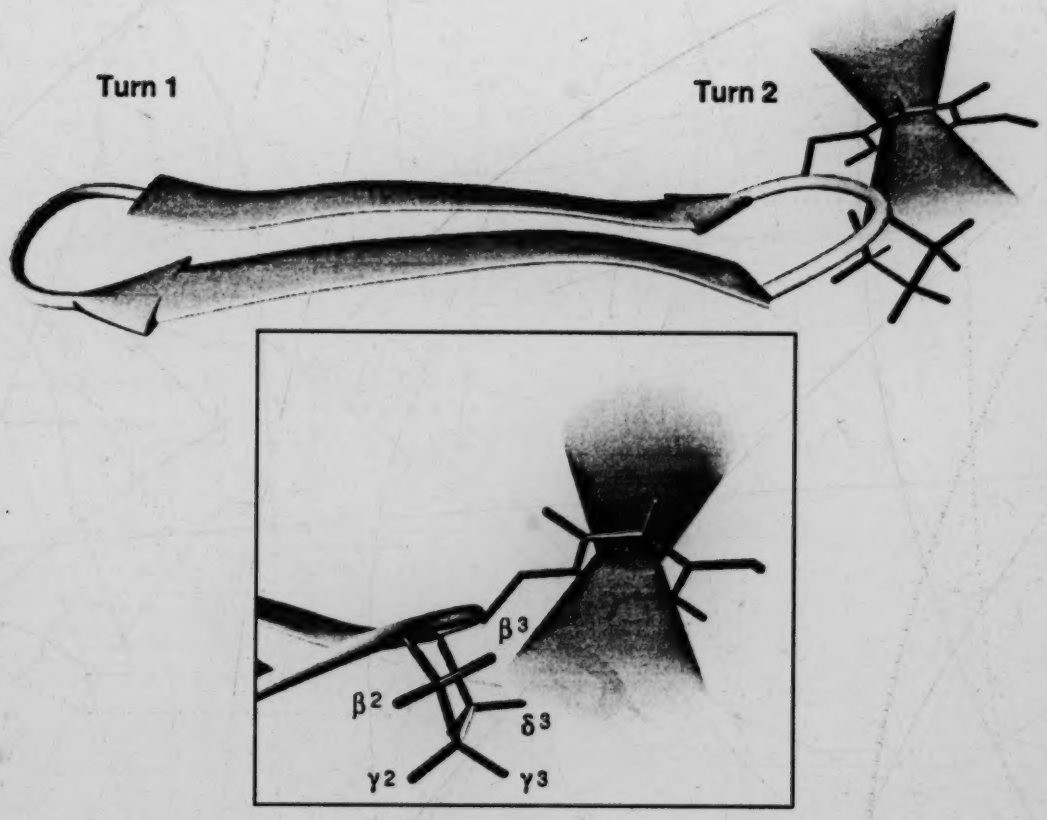

Figure 4.7. The aromatic/proline interaction. A chemical shift refined dPRO–PRO structure (side view), with a schematic representation of the tyrosine anisotropy cone of the i+1 residue in Turn 2. The inset has a close view of the turn with labeled i+2 proline protons, illustrating the spacial proximity of side chains. The δ3 hydrogen lies almost directly under the aromatic ring and is thus shielded the most.

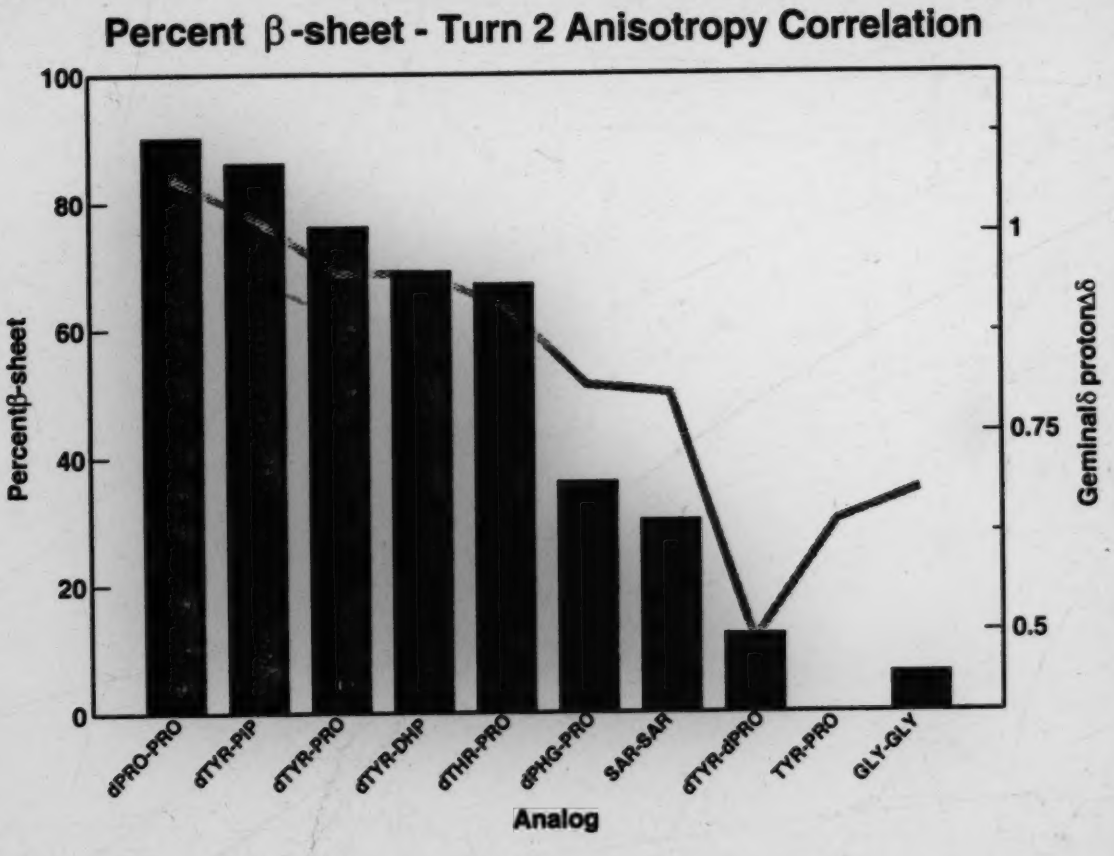

Figure 4.8. The correlation between percent β–sheet content (black bars, left axis) and geminal, δ proton proline chemical shift anisotropy (gray line, right axis). The amount of separation between the two geminal δ hydrogens of Turn 2 (in ppm), shows a strong correlation with the amount of overall β–sheet content. This difference in δ proton anisotropy is related to the amount of deformation in the β–sheet, or more specifically the amount of instability in Turn 2. With decreasing β–sheet content, the tyrosine side chain loses optimal equatorial:axial (i+1, i+2) interaction and i+2 experiences less anisotropy.

Chapter 5*

Folding and Unfolding of Small Cyclic β–sheet Peptides (GS Analogs)

5.1 Introduction

The as–yet unsolved link between protein sequence and prtoein structure is the basis for what has become known as the protein–folding problem (Honig, 1999; Dobson et al., 1998). This problem actually consists of two primary parts (Muñoz et al. 1998): 1) understanding how sequence determines structure and 2) understanding the kinetics and mechanisms of protein folding. It is the latter area where recent experimental and computational techniques have made significant inroads in the study of protein folding. Some techniques that have seen recent application in the study of protein folding include: Nuclear Magnetic Resonance (NMR) (Dobson et al., 1994; Balbach et al., 1995; Dyson and Wright, 1998; Dobson and Hore, 1998), laser induced temperature–jump methods (T–jump) (Muñoz et al. 1997; Hagen and Eaton, 2000) and molecular dynamics (MD) simulations (Karplus and Sali, 1995; Ferrara et al., 2000). In this study we have combined both experimental (T–jump and NMR) and theoretical methods (MD) to help elucidate the mechanism and kinetics of β–hairpin structure folding and unfolding.

---

* This chapter is part of an ongoing collaboration with Dr. Brian Dyer and Shelia Maness from the Los Alamos National Lab.

One approach to studying protein folding and unflolding involves the use of engineered protein models or protein fragments (Muñoz et al. 1998; Eaton et al., 1997). The information gained from model peptides is important, as these systems are thought to correspond to structural elements found at various times during the folding process. Furthermore, the relative simplicity of these small structural elements, compared to large proteins, allows a more detailed study of their formation and stability (Dinner et al., 1999). Model α–helical peptide systems, both synthetic and natural, have been used extensively over the last 40 years to study the kinetics of helix formation (Williams et al., 1996; Thompson et al., 1997). In contrast, there have been very few β–hairpin models developed to study the kinetics of β–sheet formation.

Recently, however, a linear β–hairpin model has been shown to be amenable to the study of β–sheet folding and unfolding (Muñoz et al. 1997). This particular β–hairpin model is a 16 residue fragment isolated from the C–terminal of the Ig–binding domain of protein G (sequence – GEWTYDDATKTFTVTE). The peptide contains the intrinsic fluorophore tryptophan, hence fluorescence spectroscopy can be used to monitor folding reactions of this peptide using temperature jump (T–jump) experiments. Thermodynamic parameters have been measured (following a laser induced 15° C T–jump) yielding a $\Delta H = -11.6$ kcal/mol and a $\Delta S = -39$ cal/mol/K for the folding transition. These results indicate the peptide contains β–sheet content of approximately 80% at 278 K and less than 10% at 360 K. These

thermodynamic results were subsequently used to determine the kinetics of folding (τ_f=6 μs). This folding time is about 30 times slower than that of α–helix formation in peptide systems of similar size (Williams, et al. 1996).

Although the study by Muñoz, et al. has elucidated much about the kinetics of β–hairpin formation, the exact mechanisms of β–sheet formation are still unclear. Debate has ensued concerning the mechanism of β–hairpin formation, with evidence to support two commonly held views (Kolinski, et al. 1999). One view is that the initial step in folding is the formation of the β–turn (Muñoz, et al. 1998) followed by intrastrand hydrogen bond formation. The other view posits that the initial step in folding is a hydrophobic collapse, followed by folding interactions propagating outward to create a β–hairpin (Dinner et al., 1999). Further experimental data is needed to test these views and resolve questions concerning the mechanism of β–hairpin formation.

To shed more light on the mechanism of β–hairpin formation and folding, we have chosen to use a cyclic β–hairpin model. Our model is based on gramicidin S (GS) and its synthetic analogs (Wishart et al., 1996; Kondejewski et al., 1996). The analogs used in this study are summarized in Table 5.1. GS is a cyclic, amphipathic decapeptide composed of two evenly spaced type II' β–turns separated by an antiparallel β–sheet. This peptide model is well suited to study β–hairpin formation and stability because GS analogs can be readily synthesized, the β–hairpin

structure is highly populated and this structure is largely solvent and solute independent (Wishart et al., 1996). Furthermore, since these peptides are amphipathic and contain two β–turns (Gibbs et al., 1998) they are thought to have the three key physical attributes important to β–hairpin formation (see Figure 5.1). The first feature is a hydrophobic face or site. The GS analogs used in this study actually contain two hydrophobic sites, the hydrophobic face of the peptide (containing Leu and Val residues) and the β–turn (containing Val, Tyr, Pro and Leu residues). The second feature is a β–turn, actually two type II' β–turns in this case.

By using the GS β–hairpin model in a combination with experimental data from T–jump IR, NMR and MD computer simulations, it was our expectation that these data would help answer important questions about the formation of β–hairpins. We have selected three β–hairpin (6, 10 and 14 residue) GS analogs (Table 5.1), that have previously been characterized via CD and NMR spectroscopy (Gibbs et al., 1998), to use as model β–hairpin fragments. T–jump kinetic data show an unexpectedly fast relaxation and subsequent refolding rate. This appears to be orders of magnitude faster than the β–hairpin found in the linear protein G fragment. These results prompted us to use MD in an effort to determine how peptide structure, during the folding reaction, influences the rate of β–hairpin folding.

5.2 Materials and Methods

Peptide Synthesis and Purification. All three peptides were synthesized on an

Applied Biosystems 430A automated peptide synthesizer using standard t–butyloxycarbonyl (Boc) chemistry on 2Cl–Z–PAM resin. Orthogonally protected Boc–ε–formyl lysine was used instead of Boc–ε–2Cl–Z lysine to prevent complications arising from the cyclization process. Following synthesis, peptides were cleaved from the resin with anhydrous HF in the presence of 10% anisole and 2% 1, 2–ethanedithiol. The crude linear peptides were purified prior to cyclization using reversed–phase HPLC on a Synchropak RP–4 preparative C–8 column. Cyclizations were performed at peptide concentrations of 2 mg/mL in N,N–dimethyformamide using 3 equivalents each of benzotriazoyl N–oxytri–dimethylaminophosphonium hexafluorophosphate, 1–hydroxybenzotriazole and diisopropylethylamine. Cyclization was complete after 12 hours. Then, after cyclization, the formyl protecting group was removed by heating the peptide to 37 °C in 10% methanolic HCl for 24 hours. The resulting cyclic peptides were purified by reverse phase HPLC using a linear AB gradient where solvent A is 0.1% aqueous TFA and solvent B is 0.1% TFA in acetonitrile. Peptide composition was verified via electrospray mass spectrometry.

Sample Preparation for Infrared Spectroscopy. Samples were dissolved in either D_2O or a mixture of 50/50 weight percent D_2O and glycerol. Sample concentrations were measured with a Hewlett Packard 8452A Diode Array Spectophotometer using the ultraviolet absorbance (λ = 274) of tyrosine. Peptide concentrations were determined to be 8 mM for the 6–mer, 5 mM for the 10–mer and 2 mM for the 14–mer.

Infrared Spectroscopy. Prior to T–jump analysis, static Fourier transform infrared (FTIR) spectra were measured on a BioRad FTS–40 interferomter to determine the temperature dependence (stability) of the peptide structure. Spectra were acquired over a broad temperature range (from 5–85 °C) using approximate 5 °C intervals. Single–beam transmittance spectra were collected for both a peptide sample and a reference in quadruplicate with 32 scans per set at each temperature monitored. These data were subsequently converted to absorbance measurements. The temperature dependent data show the approximate change in optical density one should expect between two different temperatures.

Temperature–jump Spectroscopy. All T–jump IR studies were performed by Shelia Maness (LANL). Transient infrared absorption of the amide I' stretching of the peptide sample and reference were monitored using a Laser Photonic diode with a range of approximately 1600 cm^{-1} to 1700 cm^{-1} and detected using a Kolman Technologies Infrared detector. A Quanta–Ray DCR–4 Nd:YAG laser was used in combination with a Raman shifter filled with H_2 gas to generate a two micron pump beam — the source for the temperature jump (see Figure 5.2). The pump beam generates bulk heating of the solvent while the probe beam monitors the amide I' stretching and vibrational changes in the peptide. Steady–state voltage measurements, between the probe beam and detector, are recorded prior to and after each data collection period. The steady–state voltages (measured in the absence of the pump beam) are proportional to the amount of transmittance. The steady–state voltages are equivalent to the initial intensity (I_o). In order to convert transmittance

to overall change in absorbance (ΔA) the following equation is used:

$$[5.1] \quad \Delta A = -\log [(I_o + \Delta I)/I_o]$$

Where ΔI is the change in intensity measured when both the pump and probe beams are irradiating the peptide sample (during a typical T–jump experiment).

NMR Spectroscopy. The GS–14 temperature series experiment was performed on a Varian Unity INOVA 500 MHz NMR spectrometer. The GS–14 sample was prepared in 500 µl 90 % H_2O/10% D_2O to give a final concentration of 1–2 mM. 0.1 mM 3–(trimethylsilyl)–1–propanesulfonic acid (DSS) was added as an internal chemical shift reference. The sample pH ranged between 4.5–5.5. Spectra were collected at 1K increments from 298 to 328K.

Unrestrained Molecular Dynamics. A distance restrained representative structure of GS–14 was solvated in a rectangular box with an average of 900 SPC (Berendsen et al., 1981) water molecules. Simulations ranging from 3 to 10 nanoseconds in length over temperatures of 300 to 600 K were calculated using the software package GROMACS v2.0 (Berendsen, et al., 1995). During the simulations, weak individual coupling of peptide and solvent to a bath of constant temperature was maintained using a coupling time τ_T of 0.1 picoseconds was used for each temperature. Pressure coupling to a pressure bath (reference pressure 1 bar) was performed with a coupling time τ_P of 1.0 ps. The SETTLE algorithm was used to constrain water bond lengths and angles (Miyamoto and Kollman, 1992).

5.3 Results and Discussion

T–jump IR. A common approach to study fast folding events is to initiate a rapid change in solution conditions to induce protein unfolding (Callender, et al. 1998). Subsequent to this change, a measurement of the relaxation (unfolding) rate of the molecule is recorded, usually via optical spectroscopy. In this study, we have chosen to use laser–induced T–jump spectroscopy to induce rapid solution condition changes to initiate the unfolding reaction, followed by IR spectroscopy for measurement of molecular relaxation rates. Laser–induced T–jump is an excellent method to study protein folding because as one jumps from one temperature to another, it changes the equilibrium position of the ensemble of possible states (conformers) faster than processes that maintain the systems equilibrium (Eigen and De Maeyer, 1963).

IR absorption spectroscopy of the amide I mode in polypeptides (characteristic of backbone amide carbonyl stretching) is a particularly useful probe to study protein folding. Amide I stretching is a reliable indicator of secondary structure, due to its sensitivity to hydrogen bonding, dipole–dipole interactions and geometry of the peptide backbone (Susi and Byler, 1986). In the present study, D_2O was used as solvent. This is because H_2O can overlap the amide I band as far down as 1200 cm^{-1} (Callender et al., 1998). It is important to note, there is a nomenclature distinction between protonated and deuterated amide I modes. Deuterated amide I modes are represented as amide I'. Empirical evidence suggests that: α–helical region amides absorb at ~1654 cm^{-1}; β–sheet amides absorb at ~1615

and ~1675 cm^{-1}; β–turns absorb at ~1668, ~1675, ~1686 cm^{-1}; and random coil amides absorb at ~1645 cm^{-1} (Callender et al., 1998). For these studies we followed the presence or absence of absorption bands at approximately 1618 cm^{-1}.

Our model β–hairpin system shows very fast relaxation kinetics, in response to a laser induced T–jump. Relaxation appears to be complete, for all peptides, after just 60 nanoseconds (ns). This is orders of magnitude faster than the time measured for linear peptide β–hairpin formation (Muñoz et al. 1997). Figure 5.3 shows the change in optical density (OD) as a function of time for each of the three GS analogs. These curves illustrate the speed at which the peptides unfold (maximum change in optical density) in just 60 ns, then slowly return to a folded state (no change in optical density) after a few microseconds. Our hypothesis is that the protein G hairpin formation is limited by diffusion, whereas diffusion is not a factor with these cyclic peptides. T–jump IR kinetic studies conducted in 50% glycerol (data not shown), support this hypothesis. The glycerol studies indicate, that there is no viscosity dependence on the kinetic rates of the cyclic peptides. Indeed, the (un)folding rate is the same no matter what solvent is used. Thus, these T–jump IR measurements appear to give an intrinsic β–sheet formation rate, in the absence of diffusion. Although there is no viscosity dependence on the rates of (un)folding, there is a slight dependence on the size of the peptide where the rate of (un)folding is longest for GS–14 (i.e. 59 ns).

Table 5.2 summarizes the results of the T–jump experiments. On average, a

temperature increase of approximately 10 °C followed each laser pulse. Following the T–jump, changes in absorbance at 1618 cm^{-1} were recorded.

NMR. Proton chemical shifts are very sensitive to their local environments, thus they are good indicators of structure, in particular, secondary and tertiary structure (Wishart and Sykes, 1994). Because of this, their utility in monitoring protein folding has been well established (Dyson and Wright, 1998; Dobson and Hore, 1998). It has been shown that the line width of a particular resonance in the NMR spectrum gives important indications as to the type of environment the nuclei resides in. Generally speaking, broad line widths may indicate a couple of different things. 1) Fast exchangeing protons, in the case of protons with relatively low pKa (amide protons) and 2) conformational exchange (protons with higher pKa), where more than one conformer is present. Broad line widths due to conformational exchange is also known as exchange broadening. It is important to note, fast relaxation rates (T_2) also cause broad line widths, however, this is not a factor with these small molecular weight peptides.

In an attempt to correlate the T–jump results with an additional experimental technique, we measured 1–D proton NMR spectra of GS–14. A series of 1–D NMR experiments were recorded at increasing temperature for GS–14. By collecting 1–D experiments from 25–55 °C (temperature series experiment), it is possible to get an idea of the extent of structural stability for a protein or peptide. Figure 5.4 shows a stack plot of the GS–14 temperature series experiment. Two views of the amide proton region are plotted. Clearly visible are the increasing

linewidths as temperature increases for many of the amide protons in the peptide. Broad line widths are apparent in the lysine residues, which are located near the middle of the strands, and the tyrosine residues that are located in the turns. Our hypothesis is (also indicated by broad α–proton line widths, data not shown) that the peptide is in a state of conformational heterogeniety at high (+ 45 °C) temperatures as indicated by exchange broadening. However, based on peak intensity of many resonances, the population of unfolded peptide is relatively small compared to the folded peptide. The broad line widths of the lysine and tyrosine residues, demonstrate that both the turn and sheet regions (of the smaller population) are unfolded.

Unrestrained MD. The determination of structural characteristics of peptide or protein intermediates during folding reactions are crucial to understanding the mechanisms of folding (Kim and Baldwin, 1990). Since experimental methods (such as NMR, T–jump, fast flow CD) yield limited information on detailed structural transitions during folding, empirical MD methods provide perhaps the best approach to model structural details at the atomic level. A number of different MD approaches to study peptide and protein folding have appeared throughout the literature (Pande and Rokhsar, 1999; Dinner et al., 1999; Ferrara et al., 2000; Kolinski et al., 1999; Bryant, et al., 2000; Garcia and Sanbonmatsu, 2001). These methods are all somewhat limited in the length of simulation as all of these approaches are highly CPU intensive.

Since regular unrestrained MD simulations are generally limited to temporal trajectories on the order of tens of nanoseconds, it has not been practical to simulate the folding of small proteins (or peptide models) as this would require MD runs of milliseconds (CPU years). One strategy which allows the study of conformational and folding changes in peptides and proteins is to simulate unfolding rather than direct folding (Pande and Rokhsar, 1999). These unfolding simulations are usually carried out under conditions that favor or accelerate the unfolding reaction (high temperature, low pH etc.) into an accessible time range (Tirado–Rives et al., 1997; Lazaridis and Karplus, 1997). A key advantage to studying unfolding as opposed to folding (in addition to the savings in computation time) is that the simulations proceed from a well–defined starting structure. Hence, it is possible to examine the actual transitions occurring as the peptide or protein unfolds and to characterize any intermediates during the process. Many unfolding transitions (or transition states) are assumed to mimic latter stages of refolding (Pande and Rokhsar, 1999).

Using simulations from three to ten nanoseconds in length, we have studied 'complete' unfolding events of the fourteen residue GS analog (GS–14) at temperatures of 500 and 600 K. We also simulated early stages of unfolding at temperatures of 300–320 K. The trajectories calculated at different temperatures and durations allowed the determination of a relatively complete unfolding pathway for this model peptide. Our results indicate that unfolding occurs in discrete steps extending over varying lengths of time. Because these simulations are artificially accelerated, it is inappropriate to mention exact durations (in picoseconds) of each of these unfolding steps.

Figure 5.5 illustrates the unfolding trajectory at 500 K for GS–14, as calculated using an extended run of unrestrained molecular dynamics in a solvent bath. Each structure corresponds with a discrete step, or transition state, during the unfolding process. The backbone, D–tyrosine and proline side–chain (β–turn residues) atoms are shown for clarity. The starting structure (Start) is 10 ps into the unfolding reaction. As is evident by the superimposed ribbon diagram, the β–sheet is still very stable early on in the trajectory. By the time the simulation reaches Step 1, most of the β–sheet structure is still intact, however a bend along the plane of the sheet (at 390 ps) represents a significant destabilization. Step 2 (900 ps) shows a total deformation of the β–sheet structure with large amounts of twisting and solvent exposure evident. Step 3 (1640 ps) shows that a β–sheet–like structure has been restored. Although there is antiparallel sheet structure, a large bend perpendicular to the plane of the sheet does not allow a true, β–sheet to be formed. In Step 4 (2090 ps), a return to the open, twisted state similar to Step 2 is adopted. By Step 5 (3800 ps), the most interesting state, shows a return of the antiparallel sheet–like structure. As shown by the superimposed ribbon diagram and the position of the β–turn residues, the sheet appears to be initiated and terminated by each proline residue. However it is apparent that, large deviations of dihedral angles (from the starting structure) throughout the entire backbone are required to form this sheet–like structure.

The correlation between folded and unfolded states with molecular radius of gyration is a common measurement in MD studies (Dinner et al., 1999; Pande and Rokhsar, 1999). The radius of gyration essentially describes the compactness of a molecule. Hence, changes in radius of gyration correspond to changes in (un)folded states. The unfolding steps mentioned above correlate well with the molecular radius of gyration, calculated from 4 ns simulations conducted at 500 K (see Figure 5.6). The radius of gyration throughout the trajectory shows distinct dwell times within each state, whereas the transit times between states are very short. Sheet structure, or sheet–like structure, corresponds to an average radius of gyration of approximately 7.50 Å. In contrast, unfolded twisted structure has a slightly lower radius of gyration with an average of 6.75 Å. Also evident in this figure is the brief interruption of the open–twisted forms (Steps 2 and 4) with a sheet–like conformation appearing in Step 3. Followed by the sheet–like conformation of Step 5.

From these results, there appear to be at least two possible transition states found during an (un)folding reaction: an open twisted form (as in Steps 2 and 4) and sheet–like structures (as in Steps 3 and 5). It is not correct to assume that the reverse order of these states would be observed during a folding reaction since folding does not occur at 500 K and the 500 K trajectory finishes at 4ns with a somewhat sheet–like structure. Indeed, a 600 K simulation ended (at 3.5 ns) with the completely unfolded state. It may be more realistic to think that a cycling between these states occurs during the folding process.

5.4 Conclusion

The results of these studies both experimental (T–jump IR and NMR) and theoretical (all–atom MD), show rapid unfolding events within small cyclic peptides in response to increasing temperature. The T–jump results in particular, show the unfolding reactions of the peptides occurs in less than 60 ns. This relaxation is three orders of magnitude faster than the protein G β–hairpin. We believe, the most likely explanation for this is that since the protein G hairpin is linear, it has much more conformational space to sample than the cyclic GS peptides. Therefore, both folding and unfolding will take longer for the protein G hairpin. The slightly higher molecular weight (1864 amu) of the protein G peptide, probably has negligible effect on the differing relaxation rates.

The NMR temperature series experiment revealed a conformational heterogeniety between folded and unfolded states, based on exchange broadening. However, the unfolded conformer(s) represents a smaller population than the folded conformer at high (+ 45 °C) temperature. These results corraborate the T–jump results, in that we observe unfolded peptide at ~50 °C. The fact we do not see just one (unfolded) population at high temperature, as with the T–jump data, is indicative of the fundamentally different experimental techniques (i.e. NMR = steady–state whereas laser induced T–jump is on the order of picosecond time scale). This is supported by the aforementioned feature of laser induced T–jump, in that the equilibrium position of the ensemble of possible conformers is changed

faster than chemical processes are able maintain equilibrium, hence unbalanced populations (Eigen and De Maeyer, 1963).

It has been stated, via the principle of microscopic reversibility, that refolding will occur by the reverse of the unfolding pathway. Therefore, it is natural to assume that the nature of the refolding pathway will be preserved at lower temperature (Pande and Rokhsar, 1999; Daggett and Levitt, 1999). It was on this basis that we simulated unfolding in an attempt to identify possible intermediates along the folding pathway. By careful examination of the structural intermediates generated from these MD simulations of unfolding, it is clear at least two unfolding intermediates exist. In addition, these results point to hydrophobic effects, more than likely, have greater influence to (un)folding intermediate formation. This is evident by the common structure of State 5, where the turn forming residues no longer promote turn formation but a sheet–like structure still exists. That being said, however, it is difficult to determine to what extent either β–turn residues or hydrophobic residues have on intermediate formation, due to the 'unnatural' cyclic constraint of these GS analogs.

It may be possible in future studies, to use the unfolding intermediates in refolding experiments, at *in vivo* temperatures, to 'visualize' a much longer folding time–line. However, limitations exist with this method. A known problem with this type of experiment is that at high temperatures, certain low temperature folding intermediates may not appear (Pande and Rokhsar, 1999). Therefore, other folding pathways may exist that are not seen at these high temperatures.

References

Balbach, J., Forge, V., van Nuland, N.A.J., Winder, S.L., Hore, P.J. and Dobson, C.M. (1995) *Nat. Struct. Biol.* 2:865–870.

Berendsen, H.J.C., van der Spoel, D. and van Drunen, R. (1995) *Comp. Phys. Comm.* 91:43–56.

Berendsen, H.J.C., Postma, J.P.M., van Gunsteren, W.F. and Hermans, (1981) *J. Intermolecular forces*, B.Pullman ed. :Dordrecht.

Bryant, Z.B., Pande, V.S. and Rokhsar, D.S. (2000) *Biophys. J.* 78:584–589.

Callender, R.H., Dyer, R.B., Gilmanshin, R. and Woodruff, W.H. (1998) *Annu. Rev. Phys. Chem.* 49:173–202.

Daggett, V. and Levitt, M. (1993) *J. Mol. Biol.* 232:600–619.

Dinner, A.R., Lazaridis, T. and Karplus, M. (1999) *Proc. Natl. Acad. Sci. USA* 96:9068–9073.

Dobson, C.M., Evans, P.A. and Radford, S.E. (1994) *Trends Biochem. Sci.* 19:31–37.

Dobson, C.M. and Hore, P.J. (1998) *Nat. Struct. Biol.* 5:S04–S07.

Dobson, C.M., Sali, A. and Karplus, M. (1998) *Angew. Chem. Int. Ed.* 37:868–893.

Dyson, J.H. and Wright, P.E. (1998) *Nat. Struct. Biol.* 5:S4999–S503.

Eaton, W.A., Muñoz, V., Thompson, P.A., Chan, C.–K. and Hofrichter, T. *Curr. Opin. Struct. Biol.* 7:10–14.

Eigen, M. and De Maeyer, L.D. (1963) In *Technique of Organic Chemistry*, ed. S.L. Friess, E.S. Lewis and A. Weissberger, 8:895–1054. New York: Interscience.

Ferrara, P., Apostolakis, J. and Caflisch A. (2000) *Proteins* 39:252–260.

Garcia, A.E. and Sanbonmatsu, K.Y. *Proteins* 42:345–354.

Gibbs, A.C., Kondejewski, L.H., Gronwald, W., Nip, A.M., Sykes, B.D., Hodges, R.S. and Wishart, D.S. (1998) *Nat. Struct. Biol.* 5:284–288.

Hagen, S.J. and Eaton, W.A. (2000) *J. Mol. Biol.* 301:1019–1027.

Honig, B. (1999) *J. Mol. Biol.* 293:283–293.

Karplus, M. and Sali, A. (1995) *Curr. Opin. Struct. Biol.* 1:58–73.

Kim, P.S. and Baldwin, R.L. (1990) *Annu. Rev. Biochem.* 59:631–660.

Kolinski, A.K., Ilkowski, B. and Skolnick, J. (1999) *Biophys. J.* 77:2942–2952.

Kondejewski, L.H., Farmer, S.W., Wishart, D.S., Hancock, R.E.W. and Hodges, R.S. (1996) *Int. J. Pept. Protein Res.* 47:460–466.

Lazaridis, T. and Karplus, M. (1997) *Science* 278:1928–1931.

Miyamoto, S. and Kollman, P.A. (1992) *J. Comp. Chem.* 13:952–962.

Muñoz, V., Henry, E.R., Hofrichter, J. and Eaton, W.H. (1998) *Proc. Natl. Acad. Sci. USA* 95:5872–5879.

Muñoz, V., Thompson, P.A., Hofrichter, J. and Eaton, W.A. (1997) *Nature* 390:196–199.

Pande, V.S. and Rokhsar, D.S. (1999) *Proc. Natl. Acad. Sci. USA* 96:9062–9067.

Susi, H. and Byler, D.M. (1986) *Methods Enzymol.* 130:290–311.

Thompson, P.A., Eaton, W.A. and Hofrichter, J. (1997) *Biochemistry* 36:9200–9210.

Tirado–Rives, J., Orozco, M. and Jorgensen, W.L. (1997) *Biochemistry* 36:7313–7329.

Williams, S., Causgrove, T.P., Gilmanshin, R., Fang, K.S., Callender, R.H., Woodruff, W.H. and Dyer, R.B. (1996) *Biochemistry* 35:691–697.

Wishart, D.S., Kondejewski, L.H., Semchuck, P.D., Sykes, B.D. and Hodges, R.S. (1996) *Lett. Pep. Sci.* 3:53–60.

Wishart, D.S. and Sykes, B.D. (1994) *Methods Enzymol.* 239:363–392.

Table 5.1 GS Analogs

Name	Sequence[a]	Molecular Weight[b]
GS–6	KYPKYP	776.95
GS–10	VKLYPVKLYP	1201.53
GS–14	VKLKVYPLKVKLYP	1670.17

a. All tyrosine residues are of D–stereochemistry.
b. Theoretical molecular weight.

Table 5.2 Summary of T–Jump Experiments

Analog	Initial Temp.[a]	Final Temp.[b]	ΔT^c	ΔA (mOD)[d]	τ (obs.)[e]
GS–6					
Average	40.5	51.3	10.8	3.75	38
Std. Dev.	0.7	0.6	0.5	0.18	7
GS–10					
Average	40	50.2	10.4	2.83	36
Std. Dev.	0.1	0.8	0.8	0.63	9
GS–14					
Average	40.2	51.0	10.8	2.68	59
Std. Dev.	0.1	0.5	0.6	0.08	4

a. Initial temperature of sample.
b. Final temperature of sample after temperature jump.
c. Overall change in temperature.
e. ΔA (mOD), is the average change in absorbance at 1618 cm^{-1}.
f. τ (obs), is the average relaxation time in nanoseconds.

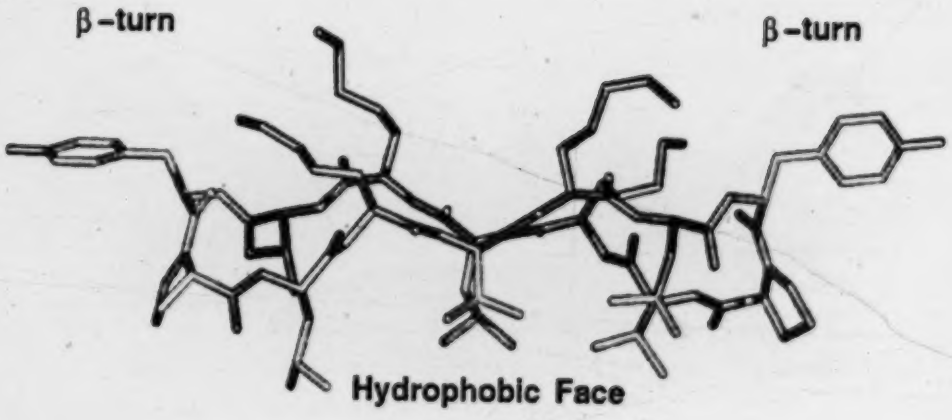

Figure 5.1. GS analog β–turns and hydrophibic face.

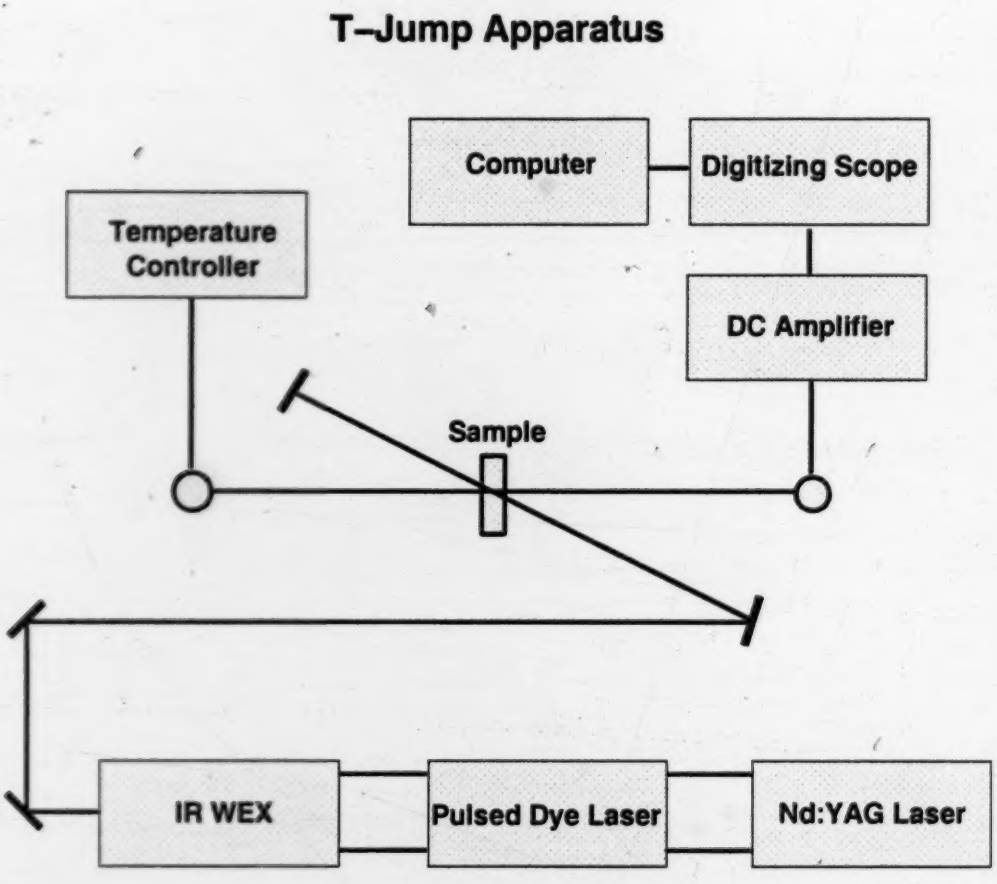

Figure 5.2. Temperature–jump apparatus. The Nd:YAG laser is the source for the temperature jump. The sample gets irradiated, the signal subsequently gets digitized and amplified then is recorded by the IR WEX (which is in line with the Nd:YAG laser).

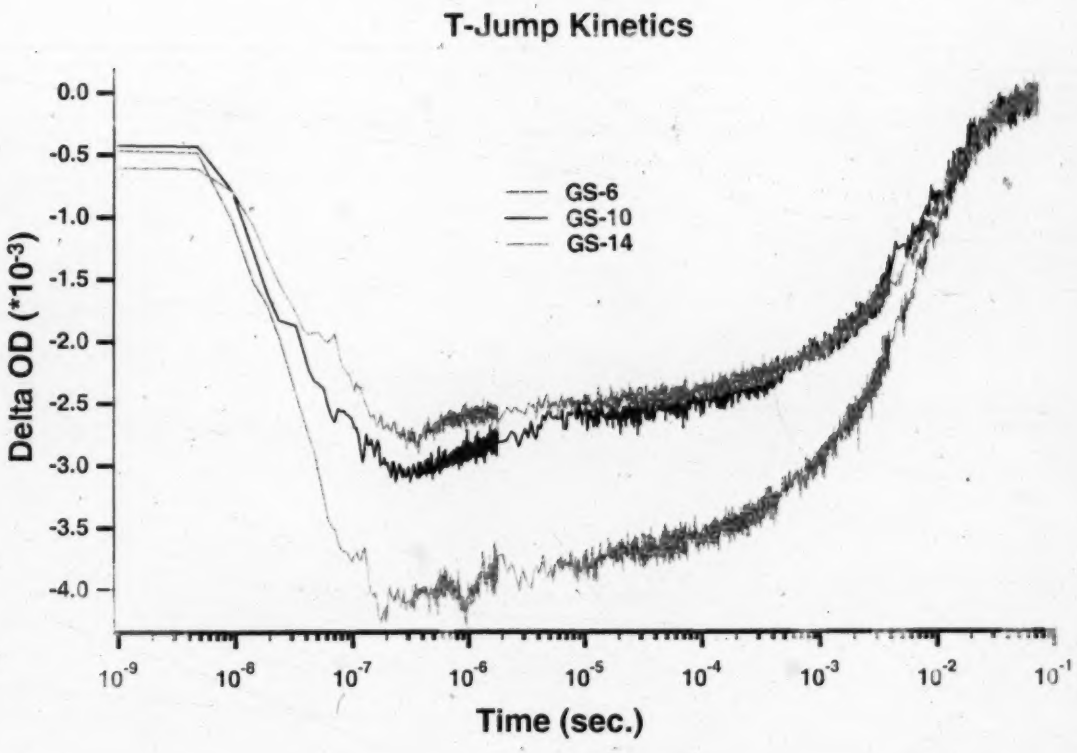

Figure 5.3. T–jump kinetic curves. Top (green) = GS–14, middle (blue) = GS–10 and bottom (red) = GS–6. As is shown by the curves, an initial change in OD is indicative of the 60 ns (or less) relaxation time. Then folding occurs over microseconds until the sample no longer gives a change in OD.

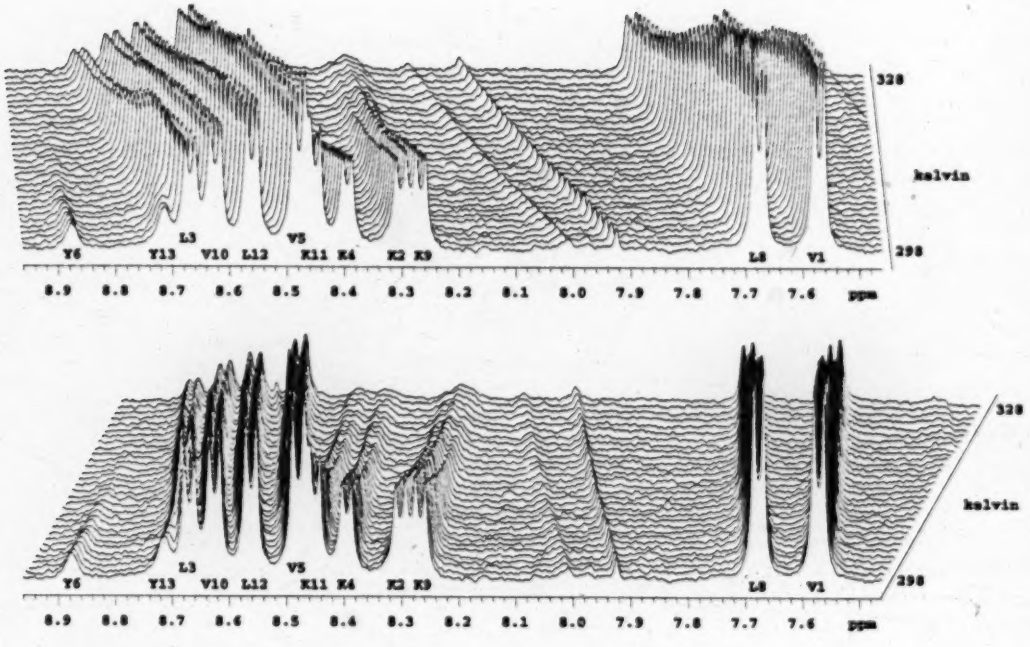

Figure 5.4. NMR stack plot. Two views of the amide proton region are shown. Visible are the broad linewidths at high temperatures for most of the resonances. These broad linewidths are indicative of peptide denaturation.

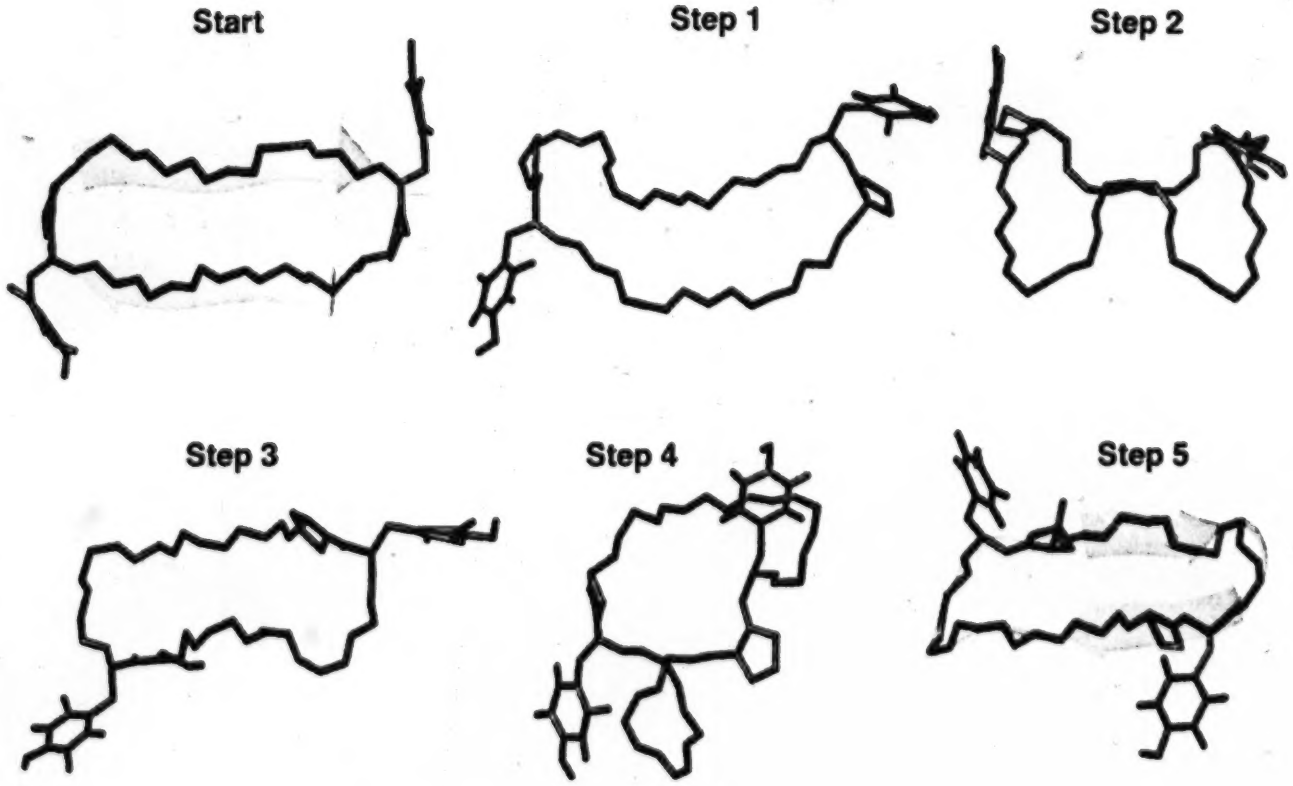

Figure 5.5. See next page.

Figure 5.5. The unfolding trajectory at 500 K. The Start is just picoseconds into the simulation and the β–sheet structure is still stable. Step 1 (at 390 ps), shows the destabilized β–sheet just before it loses all sheet–like character. Step 2 (900 ps), a total deformation of the β–sheet and high solvent exposure. Step 3 (1640 ps), a restoration of sheet–like structure. Step 4 (2090 ps), random coil, unfolded structure. Finally, in Step 5 (3800 ps) the formation of a skewed β–sheet.

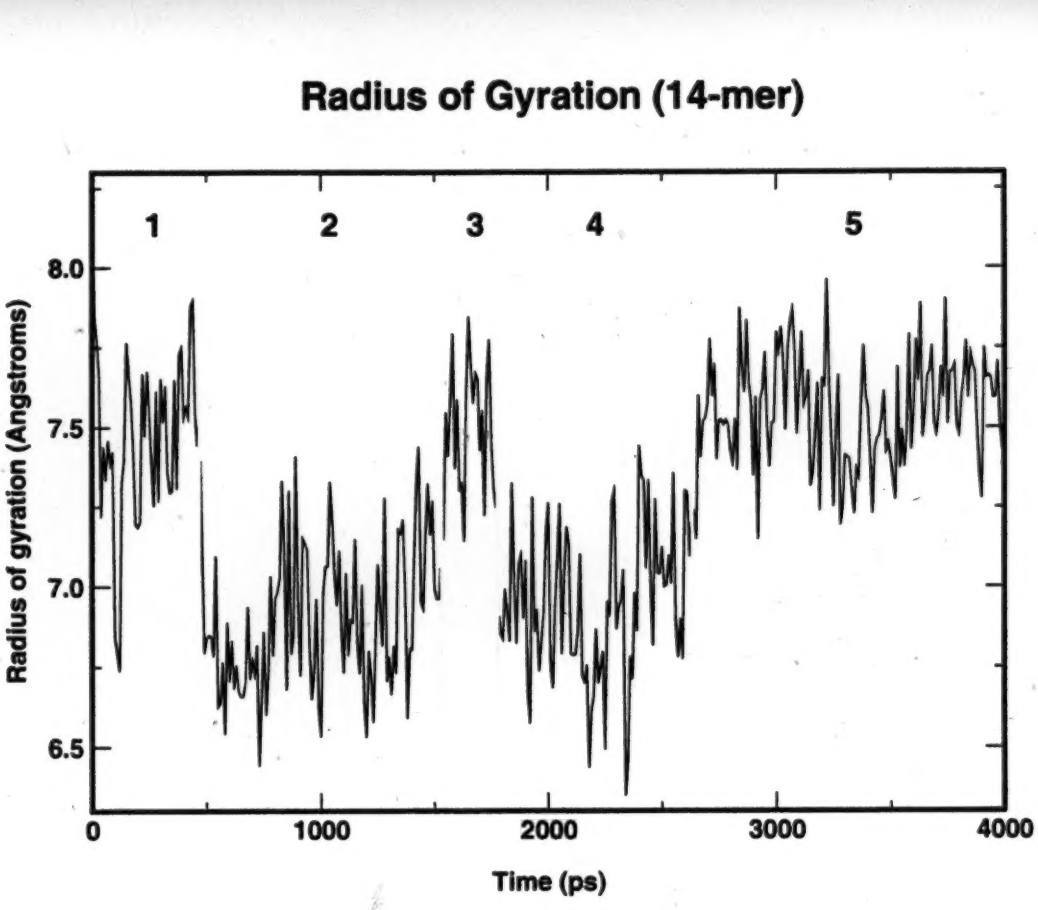

Figure 5.6. Radius of gyration at 500 K. The change in radius of gyration through out the simulation shows clear intermediate dwell times and short transition times through out the simulation.

Chapter 6

General Discussion and Conclusions

This thesis focuses on two structurally diverse molecules both of which are members of a therapeutically important class of antibiotics – the antibacterial peptides. The recent occurrence of antibiotic resistant bacteria has promoted a resurgence of study on this venerable class of antibiotics (Hancock, 1997; Hancock and Chapple, 1999; Hwang and Vogel, 1998). Indeed it is widely believed that antibacterial peptides will make excellent candidates as potential therapeutics because their mechanism of action involves interaction with a unique and ubiquitous target – the bacterial cell membrane (Huang, 2000; Oren and Shai, 1998). The intent of this thesis was to describe the synthesis, structure and dynamics of a series of specially designed gramicidin S and leucocin A analogs. These studies were undertaken with the hopes of elucidating structural requirements for antibacterial peptide activity. More specifically, in Chapter 2, I describe the synthesis and structural characterization of a number of different sized GS analogs. This study showed an obvious structural periodicity occurring within the peptides, a periodicity that arises from the peptide ring size as well as a number of other parameters. In Chapter 3, I describe the synthesis and characterization (both molecular constitution and biological activity) of the D–enantiomer of a class IIa bacteriocin known as leucocin A. This study revealed an important detail in leucocin A's mechanism of action. That is, the requirement of a chiral interaction step. Chapter 4, details the

structural determinants of type II' β–turn formation by way of β–hairpin formation and stability. The results of this study may aid in the design of cyclic peptides, linear β–hairpins and peptidyl mimetics. Finally, in Chapter 5, I describe the folding and unfolding of GS analogs at both the temporal and structural levels. These results clearly indicate the dynamic nature of the GS analogs at elevated temperatures. It is my contention that these kinds of detailed structural characterizations of two different classes of antibacterial peptides, gramicidin S (β–sheet) and leucocin A (α–helical), will help elucidate mechanisms of action and assist in the design of novel antibacterial peptides, of model secondary structural elements (β–turns and β–hairpins) and of peptidyl mimetics.

Chapter 2

Many small cyclic peptides (especially those with less than 15 residues) contain a wide variety of coded/non–coded amino acids and post–translationally modified residues. Some of the more common, naturally occurring, cyclic peptides include cyclosporin A (Rüegger et al., 1976), valinomycin (Shemyakin et al., 1965), virginiamycins (Kingston et al., 1966), vernamycin A (Meyers et al., 1965), tyrocidine (Lipmann, et al., 1941), actinomycin (Goldberg et al., 1962) and mycobacillin (Sengupta, et al., 1971). Although much is known about the primary sequences of these peptides much less is known about their three–dimensional structures. Robert Schwyzer (Schwyzer, 1958) was one of the first scientists to think about the three–dimensional structures of cyclic peptides, in particular the antibacterial gramicidin S. He predicted that the number of amino acids in a cyclic peptide would influence the type of secondary structure adopted by the peptide.

This hypothesis remained untested until 1996 when preliminary CD data revealed a periodicity in secondary structure of a series of different length GS analogs (Kondejewski et al., 1996). This result nicely corroborated Schwyzer's hypothesis, however, the exact details of this periodicity remained unknown. These more detailed findings are the basis for Chapter 2.

Chapter 2 reports the full three–dimensional characterization, via NMR and CD spectroscopy, of a series of longer GS analogs. Indeed, we were able to confirm Schwyzer's hypothesis that only peptides with 2(2n + 1) residues (where n=1, 2, 3...) have the ability to form β–sheets. This study represents the first three–dimensional confirmation of Schwyzer's hypothesis. However, we also show that a numbe r of details not mentioned by Schwyzer also need to be fulfilled in order for cyclic peptides to form β–sheets. Hence we proposed a few amendments to Schwyzer's original rule. First, β–sheet formation can only occur in peptides that contain two equally spaced type II' or type I' β–turns. These mirror image turns are required in order to compensate for the natural left–handed twist of antiparallel β–sheets. Second, appropriate placement of 'turn–forming' residues through out the peptide is required. Third, intrinsic secondary structural propensities of amino acids can dramatically influence the stability of β–sheet structure. Fourth, the number and placement of D–amino acids is an important consideration when predicting β–sheet formation. Fifth, cyclic peptides containing evenly spaced type I' or type II' β–turns and 4n residues (where n=1, 2, 3...), will always form random coil structures.

Similarly, cyclic peptides containing an odd number of residues are incapable of forming stable β–sheets (Morita et al., 1996).

Chapter 3

In 1948 Alexander Ogston published an account of his proposed three–point attachment model (Ogston, 1948). The three–point attachment model is the prototypical description of enzyme–substrate specificity. The model simply states, a substrate with binding sites A, B, and C will be recognized by an enzyme with binding sites A', B' and C' whereas the enantiomer of the substrate (with binding sites C, B and A) will not be recognized by the enzyme. This concept, although somewhat antiquated, is the basis for many studies on chiral recognition, including enantiomeric (and diastereomeric) syntheses. In an attempt to determine if chirality plays a role in leucocin A's antibacterial action, we synthesized and assayed for activity the unnatural enantiomer of leucocin A.

Chapter 3 describes the synthesis and characterization of the all–D–amino acid leucocin A. This study represents the first synthesis of an all–D–amino acid class IIa bacteriocin. Solid phase peptide synthesis with Fmoc protected D–amino acids was employed to give an overall yield of 6% D–LeuA, at over 95% purity. Following the characterization of D–LeuA, a large number of bioactivity assays were performed. Interestingly, the results of these assays differed from previous studies of all–D–amino acid antibacterial peptides in that D–LeuA was found to be devoid of activity. One may assume these differences are a result of the structural variation between the peptides. The three–dimensional structure of LeuA is very

different from all α–helical, bacteriocidal enantiomers like plantaricin A. LeuA contains an amphipathic α–helix, as does plantaricin A, but differs in that LeuA also contains an N–terminal amphipathic three stranded β–sheet (Gallager et al., 1997; Wang et al., 1999). Hence, the different activity of these all–D–amino acid peptides, indicates an amphipathic α–helix by itself, has a limited role in chiral recognition and that receptor attachment points are required from other structural elements.

Chapter 3 also illustrates the differences between LeuA and its closely related homolog, CbnB2. Interestingly, the N–terminal structure for the two peptides are actually very different despite the high level of sequence homology, whereas structurally the C–termini are very similar. Therefore, it is easy to assume the N–terminus accounts for the differences in antibacterial spectrum of action between the two peptides. However, our data suggests the C–termini may play a significant role in specifying antibacterial spectrum of action. The bacteriocin fragment studies support this conclusion (i.e. C–terminal CbnB2 and N–terminal LeuA fragments were inactive by themselves). In addition, the results of the fragment studies suggests that the integrity of the entire sequence is necessary for activity of class IIa bacteriocins.

Chapter 4

Recent experiments have shown that 14–residue GS analogs have a wide range of therapeutic indices depending on the secondary structure adopted (Kondejewski et al., 1999). Kondejewski et al. report on a series of 14 residue GS

analogs differing at only one chiral center. The results of this study indicate a clear correlation showing high amphipathicity (high β–sheet content) yields high hemolytic activity and low antibacterial activity in the diastereomers. The diastereomers possessing the most attractive therapeutic indices (hemolytic activity/antimicrobial activity), greater than 60 in some cases, possessed some of the lowest amphipathicities. Therapeutic indices of the parent β–sheet peptide where less than 0.01. These findings prompted the study reported in Chapter 4. It was our intention in this chapter to further define the rules regarding secondary structure formation in 14–residue GS analogs. Specifically, we wished to detail our 'first' amendment to Schwyzer's 2(2n + 1) rule. Therefore in Chapter 4, I describe the structural determinants of type II' β–turn formation. We used a combination of NMR and molecular dynamics to determine β–hairpin content, a property that is intrinsically related to type II' β–turn stability. By substituting a variety of coded and non–coded amino acids into one turn of a model 14–residue GS analog, it was possible to probe the conformational space of the type II' β–turn. These substitutions allowed us to examine the roles of backbone chirality, side–chain steric restriction and side–chain/side–chain interactions on type II' β–turn formation and stability.

The study in Chapter 4 is unique in that unlike most molecular dynamics simulation studies, we were able to experimentally (via NMR) determine initial atomic coordinates as input for these simulations. The calculated 10 ns molecular

dynamics trajectories, in turn, yielded information relating to the experimentally determined structures. It was shown that β–sheet content as determined by NMR is not necessarily a 'static' phenomenon but more of a dynamic or temporal property. Therefore, amount and stability of the β–sheet depends strongly on the dihedral angles favored in a particular β–turn. As Chapter 4 reports, the results of this study demonstrate that backbone heterochirality (which determines equatorial and axial side–chain orientation at the i+1 and i+2 residues of the turns) may account for up to 60% of type II' β–turn stabilization. Steric restriction through side chain N–alkylation may provide up to 20% of type II' β–turn stability. Finally, it was shown that aromatic/proline side–chain interactions (i.e. side–chain/side–chain) appear to account for ~10% of type II' β–turn stabilization.

Chapter 5

In order to study the secondary structural elements found in proteins, it is often easier and more efficient to use peptide model systems. Ideally, these peptide model systems contain a relatively small number of residues, are easily synthesized, soluble and monomeric. Peptide model systems have proven to be an invaluable tool in the study of many aspects of secondary structure and function ranging from amino acid propensity measurements to protein folding studies. Although, many α–helical peptide model systems have been developed over the years, far fewer β–sheet models systems have been developed. Our earlier studies in Chapter 2 and 4, identified the utility of GS as a model β–hairpin system. It was on this basis that the GS –hairpin system was used to study the kinetics of β–hairpin folding.

In Chapter 5, I describe the folding and unfolding of three different sized β–sheet, GS analogs. Temperature–jump studies indicate relaxation kinetics to be very fast for all 3 peptides. These relaxation kinetics yielded folding rates that were orders of magnitude faster than what was found for a linear β–hairpin model (Muñoz et al., 1997). The differences between relaxation rates of our cyclic β–hairpin model and the linear β–hairpin model of Muñoz and Eaton, arise from the fact that the linear β–hairpin model is limited by diffusion whereas diffusion is not a factor for the cyclic β–hairpins. In an attempt to correlate the experimental T–jump results with atomic resolution structures, we performed unrestrained molecular dynamics simulations of peptide folding and unfolding over an extended period of time. Although the molecular dynamics simulations did not directly simulate peptide folding, the unfolding trajectories indirectly showed interesting information relating to possible folding intermediates. Specifically, there are at least two primary intermediates, one being totally unfolded and the other exhibiting a sheet–like state. It appears that the sheet–like state can contain a wide range of partially folded (hydrogen bonded) conformations.

A few additional experiments may provide further insight to the studies in Chapter 5. For example, it may be interesting to measure MD trajectories starting with the intermediate unfolded states at low (in vivo) temperatures. This may allow one to simulate folding by way of a multitude of shorter simulations rather than very long micro or millisecond trajectories. Further characterization of the putative

bacteriocin receptor (Chapter 3) would also be interesting. A future synthesis of an all-D-amino acid non α-helical class IIa bacteriocin may help elucidate this further. All the experiments in this thesis have led to my greater understanding of synthesis, structure and characterization of antibacterial peptides.

References

Gallagher, N.L.F., Sailer, M., Neimczura, W.P. Nakashima, T.T., Stiles, M.E. and Vederas, J.C. (1997) *Biochemistry* 36:15062–15072.

Goldberg, I.H., Rabinowitz, M. and Reich, E. (1962) *Proc. Natl. Acad. Sci. USA* 48:2094.

Hancock, R.E.W. (1997) *Lancet* 349:418–422.

Hancock, R.E.W. and Chapple, D.S. (1999) *Antimicrob. Agents Chemother.* 43:1317–1323.

Huang, H.W. (2000) *Biochemistry* 39:8347–8352.

Hwang, P.M. and Vogel, H.J. (1998) *Biochem. Cell Biol.* 76:235–246.

Kingston, D.G.I., Sarin, P.S., Todd, L. and Williams, D.H. (1966) *J. Chem. Soc. C* 1856.

Kondejewski, L.H., Farmer, S.W., Wishart, D.S., Kay, C.M., Hancock, R.E.W. and Hodges, R.S. (1996) *J. Biol. Chem.* 271:25261–25268.

Kondejewski, L.H., Jelokhani–Niaraki, M., Farmer, S.W., Lix, B., Kay, C.M., Sykes, B.D., Hancock, R.E.W. and Hodges, R.S. (1999) *J. Biol. Chem.* 274:13181–13192.

Lipman, F., Hotchkiss, R.D. and Dubos, R.J. (1941) *J. Biol. Chem.* 141:163–169.

Meyers, E. Smith, D.A. and Perlman, D. (1965) *Antimicrobial Agents Chemother.* 5:256–260.

Morita, H., Kayashita, T., Takeya, K. and Itokawa, H. (1996) *Chem. Pharm. Bull.* 44:2177–2180.

Muñoz, V., Thompson, P.A., Hofrichter, J. and Eaton, W.A. (1997) *Nature* 390:196–199.

Ogston, A.G. (1948) *Nature* 162:963.

Oren, Z and Shai, Y. (1998) *Biopolymers* 47:451–463.

Rügger, A., Kuhn, M., Lichti, H., Loosli, H.R., Huguenin, R., Quiguerez, C. and von Wartburg, A. (1976) *Helv. Chim. Acta.* 59:1075–1092.

Schwyzer, R. (1958) *Chimia* 12:53–68.

Sengupta, S., Banerjee, A.B. and Bose, S.K. (1971) *Biochem. J.* 121:839–846.

Shemyakin, M.M., Virnagradova, E.I., Feigina, M.Y., Aldanova, N.A., Loginova, N.E., Ryabova, I.D. and Pavlenko, I.A. (1965) *Experientia* 21:548–552.

Wang, Y., Henz, M.E., Gallaher, N.L.F., Chai, S., Gibbs, A.C., Yan, L.Z., Stiles, M.E., Wishart, D.S. and Vederas, J.C. (1999) *Biochemistry* 38:15438–15447.